The Voltage-gated Sodium Channel Isoform $Na_v1.6$ Facilitates Neuronal Hyperexcitability in Genetic and Acquired Epilepsies

Bryan Scot Barker

Philadelphia, PA

B.S., University of Pennsylvania, 2013

A Dissertation presented to the Graduate Faculty
of the University of Virginia in Candidacy for the Degree of
Doctor of Philosophy

Neuroscience Graduate Program

University of Virginia
March 20th, 2018

Manoj K. Patel, PhD (Dissertation Advisor) _____

Edward H. Bertram III, MD (Executive Committee Member) _____

Jaideep Kapur, MD, PhD _____

Ed Perez-Reyes, PhD _____

Mark P. Beenhakker, PhD _____

Abstract

Voltage-gated sodium channels play a crucial role in regulating neuronal activity in the brain. One of these voltage-gated sodium channel isoforms in particular, $Na_v1.6$, is instrumental in the initiation and propagation of action potentials that is necessary for normal brain function. $Na_v1.6$ is highly expressed at the distal axon initial segment and the nodes of Ranvier, where the channel's more hyperpolarized activation allows for a lower action potential threshold. In both genetic and acquired epilepsies, proexcitatory alterations to $Na_v1.6$ can induce neuronal hyperexcitability. This hyperexcitability causes the rewiring of key neural circuits in a way that is conducive to the initiation and propagation of spontaneous seizures. Here we explore how proexcitatory changes to $Na_v1.6$ contribute to neuronal hyperexcitability in the genetic epilepsy syndrome, early infantile epileptic encephalopathy 13 (EIEE13), and the acquired temporal lobe epilepsy (TLE).

EIEE13 is a rare neurological disorder that results predominantly from missense, *de novo* mutations to the *SCN8A* gene, which encodes $Na_v1.6$. Patients with EIEE13 experience seizures beginning from birth to 18 months of age that are often refractory to clinically available treatments. In addition to seizures, EIEE13 patients suffer from mild to severe intellectual disability, developmental delay, and movement disorders. Here we are the first to electrophysiologically characterize novel, recurrent *SCN8A* mutations that account for 20% of all EIEE13 mutations known to date. As previously mentioned, patients suffering from EIEE13 are often refractory to clinically available antiepileptic drugs and literature detailing the efficacy of various treatments is sparse. To fill this knowledge gap, we test the *in vitro* efficacy of the sodium channel blocker phenytoin on a novel gain-of-function *SCN8A* mutation. We show that phenytoin shows preferential block of mutant $Na_v1.6$ channels over wild type and that phenytoin can help decrease the proexcitatory alterations in channel function that are induced by the mutation. To grasp a better understanding of the phenotypes that result from *SCN8A* mutations, we also are the first to characterize novel loss-of-function *SCN8A* mutations from patients with intellectual disability and no seizures. This work contributes to the *SCN8A* field by demonstrating the spectrum of phenotypes that can result from $Na_v1.6$ mutations and it makes a

stronger case for the screening of *SCN8A* mutations in patients with idiopathic intellectual disorders.

To grasp a deeper understanding of EIEE13 that goes beyond *in vitro* cultured cell experiments, a mouse model of EIEE13 was generated by knocking in the p.Asn1768Asp (N1768D) mutation. Mice carrying this mutation recapitulate many of the phenotypes seen in human patients including motor disorder, seizures, and SUDEP. To better understand how the N1768D mutation contributes to neuronal hyperexcitability, we electrophysiologically characterized layer II excitatory neurons of the medial entorhinal cortex (mEC) of heterozygote (D/+) and homozygote (D/D) mice. Layer II mEC neurons from D/+ and D/D are hyperexcitable in response to somatic current injection steps and synaptic stimulation. Additionally, D/+ and D/D mice show a dose-dependent increase in both persistent (I_{NaP}) and resurgent (I_{NaR}) sodium currents, two currents that strongly contribute to bursting and high frequency action potential firing. Our work using the N1768D mouse model further expands our knowledge of this rare and devastating disorder and it paves the way for future, more advanced *in vitro* and *in vivo* experiments.

Temporal lobe epilepsy (TLE) is one of the most common forms of adult epilepsy and it is marked by seizures that originate from the temporal lobe. While seizure-induced changes in the dentate gyrus (DG) and Cornu Ammonis (CA) regions have been well studied, relatively little attention has been given to alterations that occur in the subiculum, a region that acts as an output of the temporal lobe. This gap is literature is surprising as the subiculum consists of a large population of endogenously bursting neurons and is largely spared in TLE. Here we explore the neuronal excitability in subiculum excitatory neurons, and how it is altered in TLE. Specifically, we see that TLE subiculum bursting neurons are hyperexcitable in response to somatic current injection steps and synaptic stimulation. We hypothesized that alterations in sodium channel physiology contribute to this neuronal hyperexcitability seen in the subiculum in TLE. Outside-out patch clamp recordings revealed proexcitatory alterations in sodium channel physiology from TLE neurons compared to wild type. Additionally, we saw significant increases in both persistent (I_{NaP}) and resurgent (I_{NaR}) sodium channel currents in TLE subiculum neurons compared to controls. We believed that proexcitatory changes to $Na_v1.6$ in particular were the predominant driver of subiculum neuronal hyperexcitability in TLE. To test this hypothesis we applied the TTX metabolite 4,9-anhydro-tetrodotoxin (4,9-ah-TTX), which has

higher affinity for $Na_v1.6$ over other sodium channel isoforms, to TLE subiculum neurons. We saw that 4,9-ah-TTX significantly reduced TLE subiculum neuron hyperexcitability and caused significant reductions in both I_{NaP} and I_{NaR} currents. These findings shed more light on the intrinsic changes that occur in TLE and expand our existing knowledge of the cellular and synaptic reorganization that occurs in the disorder. Additionally, this data makes a stronger case to continue the push to develop the elusive $Na_v1.6$ selective blocker, a drug that could be the next promising treatment option for patients suffering from TLE.

Table of Contents

Publications

J.L. Wagnon, **B.S. Barker**, J.A Hounsell, C. Haaxma, A. Shealy, T. Moss, S. Parikh, R.D. Messer, M.K. Patel and M.H. Meisler. Pathogenic mechanism of recurrent mutations of *SCN8A* in epileptic encephalopathy. *Annals of Clinical and Translational Neurology* 2015; 3:114–23

B.S. Barker, M. Ottolini, J.L Wagnon, R. Hollander, M.H. Meisler and M.K Patel. The *de novo SCN8A* encephalopathy mutation p.Ile1327Val displays elevated sensitivity to inhibition by the anticonvulsant phenytoin. *Epilepsia* 2016; *57(9):1458–1466*

M.A. Wheeler, C.J. Smith, M. Ottolini, **B.S. Barker**, A.M. Purohit, R.M. Grippo, R.P. Gaykema, A.J. Spano, M.P. Beenhakker, S. Kucenas, M.K. Patel, C.D. Deppmann, and A.D. Güler. Remote magnetic control of the nervous system *in vivo*. *Nature Neuroscience* 2016; 19(5):756- 61

D. Warthen, M. Ottolini, **B.S. Barker**, P. Lambeth, R. Gaykema, B. Newmyer, Y. Ohmura, E. Perez-Reyes, A. Güler, M.K. Patel, and M. Scott. Activation of pyramidal neurons in mouse medial prefrontal cortex selectively enhances performance in several food-rewarded operant tasks. *Frontiers in Behavioral Neuroscience* 2016; 10:63

J.L. Wagnon*, **B.S. Barker***, M. Ottolini, Y. Park, A. Volkheimer, P. Valdez, M.E.M. Swinkels, M.K. Patel, and M.H. Meisler. Loss-of-function mutations of *SCN8A* in intellectual disability without seizures. *Neurology Genetics* 2017; Aug; 3(4): e170

*Co-First Authors

M. Ottolini*, **B.S. Barker***, R. Gaykema, M.H. Meisler, M.K. Patel. Aberrant sodium channel currents and hyperexcitability of medial entorhinal cortex neurons in a mouse model of *SCN8A* encephalopathy. *Journal of Neuroscience,* 2017 37(32):7643-7655.

*Co-First Authors

B.S. Barker, A. Nigam, M. Ottolini, R. Gaykema, N.J. Hargus and M.K. Patel. Pro-excitatory alterations in sodium channel activity facilitate subiculum neuron hyperexcitability in temporal lobe epilepsy. *Neurobiology of Disease,* 2017**;** 108:183-194

Acknowledgements

Wisdom I Know is Social. She Seeks Her Fellows

-Thomas Jefferson

This work was a collaborative effort involving a number of very supportive and talented people that I have had the pleasure of working with over the past few years. In Chapters III-V, Matteo Ottolini was invaluable for his assistance with the electrophysiology recordings, cell culture transfections and current-clamp data analysis. Ron Gaykema's biochemical technical expertise was crucial for conducting the demanding PCR genotyping of the N1768D mice as well as running the immunohistochemistry necessary to complete Chapters IV & V. This work would also not have been possible without our collaborators at the University of Michigan, Jacy Wagnon and Miriam Meisler. Jacy and Miriam were responsible for a significant portion of the work performed in Chapters III & IV, specifically generating the N1768D mice, producing the $Na_v1.6$ cDNA clones, and performing Western blot staining. Lastly, the preliminary data that acted as a foundation for Chapter V was provided by previous outstanding students of the Patel lab, Aradhya Nigam and Nick Hargus, whose departures left big shoes to fill.

I would also like to extend my thanks and appreciation to Bettina Winckler, Nadia Cempre and the Neuroscience Graduate Program for their support and for giving me the opportunity to pursue my PhD in Neuroscience. This document would not be possible without my thesis committee consisting of Drs. Edward Bertram, Jaideep Kapur, Ed Perez-Reyes and Mark Beenhakker who provided mentorship and critical feedback necessary to complete the work presented below. Lastly, I would like to thank Dr. Manoj K. Patel for his mentorship and for providing me with an excellent PhD experience. Without hesitation, Dr. Patel took a risk welcoming me to his lab without a prior rotation and his belief in me will never be forgotten. Dr. Patel was invaluable in all his roles; a mentor, teacher, reviewer, AES co-socialite and my good friend.

This research was supported by the Neuroscience Graduate Program Training Grant, the American Epilepsy Society Predoctoral Research Fellowship, and the 2016-2017 & 2017-2018 University of Virginia Wagner Fellowship Research Grants.

List of Abbreviations

4,9-ah-TTX	4,9-anhydro-tetrodotoxin
4-AP	4-aminopyradine
ACSF	artificial cerebrospinal fluid
ADP	after depolarizing potential
AED	anti-epileptic drug
AIS	axon initial segment
Ala	alanine
Ank G	ankyrin G
ANOVA	analysis of variance
AP	action potential
Arg	arginine
Asn	asparagine
Asp	aspartic acid
ATP	adenosine triphosphate
AUC	area under the curve
BSA	bovine serum albumin
CA1	Cornu Ammonis area 1
CA2	Cornu Ammonis area 2
CA3	Cornu Ammonis area 3
CDC	Center for Disease Control
cDNA	complementary DNA
CHS	continuous hippocampal stimulation
CNQX	6-cyano-7-nitroquinoxaline-2,3-dione
CNS	central nervous system
CSF	cerebrospinal fluid
DG	dentate gyrus
DMEM	Dulbecco's modified eagle media
DRG	dorsal root ganglion
EDTA	ethylenediaminetetraacetic acid
EEG	electroencephalogram
EIEE13	early infantile epileptic encephalopathy 13
fAHP	fast after hyperpolarization
FBS	fetal bovine serum
GABA	gamma-aminobutyric acid
GFP	green fluorescent protein
Gln	glutamine
Glu	glutamic acid
Gly	glycine
GTP	guanosine-5'-triphosphate
HA	hemagglutinin
HEK	human embryonic kidney
i.p.	intraperitoneal
ILAE	International League Against Epilepsy
Ile	isoleucine

I_{NaP}	persistent sodium current
I_{NaR}	resurgent sodium current
IPSC	inhibitory post synaptic potential
KA	kainic acid
kD	kilodalton
Leu	leucine
Lys	lysine
mEC	medial entorhinal cortex
mRNA	messenger RNA
Na	sodium
NaChBac	bacterial sodium channel
NADPH	nicotinamide adenine dinucleotide phosphate
NEAA	nonessential amino acid
OMIM	online Mendalian inheritance in man
PCR	polymerase chain reaction
PNS	peripheral nervous system
PV	parvalbumin
PV-IR	parvalbumin-immunoreactive
R_i	input resistance
RMP	resting membrane potential
R.O.D	relative optical density
RT-PCR	reverse transcription polymerase chain reaction
SE	status epilepticus
SEM	standard error of the means
Ser	serine
SUDEP	sudden unexpected death in epilepsy
TALEN	transcription activator-like effector nucleases
TEA	tetraethylammonium
Thr	threonine
TLE	temporal lobe epilepsy
Trp	tryptophan
TTX	tetrodotoxin
Val	valine
WHO	World Health Organization
WT	wild type
YFP	yellow fluorescent protein

I. Introduction

Epilepsy

Definitions

Epilepsy is a severe neurological disorder characterized by a prolonged predisposition to the occurrence of spontaneous seizures. As described by the International League Against Epilepsy (ILAE), a seizure is a "transient occurrence of signs and/or symptoms due to abnormal excessive or synchronous neuronal activity in the brain" (Fisher et al., 2014). Instead of being labeled a disease, epilepsy is often described as an eclectic disorder that embodies a wide variety of various diseases (Fisher et al., 2014). This description truly encompasses the heterogeneous nature of epilepsy and hints at the true spectrum of the conditions that are classified under the disorder.

In addition to providing definitions for terms related to epilepsy, the ILAE has also devised a criterion for the definition of epilepsy itself, with the hopes of aiding in the process of a clinical diagnosis. As defined by the ILAE in 2014, a patient can be diagnosed with epilepsy if they meet one of the three conditions: 1) "two unprovoked or reflex seizures that occur less than 24 hours apart" 2) "one unprovoked or reflex seizure and a probability of further seizures similar to the general recurrence risk (at least 60%) after two unprovoked seizures, occurring over the next 10 years" 3) "a diagnosis of an epilepsy syndrome" (Fisher et al., 2014).

With guidelines set to help with the diagnosis of epilepsy, the ILAE also wanted to formulate criteria for the termination of epilepsy in a patient. The word "cure" is not used when it comes to epilepsy as it implies that a patient's risk for future seizures is the same as the unaffected population. Unfortunately for epileptic patients, this low seizure probability is never achieved. Instead, the ILAE settled on the term "resolved" to reflect the fact that epilepsy does not have to be a lifelong condition (Fisher et al., 2014). A patient's epilepsy is considered resolved if either they "had an age dependent epilepsy syndrome but are now past applicable age or they have remained seizure free for the last 10 years and have been off antiseizure medicines for at least the last five years" (Fisher et al., 2014).

Significance

Epilepsy is a one of the most globally prevalent neurological disorders and it affects people of all ages. Approximately 50 million people worldwide suffer from epilepsy, with an estimated 2.4 million new cases diagnosed every year (WHO, 2018). The number of people suffering from active epilepsy, which WHO describes as patients with "continuing seizures or with the need for treatment," is between four and ten per 1000 people worldwide, with patients living in low or middle income countries accounting for 80% of all epilepsy cases (WHO, 2018).

Epilepsy can arise from a variety of etiologies that can be classified into six major categories: structural, genetic, infectious, metabolic, immune, and unknown (Scheffer et al., 2017). In addition to seizures, epilepsy patients tend to suffer from severe comorbidities including poor bone health, migraine headaches, ADHD, depression and other psychiatric conditions (Seidenberg et al., 2009). In epileptic patients, there is always a risk of mortality from sudden unexpected death in epilepsy (SUDEP). Annually, there are 1.16 SUDEP cases per 1000 epileptic patients, and SUDEP is second only to strokes when it comes to potential life lost from neurological disorders (Thurman et al., 2014).

The social and economic burdens of epilepsy can often be as devastating as the seizures patients suffer from. Epilepsy is a financial burden on both the affected and unaffected, with total direct and indirect costs in the United States being estimated to be approximately $15.5 billion per year (CDC, 2018). Epilepsy also is responsible for 0.6% of the global burden of disease, a measurement that combines years of life loss due to premature death and years spent living in poor health (WHO, 2018).

Voltage-gated Sodium Channels

Structure and Function

Voltage-gated sodium channels play a crucial role in the initiation and propagation of action potentials and the importance of these channels are reflected in the high degree of evolutionary conservation. The mammalian voltage-gated sodium channel is a complex composed of a 260 kDa α subunit usually in association with one or two smaller auxiliary β subunits (β1-β4) ranging from 33-36 kDa in size (Catterall, 2000; Catterall et al., 2005) (Figure 1.1). The sodium channel α subunit protein is composed of four domains (I-IV), with each domain consisting of six transmembrane α-helical segments (S1-S6). It's believed that the S1-S4

segments act as the voltage-sensing component whereas the reentrant P loop and S5-S6 segments form the pore-forming region (Catterall, 2000; Catterall et al., 2005). Fast inactivation is crucial for regulating normal neuronal physiology and it occurs rapidly in voltage-gated sodium channels, usually within milliseconds of the channel opening. The short intracellular linker that connects domains III and IV is a highly conserved region of voltage-gated sodium channels and it is believed to act as the sodium channel inactivation gate (Catterall, 2000). Studies using anti-peptide antibodies against this region were able to delay channel inactivation, whereas targeting other intracellular domains did not repeat this effect (Vassilev et al., 1988, 1989).

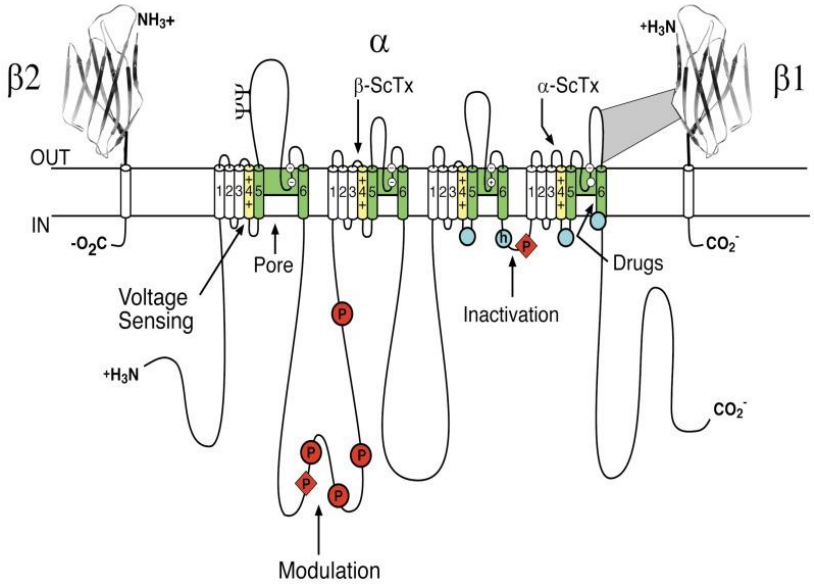

Figure 1.1. The mammalian voltage-gated sodium channel complex. Image from Catterall, 2000.

Voltage-gated Sodium Channel Isoforms and Their Expression

Eleven sodium channel α subunit genes (*SCN1A*-*SCN11A*) have been described to date and these genes map to four paralogous chromosome segments in the human and mouse genome (Plummer and Meisler, 1999). The sodium channel α-subunit genes encode for 10 sodium channel isoforms, $Na_v1.1$-$Na_v1.9$ and Na_x. Though often classified with voltage-gated sodium channels, Na_x is in fact not a voltage sensing channel. Instead, this channel has been shown to play an important role in regulating body fluid sodium level and salt intake behavior (Watanabe et al., 2000).

The various voltage-gated sodium channel isoforms display differential expression throughout the body and localize to various subcellular regions within individual cells. Recent studies have even suggested that voltage-gated sodium channel α-subunits assemble and gate as functional dimers (Clatot et al., 2017). $Na_v1.1$, $Na_v1.2$, $Na_v1.3$, and $Na_v1.6$ have the highest expression in the central nervous system. $Na_v1.1$ is believed to play a crucial role in regulating GABAergic inhibitory interneuron physiology. Homozygous null *Scn1a* mice show premature

death at P15. Heterozygous null mice develop spontaneous seizures and demonstrate a significant reduction in sodium channel current density in inhibitory interneurons. Similar reductions were not seen in excitatory neurons, suggesting $Na_v1.1$ to be predominantly expressed in inhibitory interneurons (Yu et al., 2006).

Contrary to $Na_v1.1$, $Na_v1.2$ is predominantly expressed in excitatory pyramidal neurons. More specifically, $Na_v1.2$ is found in high density in the proximal AIS where it is believed to play an important role in the backpropagation of action potentials into the soma (Hu et al., 2009). During development, high levels of $Na_v1.2$ can also be found at immature nodes of Ranvier. As the nodes mature however $Na_v1.2$ is replaced by $Na_v1.6$ (Boiko et al., 2001; Kaplan et al., 2001). Research seems to suggest that this isoform transformation is dictated by the increase in compact myelin. In *Shiverer* mice, which carry a mutation that leads to severe hypomyelination, $Na_v1.2$ persists along neuronal axons into adulthood (Boiko et al., 2001).

$Na_v1.3$ is often considered a rodent neonatal channel as its expression is highest during this period (Vacher et al., 2008). Studies from adult humans however show widespread expression of $Na_v1.3$, suggesting that the channel may play a more prominent role in mature CNS function in humans (Whitaker et al., 2001b).

Outside of the CNS, voltage-gated sodium channels can be found throughout the mammalian body. $Na_v1.7$, $Na_v1.8$ and $Na_v1.9$ are predominantly expressed in the PNS, $Na_v1.4$ shows highest expression the skeletal muscle tissue and $Na_v1.5$ is considered to be a cardiac voltage-gated sodium channel (Plummer and Meisler, 1999).

Voltage-gated Sodium Channel Isoform $Na_v1.6$

The voltage-gated sodium channel isoform $Na_v1.6$ is encoded by the *SCN8A* sodium channel α subunit gene and it shows wide expression throughout the CNS. Though present throughout the CNS, $Na_v1.6$ has its highest expression in hippocampal pyramidal cells and the granule and purkinje cells of the cerebellum (Schaller and Caldwell, 2000; Vacher et al., 2008). The expression of $Na_v1.6$ in the CNS is relatively delayed compared to other voltage-gated sodium channel isoforms. No detectable levels of $Na_v1.6$ mRNA are observed in E15 and E18 mice. At P1, $Na_v1.6$ mRNA becomes detectable and levels of the transcripts peak between P7-P14 (Schaller and Caldwell, 2000).

On the cellular level, $Na_v1.6$ can be seen in various neuronal regions. $Na_v1.6$ is present in the soma and dendrites of neurons (Caldwell et al., 2000; Krzemien et al., 2000), but the highest expression of the channel is in the distal AIS and mature nodes of Ranvier (Boiko et al., 2001; Kaplan et al., 2001; Hu et al., 2009). At the AIS and nodes of Ranvier, it is believed that $Na_v1.6$ plays a crucial role in the initiation and propagation of action potentials. Unique proexcitatory features of $Na_v1.6$ make the isoform perfect for this role. $Na_v1.6$ has a hyperpolarized $V_{1/2}$ of activation (-35.9 ± 1.5 mV) compared to $Na_v1.2$ (-24.4 ± 1.5 mV) (Rush et al., 2005). Additionally, in the $Na_v1.6$ rich distal AIS, AP threshold is more hyperpolarized (-55.5 ± 0.8 mV) compared to the soma (-42.7 ± 1.1 mV) where expression of the isoform is more sparse (Hu et al., 2009).

$Na_v1.6$ plays a significant role in the generation of persistent and resurgent sodium currents, two subthreshold currents that contribute to repetitive and high frequency AP firing (Raman and Bean, 1997; Mantegazza et al., 1998; Stafstrom, 2007). tsA-201 cells transfected with $Na_v1.6$ show a significantly larger I_{NaP} than cells expressing $Na_v1.2$ (Chen et al., 2008). Additionally, in mice carrying a null mutation for *Scn8a* protein (*Scn8a*^{tg}), both I_{NaP} (31% compared to WT) and I_{NaR} (8-18% compared to WT) are significantly reduced compared to WT mice (Raman et al., 1997).

The importance of $Na_v1.6$ in maintaining neuronal physiology and animal viability is apparent from various studies using knockout and knockdown mutations. Mice homozygous for a null mutation that results in loss of *Scn8a* function present with severe motor defects and death around 3 weeks of age (O'Brien and Meisler, 2013). Mice heterozygous for loss-of-function mutations are viable and display normal motor function but they demonstrate anxiety like behavior and EEG spike-wave discharges typical of absence epilepsy (McKinney et al., 2008; Papale et al., 2009). Underlying these behavioral phenotypes are significant disruptions in neuronal physiology that arise from the loss of $Na_v1.6$ function. Voltage-clamp recordings from dissociated *Scn8a*^{med} CA1 neurons reveal a depolarizing shift in the properties of sodium channel activation in the absence of functional $Na_v1.6$. Additionally, CA1 neurons from *Scn8a*^{med} mice display an increased AP threshold and a significant decrease in AP firing in response to somatic current injections (Royeck et al., 2008) (Figure 1.2). Similar hypoexcitable alterations are also seen in cerebellar Purkinje cells of *Scn8a*^{med} mice. Purkinje neurons from these animals

demonstrate a significant decrease in spontaneous AP firing and AP firing in response to somatic current injection steps (Khaliq et al., 2003).

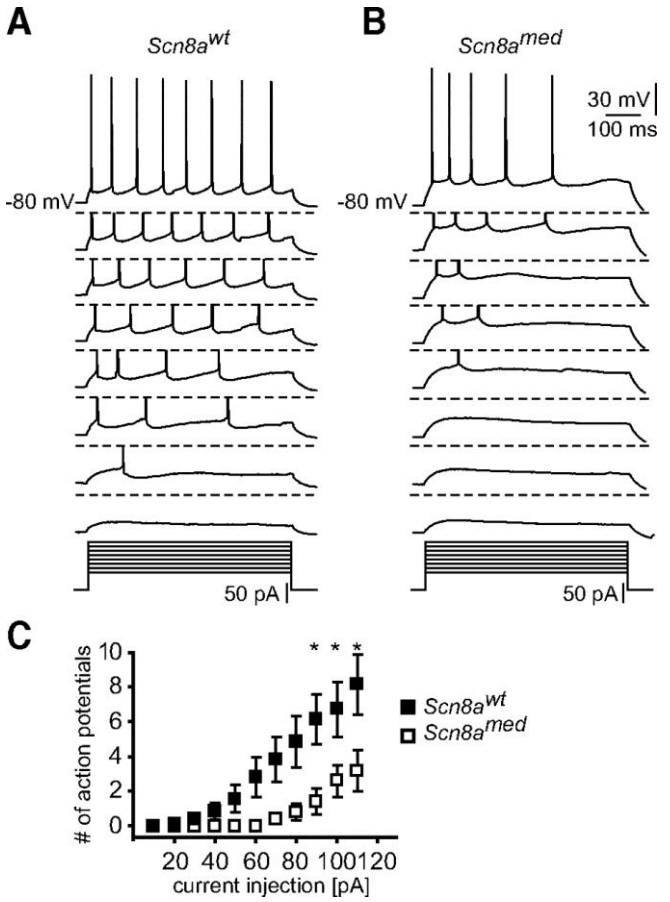

Figure 1.2. CA1 pyramidal cells from *Scn8a*^{med} mice show a decrease in spike gain compared to controls. Image taken from Royeck et al., 2008.

Voltage-gated Sodium Channels In Epilepsy

With voltage-gated sodium channels playing such a crucial role in regulating neuronal physiology, it's apparent to see how changes in channel expression or function can have devastating consequences. Alterations in sodium channel activity are key facilitators of hyperexcitability in a variety of epileptic disorders. The *SCN1A* gene, which encodes for the voltage-gated sodium channel isoform $Na_v1.1$, is the most commonly mutated gene is human epilepsy (Meisler et al., 2010). Loss-of-function mutations in *SCN1A* result in generalized epilepsy with febrile seizures plus (GEFS+) and Dravet syndrome. Dravet syndrome is one of the most widely studied epileptic sodium channelopathies and in this pediatric disease patients suffer from ataxia, intellectual disability and severe, intractable epilepsy (Catterall et al., 2010). While Dravet syndrome is the most studied channelopathy, gain-of-function alterations to voltage-gated sodium channels are more commonly seen in epileptic diseases. Mutations to *SCN2A* that result in proexcitatory alterations to $Na_v1.2$ can lead to the development of benign familial neonatal-infantile seizures (BFNIS) and Ohtahara syndrome (Scalmani et al., 2006; Meisler et al., 2010). Additionally, gain-of-function mutations to *SCN3A* can lead to pediatric cryptogenic partial epilepsy, though instances of these mutations are rare (Holland et al., 2008; Vanoye et al., 2014). While the literature on sodium channels in epilepsy is expansive, here we will focus primarily on two epileptic diseases: early infantile epileptic encephalopathy 13 (EIEE13), which results from gain-of-function mutations to

SCN8A, and temporal lobe epilepsy (TLE), one of the most common forms of adult acquired epilepsy.

Early Infantile Epileptic Encephalopathy 13 (EIEE13)

Background and Significance

Early infantile epileptic encephalopathy 13 (EIEE13), or *SCN8A* encephalopathy, is a severe neurological disorder that is caused predominantly by *de novo* gain-of-function mutations to the *SCN8A* gene. To date, >150 mutations of the *SCN8A* gene have been identified, with up to one-third being recurrent mutations that arise at mutational hotspot CpG dinucleotides (Wagnon et al., 2015a) (Figure 1.3). Seizure onset in *SCN8A* encephalopathy is typically between birth and 18 months of age with a median age of onset being 4 months (Ohba et al., 2014; Larsen et al., 2015; Wagnon and Meisler, 2015). In some cases, in utero seizures have even been reported with mothers describing a drumming like sensation (Singh et al., 2015; McNally et al., 2016). In addition to seizures, *SCN8A* encephalopathy patients suffer from mild to severe intellectual disability and developmental delay that is often exacerbated by uncontrolled seizures (Larsen et al., 2015; Wagnon and Meisler, 2015). Motor impairments ranging from ataxia to quadriplegia are also common in *SCN8A* encephalopathy and 50% of patients are nonambulatory (Ohba et al., 2014; Vaher et al., 2014; Blanchard et al., 2015; Larsen et al., 2015; Singh et al., 2015). Significant alterations in vesicular neurotransmitter release have been observed in a limited number of patients, and it has been hypothesized that these changes may worsen pathogenic phenotypes (Hammer and Encinas, 2017). Sudden unexpected death in epilepsy (SUDEP) has been reported in 10% of cases (Veeramah et al., 2012; Kong et al., 2015; Larsen et al., 2015; Wagnon and Meisler, 2015).

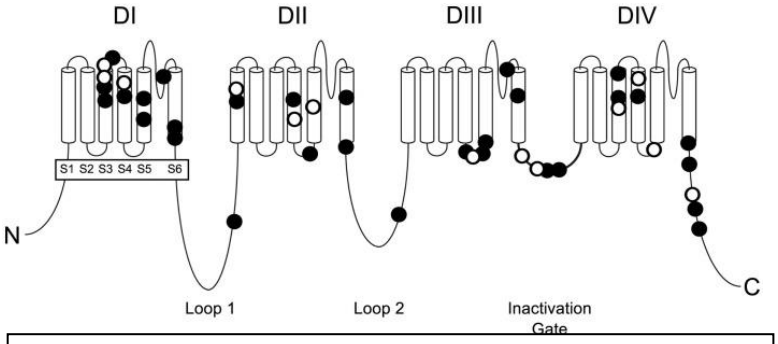

Figure 1.3. Positions of *SCN8A* missense pathogenic mutations in the sodium channel $Na_v1.6$ alpha subunit . Closed circles, mutations observed in a single patient. Open circles, recurrent *SCN8A* mutations. Image taken from Wagnon and Meisler, 2015.

To date, <20 *SCN8A* encephalopathy mutations have been characterized electrophysiologically with a majority displaying gain-of function characteristics, including increased persistent current (I_{NaP}), and impaired channel inactivation (Wagnon and Meisler, 2015; Wagnon et al., 2015a; Barker et al., 2016). The first described *SCN8A* encephalopathy mutation, p.Asn1768Asp (N1768D), was identified in a child who had refractory epilepsy at 6 months of age, intellectual disability, ataxia and SUDEP at 15 years of age (Veeramah et al., 2012). Electrophysiological characterization of the N1768D mutation in transfected cells revealed gain-of-function characteristics including increased I_{NaP}, impaired channel inactivation, and increased resurgent sodium current (I_{NaR}) (Veeramah et al., 2012; Patel et al., 2016). When transfected into cultured hippocampal neurons the N1768D mutation resulted in an increase in spontaneous firing and an increase in the number of APs in response to somatic current injections (Veeramah et al., 2012).

Though *SCN8A* encephalopathy predominantly results from *de novo* gain-of-function mutations, there are instances that contradict this norm. Previous studies have shown that gain-of-function mutations in patients with epilepsy can be inherited from both affected and unaffected parents (Butler et al., 2017). Additionally, electrophysiological characterization of mutations from patients with intellectual disability and no seizures have shown that *de novo* loss-of-function mutations occur in *SCN8A* encephalopathy (Wagnon et al., 2017). These new studies demonstrating variations in inheritance and causality of *SCN8A* mutations will continue to reshape what we know about the disorder and they make the case of *SCN8A* encephalopathy as being a spectrum disorder.

A Mouse Model of SCN8A Encephalopathy

In response to the limitations of studying *SCN8A* encephalopathy in cultured cell lines, a knock-in mouse carrying the N1768D mutation was generated using TALEN technology in combination with a targeting vector (Jones and Meisler, 2014). The production of a *SCN8A* encephalopathy mouse model allows for a better understanding of the disease by making *in vitro* brain slice electrophysiology possible as well as opening the door for an array of *in vivo* experimental assays.

The N1768D mutation is sufficient to induce seizures and SUDEP in mice. Seizures in both heterozygous and homozygous mice are usually brief, tonic-clonic generalized events that

Genotype	Preseizure phenotype	Age at seizure onset	Seizure progression	Terminal events	Median age at death (mean ± SD)	% with SUDEP
D/D	Tremor	3 weeks	No seizures prior to day of SUDEP	Sudden failure of motor function, multiple seizures within 24 h	3 weeks (3 ± 0.6)	100% (9/9)
D/−	Tremor ataxia	8 weeks	Multiple seizures per day	Impaired motor function, cluster of many seizures lasting ~2 h	9 weeks (12 ± 6)	100% (7/7)
D/+	None	8–16 weeks	0–3 Seizures per day	Not observed	14 weeks (15 ± 7)	47% (27/57)

Figure 1.4. Seizure onset and progression in mice carrying the *Scn8a*^{N1768D} mutation. From Wagnon et al., 2015.

last less than 1 minute in duration. Short periods of immobility and rapid breathing lasting 15-45 seconds typically follow seizure activity (Wagnon et al., 2015b). In the pioneering study with these mice, three strains of mutants were generated: mice homozygous for the mutation (D/D), mice heterozygous for the mutation (D/+) and mice hemizygous for the mutation (D/-) (Figure 1.4).

D/D mice are relatively undistinguishable from WT littermates the first 2 weeks of life except for a fine motor tremor that begins shortly after birth. No apparent gross brain malformations can be seen in histological analysis and the levels of $Na_v1.6$ expression does not differ from WT littermates. Around P18-22 motor function in D/D mice begin to decline, initiating with abnormalities in gait and progression to uncoordinated limb movements and the loss of the ability to right themselves. Typically within 24 hours of the start motor impairments, D/D mice experience a single, terminal tonic-clonic seizure. In D/D mice, the median age of death from this ictal event is 3 weeks of age (Wagnon et al., 2015b) (Figure 1.4).

Heterozygous D/+ mice appear phenotypically normal much longer than D/D mice, with no behavioral abnormalities occurring in the first 2-3 months of age. Seizure onset in D/+ mice begins between 8-16 weeks of age and seizures progress to up to 3 per day. SUDEP typically occurs within a month of seizure onset and the median age of death in D/+ mice that have seizures is 4 months of age. Interestingly, seizure penetrance in D/+ mice is incomplete with 50% of mice not showing any seizure phenotype within the first 6 months of age (Wagnon et al., 2015b) (Figure 1.4).

In vivo behavior assays were conducted on D/+ mice to better study the behavioral consequences of the N1768D mutation. D/+ mice show impairment in the rotarod test compared to WT littermates but do not display any deficiencies in the wire-hang test. These results suggest that rotarod deficiency is a result of a loss of coordination rather than a decrease in muscle weakness. In addition to deficits in the rotarod test, D/+ mice also show impairment in social discrimination similar to the reduced social interaction and autistic features seen in the patient carrying the N1768D mutation (Veeramah et al., 2012). Further experiments also revealed that

fear conditioning and open field tests were not significantly different in D/+ mice compared to WT littermates (Wagnon et al., 2015b).

To better understand how the N1768D mutation alters neuronal and cellular function, electrophysiological characterizations have been conducted in both D/+ and D/D mice. Studies to date seem to suggest that brain region specific alterations in excitatory neuron physiology occur in D/+ mice as a result of the N1768D mutation. In D/+ excitatory CA1 neurons, increases in I_{NaP}, spontaneous firing, and AP duration were seen in conjunction with decrease in maximum firing frequency. No changes in inactivation $V_{1/2}$, upstroke velocity, AP amplitude and AP threshold were seen. In the CA3 region of D/+ mice, only increases in I_{NaP} and spontaneous firing were observed in excitatory neurons. Cortical layer 2/3 excitatory neurons from D/+ mice did not display any significant physiological changes (Lopez-Santiago et al., 2017). Interestingly, the most drastic physiological alterations in D/+ neurons to date have been observed in layer II mEC neurons. These neurons show significant increases in I_{NaP}, I_{NaR}, inactivation $V_{1/2}$, synaptically evoked firing, AP amplitude and AP duration. Significant decreases in upstroke velocity and AP threshold were also seen and no changes in spontaneous firing were recorded. D/D layer II mEC neurons have also been electrophysiologically characterized and alterations in these neurons are similar to those observed in D/+ mice, but often with more severe changes (Ottolini et al., 2017).

In addition to studying the physiological properties of mutant neurons, work has also been conducted to discover if a cardiac phenotype exists in D/+ mice. This work stemmed from previous studies examining the *Scnb1* null mouse model of Dravet syndrome, in which these mice exhibit neurocardiac mechanisms of SUDEP (Lopez-Santiago et al., 2007; Lin et al., 2015). Similar to *Scnb1* mice, it has been shown that D/+ mice have cardiac myocyte and parasympathetic neuron hyperexcitability. Specifically, D/+ myocytes showed a prolongation of the early stages of AP repolarization, lowered threshold for AP, and an increased incidence of delayed afterdepolarization (Frasier et al., 2016).

Temporal Lobe Epilepsy

Introduction

Temporal lobe epilepsy (TLE) is one of the most common forms of adult epilepsy and it is characterized by spontaneous recurrent seizures that originate from the temporal lobe. TLE is often considered to be heterogeneous group of disorders in which the temporal lobe is the site of seizure initiation, but the etiologies, age of onset and response to treatments vary among patients (Panayiotopouos, 2005). Seizures onset in patients with TLE can widely vary, but a majority of patient's seizures begin between 4 and 16 years of age (Wieser and ILAE Commission on Neurosurgery of Epilepsy, 2004). Like age of onset, the cause of TLE can vary with each patient. Major causative factors have been identified by the ILAE however and they include: febrile seizures, trauma, hypoxia, and intracranial infection. The majority of these events usually occur before 5 years of age but variation exists among patients (Wieser and ILAE Commission on Neurosurgery of Epilepsy, 2004). TLE can be subdivided into two categories based on where seizures typically originate: mesial temporal lobe epilepsy (mTLE), or lateral temporal lobe epilepsy (lTLE). mTLE accounts for two-thirds of all TLE cases with the hippocampus being the predominant area of seizure onset in these patients (Panayiotopouos, 2005).

Based on the new ILAE guidelines, TLE is considered to have focal onset seizures and TLE itself is considered a combined generalized and focal epilepsy type (Scheffer et al., 2017). In a classic review by Richard Walter, TLE seizures are described as having a common sequence of attack. First the event begins with the patient experiencing an aura, which can range from variety of sensations including a sense of fear to the occurrence of déjà vu. Next, an autonomic phenomenon occurs and may include pilo-erection, pallor, flushing or the sudden urge to void or defecate. Respiratory arrest is also common in TLE seizures and can occur for as long as 40 seconds. Following the autonomic behavior an automatism, our automatic behavior, occurs. Lip smacking is the most commonly reported automatism, but other behaviors such as incoherent speech and behavioral arrest can occur. After the automatism, the seizure will either terminate, with the patient suffering only mild postictal confusion, or the seizure progresses out of the temporal lobe resulting in a generalized event (Walter, 1969).

The first line of treatment for patients suffering from TLE is a variety of antiepileptic drugs (AEDs). Common mechanisms of action for AEDs include inhibiting voltage-gated ion channels expressed on excitatory pyramidal neurons or activating GABAergic inhibitory interneurons. TLE is considered to be poorly controlled by pharmacological interventions and benefits of older drugs versus new ones may be minimal (Androsova et al., 2017). Surgery is

another alternative form of treatment for patients with TLE, especially ones who respond poorly to AEDs. In some cases, surgery may even lead to a better prognosis than medication alone. In a study by Sammuel Wiebe and colleagues, a group of 80 patients were split randomly into two groups. One group was prescribed AEDs for one year while the other was assigned surgery to remove tissue believed to be responsible for the origin of ictal activity. After one year, 58% of patients who received surgery were free of seizures that impaired consciousness while only 8% of patients in the AED group achieved a similar outcome (Wiebe et al., 2001). The best approach to treating TLE may be the combination of surgery and AEDs. In one study examining patients with newly intractable TLE, surgery in conjunction with AEDs resulted in a lower probability of seizures at a two year follow up than patients who relied solely on AEDs (Engel et al., 2012). Despite the variety of treatment options for patients with TLE, up to 30% will not obtain seizure control with AEDs alone (Kwan and Brodie, 2000), making the need for new treatment options paramount.

Circuits of Temporal Lobe Epilepsy

Temporal lobe epilepsy is a disease that disrupts the balance of excitation and inhibition in key neural circuits of the brain. These circuits primarily engage structures of the temporal lobe, most notably the hippocampal formation, and they are crucial for daily functions performed by the brain such as the formation of memories and navigation in space. The hippocampal formation is composed of several morphologically distinct regions: the dentate gyrus (DG), the Cornu Ammonis (CA) areas 1 through 3, and the subiculum. Other regions outside of the hippocampal formation that also contribute significantly to these crucial circuits are the thalamus and the parahippocampal region, which is composed of the presubiculum, the parasubiculum, the entorhinal cortex, the perirhinal cortex and the postrhinal cortex. The major circuits involved in TLE will be briefly reviewed below.

The Trisynaptic Circuit

The trisynaptic circuit is one the oldest studied networks and it begins in the entorhinal cortex where dense projections known as the perforant pathway connect with the dentate gyrus. Most of these fibers originate from layer II of the entorhinal cortex and they “perforate” the

pyramidal layer of the subiculum and hippocampal fissure to connect with the dentate gyrus. At the dentate gyrus perforant path fibers synapse ipsilaterally on the outer two thirds of the molecular layer (Witter, 2007). Other projections from the EC to the hippocampal formation include EC layer II and III neurons that connect with the CA3 region (Witter, 2007). Additionally, projections stemming from EC layer III neurons synapse with the CA1 and subiculum (Witter et al., 1988) and this pathway is often referred to as the temporoammonic pathway.

In the dentate gyrus, the trisynaptic circuit continues with a unidirectional connection to the CA3 region via the mossy fibers. From the CA3, the circuit proceeds along the Schaffer collaterals through the Cornu Ammonis region to the CA1 (van Strien et al., 2009). The circuit concludes with the CA1 projecting the one of two places: the entorhinal cortex or the subiculum. Projections from the CA1 to the entorhinal cortex predominantly terminate in deeper layers of the EC with layer V receiving the most innervation. Layer V neurons have been shown to have excitatory connections onto the projection cells in layer II and III which results in the formation of a recurrent neural network (Witter et al., 2000a). Instead of the EC, the CA1 can also project to the subiculum in a topographical manner. The proximal CA1 connects to the distal subiculum while the distal CA1 projects to the proximal subiculum. Like the CA1, the subiculum also sends projections to the deep layers of the EC, completing the trisynaptic circuit (van Strien et al., 2009).

Thalamolimbic Circuit

While hippocampal circuitry is usually the most commonly studied in TLE, the role of the thalamus is often understated. Multiple nuclei within the thalamus have dense projections to limbic structures involved in TLE and the thalamus may act as a seizure synchronizer. The thalamic midline nucleus reuniens is one region being examined in TLE. Studies have shown that the entorhinal cortex, CA1 and the subiculum all receive input from midline nucleus reuniens (Dolleman-Van Der Weel and Witter, 1996). Specifically, the nucleus reuniens synapse onto layer I and III of the entorhinal cortex, the stratum lacunosum-moleculare of the CA1 and the stratum moleculare of the subiculum. The nucleus reuniens and the entorhinal cortex share similar regions of connectivity in the CA1 and subiculum, which may allow the nucleus reuniens to modulate both the intrinsic connectivity of the EC and the transmission of the

parahippocampal-hippocampal system (Wouterlood et al., 1990; Dolleman-Van Der Weel and Witter, 1996).

The mediodorsal thalamus is another thalamic region that may play an important role in seizure synchronization and propagation. The mediodorsal nucleus receives inputs from a variety of limbic structures, including the subiculum, the amygdala, piriform cortex and the rhinal cortices. The mediodorsal nucleus can in turn integrate information from this variety of inputs and connect them to both the cingulate cortex and orbitofrontal cortex, which the structure has reciprocal connectivity with (Cassidy and Gale, 1998; Bertram, 2009).

The Subiculum

One of the structures that seem to plays a key role in the majority of neuronal circuits involved in TLE is the subiculum. The subiculum is a part of the hippocampal formation and it is a three layered structure that is comprised of a molecular, pyramidal and polymorphic layer. The molecular layer of the subiculum is an extension of the stratum lacunosum-moleculare and stratum radiatum of the CA1. The cell layer of the subiculum is composed primarily of large pyramidal neurons that can be distinguished from the CA1 by their lower density. Also in the pyramidal layer are inhibitory interneurons that can be distinguished from pyramidal cells by their smaller size (Stafstrom, 2005a).

The subiculum acts as an anatomical transition region between hippocampal and parahippocampal regions and it is a hub for dense input and output projections. The subiculum receives inputs from the EC which predominantly originate from layer II/III and can terminate in all layers of the subiculum (O'Mara et al., 2001). Other significant inputs to the subiculum include the CA1 and the midline nucleus reuniens as previously discussed. The subiculum is often considered to be one of the main output regions of the temporal lobe as it innervates a wide variety of targets. Through the trisynaptic circuit, the subiculum sends projections to the deep layers of the EC as well as projections back into the CA1 (Shao and Dudek, 2005). Other regions of the brain that receive input from the subiculum include: the mammillary nuclei, the midline thalamic nuclei, the lateral septal nucleus, ventral hypothalamus, the nucleus accumbens, the rhinal cortices and pre- and parasubiculum (O'Mara et al., 2001; Stafstrom, 2005a).

The subiculum is composed primarily of excitatory pyramidal neurons and a variety of smaller inhibitory interneurons. Pyramidal neurons can be further subdivided into bursting or non-bursting neurons (Figure 1.5). In a study by Staff et al., the physiology of subiculum pyramidal neurons was studied in depth. It was observed that bursting neurons, which Staff and colleagues further subdivided into weak and strong bursting categories, accounted for 68% of pyramidal neurons in the subiculum while the remaining 32% of the neural population were regular spiking neurons (Staff et al., 2000). Bursting neurons tend be located furthest away from the CA1 in the distal subiculum whereas regular spiking neurons are most commonly found near the CA1-subiculum border (Staff et al., 2000). The ionic mechanism behind the bursting phenotype in subiculum neurons is most likely multifaceted. Previous studies suggest that both calcium (Jung et al., 2001; Joksimovic et al., 2017) and sodium (Mattia et al., 1997; Barker et al., 2017) voltage-gated channels contribute significantly to the bursting phenotype. The presence of a large population of bursting neurons in the subiculum is probably linked to the region's role as a major output center of the temporal lobe. Bursting action potentials allow for a higher probability of synaptic release and backpropagation from these events can influence synaptic integration and pre- and postsynaptic coincidence detection in a manner that single action potentials cannot (Staff et al., 2000).

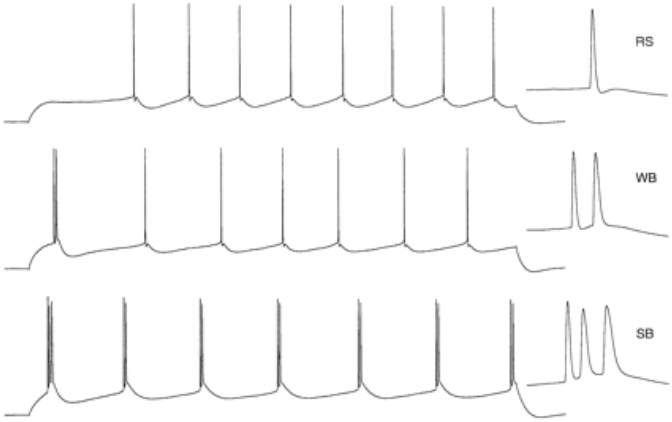

Figure 1.5. AP firing properties of subiculum pyramidal neurons to a 1-s somatic current injection. (RS) Regular spiking, (WB) Weak bursting, (SB) Strong bursting. Image taken from Staff et al., 2000.

In the healthy brain, the subiculum seems to play an important role in spatial navigation and memory retrieval. Previous studies in freely moving rats have shown that subiculum neurons can transmit spatial signals via both bursting and regular spiking neurons (Sharp and Green, 1994). Additionally, human MRI studies show that the subiculum is highly active during memory retrieval tasks (Gabrieli et al., 1997).

The Subiculum in Temporal Lobe Epilepsy

While the DG and CA regions of the hippocampus have been extensively examined in TLE, the subiculum has remained relatively understudied. With a large population of the endogenously bursting neurons and the role of a major output region of the temporal lobe, the subiculum seems prone to epileptogenic induced changes that could contribute significantly to the initiation and propagation of spontaneous seizures. In human TLE patients, subiculum neurons are relatively spared compared to other regions of the hippocampus (Dawodu and Thom, 2005; Alonso-Nanclares et al., 2011), and some studies suggest that subiculum neuronal density may even increase by 48% in sclerotic hippocampal tissue compared to non-sclerotic tissue (Alonso-Nanclares et al., 2011). This neuronal sparing may be limited to excitatory neurons however as another study by Andrioli et al., also observed an increase in neuronal density in human sclerotic hippocampi, but found significant reductions in inhibitory parvalbumun-immunoreactive (PV-IR) interneurons (Andrioli et al., 2007).

In addition to being relatively spared in TLE, it is believed that subiculum neurons become hyperexcitable as a result of epileptogenesis. In post-status epilepticus (SE) rats, significant increases in the number of bursting neurons as well as an increase in post-burst afterdepolarization has been observed (Wellmer et al., 2002), although these changes may be region specific (Knopp et al., 2005). Other studies have shown subiculum bursting neurons from TLE rats fire higher action potentials in response to somatic current injection steps and respond more robustly to synaptic stimulation (Barker et al., 2017).

Driving this subiculum hyperexcitability is proexcitatory alterations in neuronal physiology in TLE. Subiculum pyramidal neurons isolated from patients with intractable TLE show a significant increase in persistent sodium current (I_{NaP}) (Vreugdenhil et al., 2004). Brain slice recordings from TLE animals corroborate these observations, as significant increases in both I_{NaP} and I_{NaR} are seen in subiculum pyramidal neurons from epileptic rats (Barker et al., 2017).

Changes to physiology and neuronal hyperexcitability in the subiculum in TLE allow the structure to play a significant role in the initiation and propagation of spontaneous seizures. Recordings from resected brain tissue from human TLE patients suffering from intractable seizures revealed synchronous spontaneous inter-ictal like epileptiform bursts in the subiculum that were not seen in the hippocampus (Cohen et al., 2002; Wozny et al., 2005). In animal

models of TLE, previous work suggests that the subiculum may often be the sight of seizure initiation. In a study performed by Toyoda et al., looking at which brain region showed the earliest activation in spontaneous seizures, ictal activity was most often seen in the subiculum first, followed by the ventral hippocampus (Toyoda et al., 2013). To further support this observation, it has also been shown that some of the earliest and most prominent increases in preictal interneuron firing rates occur in the subiculum (Toyoda et al., 2015). The previously mentioned decrease in subiculum PV interneurons in TLE may also have significant implications in the initiation of spontaneous seizures. In a study in which PV interneurons from the subiculum of naïve mice were selectively and permanently ablated, 88% of the mice showed clusters of spike-wave discharges and 64% developed spontaneous recurrent seizures (Drexel et al., 2017).

Voltage-gated Sodium Channels in Temporal Lobe Epilepsy

Voltage-gated sodium channels play a significant role in regulating neuronal physiology and proexcitatory changes to these channels in TLE can facilitate neuronal hyperexcitability. In human TLE patients, significant alterations in voltage-gated sodium channel mRNAs are observed in the hippocampus (Whitaker et al., 2001a) and recordings from human TLE subiculum neurons reveal a significant increase in persistent sodium current (Vreugdenhil et al., 2004). Similar proexcitatory alterations to sodium channels are recapitulated in animal models of TLE. Post SE rats demonstrate aberrant sodium channel mRNA expression (Aronica et al., 2001) and proexcitatory changes in sodium channel physiology have been observed in the DG, the CA1, the subiculum and the EC of TLE rats (Ketelaars et al., 2001; Ellerkmann et al., 2003; Hargus et al., 2011; Barker et al., 2017).

The role of the voltage-gated sodium channel isoform $Na_v1.6$ in the development of neuronal hyperexcitability has been well studied since the channel is highly expressed at the AIS (Hu et al., 2009) and plays a significant role in regulating neuronal excitability (Royeck et al., 2008). Additionally, we know gain-of-function mutations to the *SCN8A* gene are sufficient to induce spontaneous seizures in humans and mice (Veeramah et al., 2012; Wagnon et al., 2015b). Proexcitatory alterations to $Na_v1.6$ have been shown to occur only days after SE and these changes can contribute significantly to neuronal hyperexcitability that drives epileptogenesis (Hargus et al., 2013). Increases in $Na_v1.6$ expression are seen in the CA3 of kindled animals

(Blumenfeld et al., 2009) and in the CA regions and EC of TLE rats (Chen et al., 2009; Hargus et al., 2011). The role of $Na_v1.6$ in neuronal hyperexcitability can be delineated using the toxin 4,9-anhydro-tetrodotoxin (4,9-ah-TTX), which has higher affinity for $Na_v1.6$ over other voltage-gated sodium channel isoforms (Rosker et al., 2007). Previous studies have shown that inhibiting $Na_v1.6$ with 4,9-ah-TTX can significantly reduce neuronal hyperexcitability and decrease enhanced persistent and resurgent sodium currents seen in TLE (Hargus et al., 2013; Barker et al., 2017).

$Na_v1.6$'s role in driving neuronal hyperexcitability has made the channel an attractive target for studies looking to prevent or decrease the occurrence of seizures in animal models of TLE. $Na_v1.6$ heterozygote *med*^{tg} mice, which have reduced $Na_v1.6$ expression, display higher afterdischarge thresholds, a slower kindling acquisition rate, and a significant decrease in seizure severity score than WT mice (Blumenfeld et al., 2009). Other studies have shown that reducing levels of $Na_v1.6$ is protective against chemically and genetically induced seizures (Martin et al., 2007; Makinson et al., 2014) and can even extend the lifespan of mice carrying mutations in the *SCN1A* gene (Martin et al., 2007). Inhibiting $Na_v1.6$ may also be a promising option for preventing the development of spontaneous seizures. In mice that had undergone KA induced SE, the administration of shRNA against $Na_v1.6$ resulted in 90% of the animals being seizure free during an 8 week recording period. In sham controls however, all animals went on to develop spontaneous seizures (Wong et al., 2018).

SCN8A Encephalopathy vs. Temporal Lobe Epilepsy

In this section we aim to provide brief comparisons between the genetic *SCN8A* encephalopathy and the acquired temporal lobe epilepsy.

Systems Affected

In S*CN8A* encephalopathy, mutations to the *SCN8A* gene, carried potentially by every cell in the body, give rise to a pathogenic phenotype. $Na_v1.6$ is predominantly expressed in excitatory neurons of the CNS, with high expression levels seen in the hippocampus and cerebellum (Vacher et al., 2008). While *SCN8A* mutations have varying consequences on channel physiology, common mechanisms include proexcitatory shifts in channel inactivation

and increases in persistent sodium current (Veeramah et al., 2012; Wagnon et al., 2015a; Barker et al., 2016). These changes in sodium channel physiology can in turn produce neuronal hyperexcitability and altered AP morphology in neuronal populations throughout the brain (Lopez-Santiago et al., 2017; Ottolini et al., 2017).

While $Na_v1.6$ is believed to play a role predominantly in excitatory neurons, studies suggest that the mutations to the *SCN8A* gene may still be disruptive for other cell types as well. Heterozygous D/+ mice display hyperexcitable cardiac myocytes which may contribute to SUDEP (Frasier et al., 2016). Preliminary data from the Patel lab has also shown that PV interneurons from D/+ mice are hypoexcitable and display aberrant AP morphology (Ottolini et al., unpublished data). Additionally, recent studies showing the role of $Na_v1.6$ in thalamic regulation (Makinson et al., 2017) suggest that mutations to the *SCN8A* gene may directly disrupt more neural circuits than previously hypothesized. No thorough characterization of cerebellar neurons carrying *SCN8A* mutations has been performed to date.

Aberrant physiology, rather than altered gene expression, seems to be the key driver of *SCN8A* encephalopathy. No increases in $Na_v1.6$ staining was observed in the EC of D/+ and D/D mice compared to WT littermates (Ottolini et al., 2017). Additionally, no changes in transcripts encoding for voltage-gated sodium, potassium, and calcium channels are seen in D/+ mice (Sprissler et al., 2016). Information on the sites of seizure initiation and the mechanisms of seizure propagation in *SCN8A* encephalopathy is simply lacking but future studies are being devised that will hopefully provide more insight.

While temporal lobe epilepsy has a relatively more focused region of interest than *SCN8A* encephalopathy, the structures of the limbic system, the mechanisms that produce hyperexcitability are much more complex. TLE produces changes in physiology and expression in a variety of ligand and voltage-gated ion channels, not just $Na_v1.6$. The assortment of changes induced by epileptogenesis can make treatment difficult as it becomes challenging to narrow in on specific therapeutic targets. Cell death and axonal sprouting are another dynamic of hyperexcitability not seen in *SCN8A* encephalopathy. In TLE, substantial neuronal death occurs to the inhibitory interneurons of DG hilus and the pyramidal neurons of the CA1, CA3 and EC layer III neurons (Sloviter and Damiano, 1981; Hargus et al., 2013). Following neuronal death, axonal sprouting occurs in the DG and CA1 and it is believed to produce excitatory feedback connections in key neural circuits (Nadler et al., 1980; Cavazos et al., 2004).

TLE seizures engage multiple neural networks, with the most prominent circuits being previously described. The location and mechanism of seizure initiation in TLE is still unclear. Some studies claim distinct regions of the brain tend to be the most common singular region of seizure onset (Toyoda et al., 2013), while others demonstrate TLE seizures as having a diffuse onset with spontaneous activity arising simultaneously in multiple sites and synchronization occurs in thalamus (Bertram, 1997, 2014).

Pharmacology

Understanding drug efficacy and how drug pharmacology may be altered in disease is crucial for successfully treating patients with epilepsy. In *SCN8A* encephalopathy, there have been no published guidelines for the treatment of the disorder. Treatment tends to focus on seizure control through drug polytherapy as uncontrolled seizures put patients at higher risk for permanent injury and SUDEP (Hammer et al., 2016). Refractory epilepsy is unfortunately common in many *SCN8A* patients but extended seizure free periods are attainable for some (Larsen et al., 2015). Studies suggest that sodium channel blockers may be the best option for patients suffering with *SCN8A* encephalopathy (Boerma et al., 2015; Larsen et al., 2015; Wagnon et al., 2015a). Disruption in sodium channel inactivation is a common pathogenic mechanism across multiple *SCN8A* mutations, and drugs that have higher affinity for the inactivated state may be advantageous in treating patients. Phenytoin is one such drug that is believed to have higher affinity for the inactivated state (Kuo and Bean, 1994). Studies have shown that phenytoin is effective in attenuating proexcitatory alterations in mutant channel physiology (Barker et al., 2016) and it has been demonstrated that the drug can provide improved seizure control for *SCN8A* encephalopathy patients (Boerma et al., 2015). While efficacy with a variety of drugs has been demonstrated in *SCN8A* encephalopathy patients, levetiracetam has been reported by multiple families to be ineffective and it may even increase seizure frequency (Hammer et al., 2016). Currently, no studies have been published demonstrating altered drug pharmacology in mutant $Na_v1.6$ channels.

Resistance to antiepileptic drugs in TLE is relatively common and up to 30% of patients cannot achieve seizure control with AEDs alone (Kwan and Brodie, 2000). Recent studies have suggested that the sodium channel blockers carbamazepine and valproate may be the most promising AED options for patients suffering from TLE but this result may not be reflective of

the entire patient population (Androsova et al., 2017). One of the reasons AEDs may be relatively ineffective in TLE patients is altered pharmacology that arises from epileptogenesis. In a kindling model of TLE, the hypoexcitatory effects of carbamazepine are reduced acutely in kindled animals compared to controls. Additionally, there is a significant increase in the EC_{50} when treating cells from kindled animals compared to controls (Vreugdenhil and Wadman, 1999). In experiments utilizing brain tissue from carbamazepine resistant TLE patients, the use-dependent block typically produced by carbamazepine was significantly diminished (Remy et al., 2003a). Additionally, it has been observed that the effects of carbamazepine on the recovery from inactivation are attenuated in TLE animals (Schaub et al., 2007).

Diminished efficacy is not just seen with carbamazepine as other studies have shown that the ability of phenytoin and lamotrigine to produce tonic block is significantly diminished in epileptic cells compared to controls (Remy et al., 2003b). Interestingly in studies using kindling animal models and cells from epileptic patients, the effects of valproate remain relatively unchanged (Vreugdenhil et al., 1998; Vreugdenhil and Wadman, 1999).

Overview of Dissertation Data

The following chapters will show data demonstrating how proexcitatory alterations to the voltage-gated sodium channel $Na_v1.6$ can lead to neuronal hyperexcitability in two separate epilepsy syndromes: *SCN8A* encephalopathy and TLE. In Chapter III, we electrophysiologically characterize both gain-of-function and loss-function mutations to the *SCN8A* gene. This work is a significant contribution to the field as we were the first to characterize recurrent *SCN8A* encephalopathy mutations that account for 20% of all mutations known to date. We hope our work in Chapter III leads to a better understanding of these recurrent mutations that enables more effective treatments for patients. Also in Chapter III, we are the first group to describe two loss-of-function *SCN8A* mutations in patients with intellectual disability but no epilepsy. This work is significant because it demonstrates that varying mutations to the *SCN8A* gene can produce a phenotypic spectrum in patients. At the conclusion of Chapter III, we explore the efficacy of the sodium channel blocker phenytoin on a novel gain-of-function *SCN8A* mutation. A significant portion of *SCN8A* patients suffer from intractable epilepsy and it remains unclear which AEDs are most efficacious in these patients. Our work is a noteworthy contribution to the field as it

demonstrates that phenytoin diminishes the proexcitatory alterations seen in a gain-of-function mutation. More importantly, this work makes a stronger case for sodium channel blockers, like phenytoin, as a first option for treating patients with *SCN8A* encephalopathy.

In Chapter IV, we electrophysiologically characterize mEC layer II neurons from a mouse model of *SCN8A* encephalopathy. This work provides novel data to the field as we are the one of the first groups to study neuronal physiology in brain slices from animals carrying a *SCN8A* mutation. This work is significant because it expands our knowledge of *SCN8A* encephalopathy beyond cultured cell *in vitro* experiments. Additionally, this data opens the door for future, more advanced *in vitro* and *in vivo* experiments using this model that will vastly improve our knowledge of the disease.

In Chapter V, we study how proexcitatory alterations to sodium channel physiology contribute to subiculum hyperexcitability in TLE. Additionally, we show that blocking $Na_v1.6$ significantly reduces subiculum neuron hyperexcitability. This work is a significant contribution to the field as it is one the first to directly implicate $Na_v1.6$ in facilitating neuronal hyperexcitability in the subiculum. The subiculum remains a vastly understudied region of the hippocampus in TLE and work demonstrating mechanisms of hyperexcitability in the subiculum is highly novel.

Overall, the data presented in these chapters describes why studying alterations to $Na_v1.6$ is applicable in multiple epileptic disorders. We believe this work is significant to the epilepsy field not only because it advances our knowledge of the mechanisms of disease, but it makes a strong argument for $Na_v1.6$ as a promising target for future antiepileptic drugs. In TLE 30% of patients do not respond to currently available AEDs, a number that has not changed significantly in decades. In *SCN8A* encephalopathy, data describing the efficacy of AEDs in patients is sparse, but it is believed that long term complete seizure control is uncommon. For this reason, research that leads to the eventual development of more efficacious AEDs is crucial to the epilepsy field and that is what we hope we have provided in the data presented in this dissertation.

II. General Methods

Cell Culture

DRG-neuron–derived ND7/23 cells (Sigma Aldrich, St. Louis, MO, USA) were grown in a humidified atmosphere of 5% CO_2 and 95% air at 37°C in Dulbecco's Modified Eagle's Medium (DMEM, 1X) supplemented with 10% fetal bovine serum (FBS), non-essential amino acids (NEAA) and sodium pyruvate. Cells were plated onto Petri dishes 48 h prior to transfection and transfected for 5 h in non-supplemented DMEM using Lipofectamine 3000 according to the manufacturer's instruction (Life Technologies, Carlsbad, CA, USA) with 5 μg of $Na_v1.6$ α subunit cDNA and 0.5 μg of the fluorescent m-Venus bioreporter. Electrophysiological recordings of fluorescent cells were made 48 h after transfection.

Voltage Clamp Electrophysiology

Recordings were carried out in the presence of 500 nM tetrodotoxin (TTX) to block endogenous sodium currents in the neuron-derived ND7/23 cells. Currents were recorded using the whole-cell configuration of the patch clamp recording technique. Currents were amplified and low-pass filtered (2 kHz) and sampled at 33 kHz. The intracellular recording solution contained (in mM): 140 CsF, 2 $MgCl_2$, 1 EGTA, 10 HEPES, 4 Na_2ATP, 0.3 NaGTP (pH adjusted to 7.2 with CsOH, osmolarity adjusted to 300 mosM with sucrose). Cultured ND7/23 cells were bathed in solution containing (in mM): 130 NaCl, 3 KCl, 1 $CaCl_2$, 5 $MgCl_2$, 0.1 $CdCl_2$, 10 HEPES, 30 TEA (pH adjusted to 7.4 with NaOH, osmolarity adjusted to 310 mosM with sucrose). Experiments were performed at room temperature (20–22°C). After establishing the whole cell configuration, a minimum series resistance compensation of 75% was applied. Capacitive and leak currents were subtracted using the P/N-4 protocol for all experiments, except steady-state inactivation protocols. The current-voltage relationship was determined using a 100 ms voltage pulse from −80 to +70 mV in steps of 5 mV from a holding potential of −120 mV at 2 sec intervals. Conductance as a function of voltage was derived from the current-voltage relationship using the equation $g = I_{Na}/(V - E_{Na})$, where V is the test potential and E_{Na} is the reversal potential. The voltage dependence of activation data were fitted by a Boltzmann function:

$$y = 1/(1 + \exp[(V - V_{1/2}/k)]$$

where y is the normalized conductance (g/g_{max}) or the normalized current for activation and inactivation respectively, $V_{1/2}$ is voltage of half-maximal activation or inactivation, and k is the slope factor. Decays of macroscopic currents were fitted to a single exponential function and time constants were determined using the equation:

$$y = A_1 [1 - \exp(-t/\tau_1)] - \text{single}$$

where A_1 is the coefficient for the exponential, t is time (ms), and τ_1 is the time constant. For steady-state inactivation, neurons were held at −120 mV and test potentials from −115 mV to −10 mV for 500 ms at 5 mV increments were applied. The second pulse to −10 mV for 40 ms was used to assess channel availability. Correction for passive and leak currents was achieved by subtracting the last sweep with the greatest depolarizing potential (−10 mV) since this sweep displays no sodium channel current. Currents during the second pulse were normalized for each cell with the largest current as 1.0 and fit to the Boltzmann function. Deactivation was estimated from current decay, using a 0.5 ms short depolarizing pulse to −10 mV followed by a 50 ms repolarizing pulse to potentials ranging from −40 to −120 mV at 5 mV increments. Deactivation kinetics was determined by fitting decaying currents with a single exponential function. For recovery from inactivation, cells were held at −120 mV and depolarized to a test potential of 0 mV for 1 sec to inactivate Na channels. Recovery was determined at times between 1 msec and 60 sec at a test potential of -90 mV. A 40 msec pulse to -10 mV was subsequently applied to assess the extent of channel recovery. For each cell, current amplitudes during this test pulse were normalized so that the largest current during the conditioning potential was 1.0. Data were fit to a double exponential function:

$$y = A_1 (1 - \exp[-t/T_1]) + A_2 (1 - \exp[-t/T_2])$$

where A_1 and A_2 are the coefficients for the fast and slow exponentials, t is the time (in msec), and T_1 and T_2 are the fast and slow time constants, respectively.

Coimmunoprecipitation and Western Blotting

HEK 293 cells were transfected with 3 μg of cDNA encoding the C-terminal domain of $Na_v1.6$ and 3 μg of the test construct. Cell extracts were prepared and immunoprecipitated as described previously (O'Brien et al., 2012). Cells were lysed in 1 mL of buffer containing 20 mmol/L Tris-HCl, pH 7.5, 137 mmol/L NaCl, and 1% NP-40 with protease inhibitors (Roche complete mini, EDTA-free, Indianapolis, IN, USA). Lysates were incubated with 20 μL anti-HA antibody-coated agarose beads (sc-7392AC, Santa Cruz Biotechnology, Santa Cruz, CA, USA) overnight at 4°C. Immune complexes on the beads were washed four times and eluted by boiling in 2X electrophoresis sample buffer at 95°C for 5 min. Western blotting was carried out as described previously (Wagnon et al., 2015b). Blots were immunostained with rabbit polyclonal anti-HA (H6908, Sigma Aldrich), rabbit polyclonal anti-GFP (G1544, Sigma Aldrich), rabbit polyclonal anti-myc (C3956, Sigma Aldrich), or rabbit polyclonal anti-Gb2 (sc-380, Santa Cruz Biotechnology).

Brain Slice Preparation and AP Recordings

Horizontal brain slices (300 m) were prepared from both rats and mice in a similar manner. Rodents were anesthesized with isoflurane, decapitated, and brains rapidly removed and placed in chilled (4°C) artificial CSF (ACSF) containing the following (in mM): 125 NaCl, 2.5 KCl, 1.25 NaH_2PO_4, 2 $CaCl_2$, 1 $MgCl_2$, 0.5 L-ascorbic acid, 10 glucose, 25 $NaHCO_3$, and 2 pyruvate oxygenated with 95% O_2 and 5% CO_2. Slices were prepared using a Vibratome 1000 Plus (Vibratome), transferred to a chamber containing oxygenated ACSF, incubated at 37°C for 35 min, and then stored at room temperature. For recordings, slices were held in a small chamber superfused with heated (32°C) oxygenated ACSF. mEC layer II or subiculum pyramidal neurons were visually identified by infrared video microscopy (Hamamatsu) using a Zeiss Axioscope microscope. Whole-cell voltage and current-clamp recordings were performed using an Axopatch 700B amplifier (Molecular Devices, pCLAMP 10 software) and a Digidata 1322A (Molecular Devices). Electrodes were fabricated from borosilicate glass using a Brown-Flaming puller (Model P97; Sutter Instruments) and had resistances of 3.5– 4.0 mΩ when filled with an intracellular recording solution containing the following (in mM): 120 K-gluconate, 10 NaCl, 2 $MgCl_2$, 0.5 K_2EGTA, 10 HEPES, 4 Na_2ATP, 0.3 NaGTP, pH adjusted to 7.2 with KOH. Currents were amplified, low-pass filtered (2 kHz) and sampled at 33 kHz. APs were evoked with a series of current injection steps from -20 pA to 470 pA in 10 pA steps for 300 ms at 5 s

interpulse intervals. In some experiments, a brief, 4 ms depolarizing current pulse was used to evoke APs. To standardize our tests, the resting membrane potential (RMP) was recorded and then maintained at -65 mV by injection of DC current. Cell input resistance (R_i) was calculated by dividing the steady-state voltage response evoked by varying current injections ($\Delta V/\Delta I$) from -20 pA until the current pulse just before that which evoked an AP. Data points were then fit with a linear line to determine R_i values. Threshold was determined as the voltage at which the slope of the AP exceeded ≥20 V/s. AP amplitudes were measured from threshold to the AP peak. AP duration (APD) was measured from threshold to the point at which the AP returned to the same potential. APD_{50} and APD_{90} were determined from this duration. Upstroke velocity was determined from phase plots using the maximum of the first derivative (dV/dt). In some experiments, APs were evoked using a bipolar platinum iridium stimulating electrode (WPI) placed 1 mm distant from the region that was being recorded. A 400 μs stimulus of varying current amplitude (1 to 3.2 mA) was applied every 15 s via a digital stimulator (Digitimer). To evoke APs consistently, the stimulus amplitude was increased until there were no failures in spike initiation (1T). Duration of the evoked somatic response evoked by either electrical stimulation or via short depolarizing current pulses was determined as the interval between the start of the deviation from the RMP to the point at which the response returned to the RMP.

Brain Slice Na Channel Electrophysiology

All Na channel current recordings, except for persistent Na current (I_{NaP}) and resurgent Na current (I_{NaR}), were recorded using the outside-out recording configuration of the patch-clamp recording technique. Currents were amplified, low-pass filtered (2 kHz), and sampled at 33 kHz. Glass pipettes had resistance of 1.8 –2.5 mΩ when filled with the following electrode solution (in mM): 140 CsF, 2 $MgCl_2$, 1 EGTA, 10 HEPES, 4 Na_2ATP, and 0.3 NaGTP, pH adjusted to 7.3 with CsOH, osmolarity adjusted to 310 M with sucrose. Outside-out patches were superfused with solution containing the following (in mM): 150 NaCl, 2.5 KCl, 2 $CaCl_2$, 1 $MgCl_2$, 1.25 NaH_2PO_4, 0.5 L-ascorbic acid, 2 pyruvate, 10 glucose, 25 $NaHCO_3$, pH adjusted by bubbling 95% O_2 and 5% CO_2, osmolarity adjusted to 320 mM with sucrose. All experiments were performed at 32°C. Capacitive and leak currents were subtracted using the P/N-4 protocol. The current–voltage (I–V) relationship was determined using a 100 ms voltage pulse from -80 to +40 mV in steps of 5 mV from a holding potential of -120 mV at 2 s intervals. Conductance as a

function of voltage was derived from the I–V relationship and fitted by a Boltzmann function as described previously in this section.

For steady-state inactivation, neurons were held at -120 mV and test potentials from -115 mV to -10 mV for 500 ms at 5 mV increments were applied. The second pulse to -10 mV for 40 ms was used to assess channel availability. Currents during the second pulse were normalized for each cell with the largest current as 1.0 and fit to the Boltzmann function.

I_{NaP} was determined in brain slice preparations using voltage ramps from -100 mV to -10 mV at a rate of 65 mV/s. I_{NaP} was recorded in bath solution containing the following (in mM): 30 NaCl, 120 TEA-Cl, 10 $NaHCO_3$, 1.6 $CaCl_2$, 2 $MgCl_2$, 0.2 $CdCl_2$, and 5 4-AP, 15 glucose, pH 7.4 when oxygenated with 95% O_2 and 5% CO_2; temperature 32°C, and a pipette solution containing the following (in mM): 140 CsF, 2 $MgCl_2$, 1 EGTA, 10 HEPES, 4 Na_2ATP, and 0.3 NaGTP, pH adjusted to 7.3 with CsOH, osmolarity adjusted to 310 mM with sucrose. Ramp voltage recordings displayed an inward current that was referred to as I_{NaP}. To determine the peak I_{NaP} current, voltage ramp protocols were repeated in the presence of TTX (1 μM). Traces obtained in the presence of TTX were subtracted from those obtained in its absence. TTX was reconstituted in ACSF.

I_{NaR} was also recorded in brain slice preparations using a bath solution containing the following (in mM): 100 NaCl, 26 $NaHCO_3$, 19.5 TEA-Cl, 3 KCl, 2 $MgCl_2$, 2 $CaCl_2$, 2 $BaCl_2$, 0.1 $CdCl_2$, 4 4-AP, and 10 glucose, pH 7.4 when oxygenated with 95% O_2 and 5% CO_2; temperature 32°C, using the same pipette solution as that for recording I_{NaP}. Neurons were held at -100 mV and depolarized to +20 mV for 20 ms, followed by either a single repolarizing step to -30 mV for 100 ms to determine the peak I_{NaR} or a series of repolarizing steps from -100 mV to -10 mV to determine the voltage dependence of I_{NaR}. Protocols were again repeated in the presence of TTX (1 μM) to determine I_{NaR} current amplitudes and gating.

Data Analysis

Electrophysiology data analysis was performed using Clampfit software version 10 (Molecular Devices) and MATLAB (The MathWorks). All values represent means ± SEM. Statistical significance was determined by using one of the following statistical tests: a Student's t-test, a Student's t-test with Welch's correction, a standard one-way or two-way ANOVA

followed by Tukey's or Dunn's *post hoc* test for parametric data or the Rank Sum test for non-parametric data (GraphPad Prism 6).

III. Pathogenic Mechanisms of *de novo SCN8A* Mutations in a Rare Genetic Channelopathy

IIIa. Pathogenic Mechanisms of Recurrent Gain-of-Function Mutations of *SCN8A* in Epileptic Encephalopathy.

Rationale

In Chapter IIIa, we electrophysiologically characterize 4 novel gain-of-function mutations that occur at the CpG dinucleotide mutation hotspots arginine 1617 and arginine 1872. Mutations at these two residues are recurrent, and account for a significant number of all EIEE13 mutations discovered. The work in Chapter IIIa is a significant contribution to the field because to date <20 *SCN8A* mutations have been physiologically characterized. The better we understand the mechanisms in which these mutations cause neuronal hyperexcitability and seizures the more likely we are to implement or develop more efficacious treatments for patients.

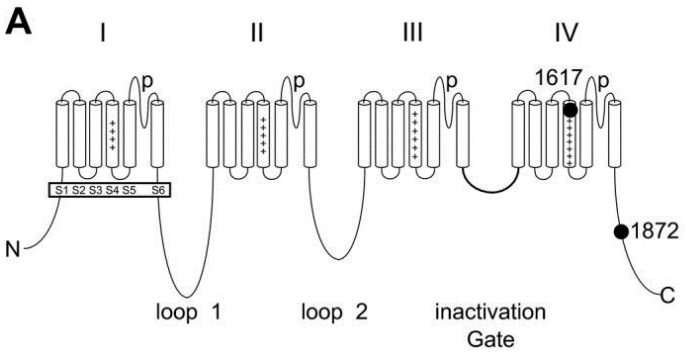

B

	Arg1617	Total #	Arg1872	Total #
Reference codon sequence	CGA (Arg)	-	CGG (Arg)	-
Coding strand mutation	TGA (Stop)	0	TGG (Trp)	4
Noncoding strand mutation	CAA (Gln)	5	CAG (Gln)	4
Other		-	CTG (Leu)	2
	Total	5		10

Figure IIIa.1. Recurrent mutations of arginine residues 1617 and 1872 in *SCN8A*. (A) Four-domain structures of the voltage-gated sodium channel α subunit. The positions of the recurrently mutated residues Arg1617 (the outermost charged residue in the S4 transmembrane segment of domain IV) and Arg1872 (near the middle of the cytoplasmic C-terminal domain) are shown. (B) CpG mutation hot spots in the codons for Arg1617 and Arg1872.

Introduction

The two amino acid residues, Arg1617 and Arg1872, are the sites of mutation in 20% of EIEE13 patients. Arg1617 is located in the voltage-responsive S4 transmembrane segment of domain IV (Figure IIIa.1A). The substitution p.Arg1617Gln has occurred in five unrelated individuals (Rauch et al., 2012; Ohba et al., 2014; Dyment et al., 2015; Kong et al., 2015; Larsen et al., 2015). Arg1872 is located in the cytoplasmic C-terminal domain (Figure IIIa.1A). Two

missense mutations of Arg1872 were described in seven patients (Carvill et al., 2013; Ohba et al., 2014; Larsen et al., 2015; Takahashi et al., 2015) and we describe a third substitution in two patients, making this the most frequently mutated residue. The CpG dinucleotides in the codons for Arg1617 and Arg1872 are mutational hotspots (Figure IIIa.1B). Recurrence in unrelated patients and absence from unaffected individuals (http:// exac.broadinstitute.org) provides strong evidence that these mutations are pathogenic. Our data demonstrate that these mutations result in impaired channel inactivation that underlies neuronal hyperexcitability and seizures.

Methods

Clinical Exome Sequencing

The c.5615G>T mutation (p.Arg1872Leu) in Case 1 was identified by whole exome sequencing at the Genomic Medicine Institute at the Cleveland Clinic (Cleveland, OH, USA). The c.5615G>T mutation (p.Arg1872Leu) in Case 2 was identified by whole exome sequencing at the Johns Hopkins Medical Institute (Baltimore, MD, USA). The c.5615G>A mutation (p.Arg1872Gln) in Case 3 was identified in the clinical exome sequencing laboratory at Radboud University (Nijmegen, the Netherlands).

Standard Protocol Approvals, Registrations, and Patient Consents

An institutional review board (IRB) approval was obtained and the parent or legal guardian of each patient gave informed consent.

Site-Directed Mutagenesis of the $Na_v1.6$ cDNA and C-terminal Constructs

The amino acid substitutions p.Arg1617Gln, p.Arg1872Leu, and p.Arg1872Trp were introduced into the tetrodotoxin (TTX)-resistant derivative of the full length $Na_v1.6$ cDNA clone (Herzog et al., 2003) as described previously (Veeramah et al., 2012). Site-directed mutagenesis was carried out with the QuikChange II XL kit (Agilent Technologies, Santa Clara, CA, USA). The entire 6-kb open reading frame was sequenced to confirm the absence of other mutations. The pHA-$Na_v1.6$-CT cDNA construct containing the 213 amino acid C-terminal domain of $Na_v1.6$ with an N-terminal HA epitope tag (Laezza et al., 2009) was kindly provided by Dr.

David Ornitz, Washington University. The substitution p.Arg1872Trp was introduced as above and the open reading frame was completely sequenced.

Plasmids Encoding Sodium Channel– Interacting Proteins

The sodium channel β subunit cDNA construct pNa_vβ1- EYFP was kindly provided by Dr. Jeanne Nerbonne (Marionneau et al., 2012). The fibroblast growth factor 14 cDNA construct pFGF14- 1b-myc tag was a gift from Dr. David Ornitz (Laezza et al., 2009). Plasmids p$G\beta_2$IRES-YFP and p$G\gamma_3$IRES-cyan encoding the G-protein subunits $G\beta_2$ and $G\gamma_3$ were kindly provided by Dr. Massimo Mantegazza (Mantegazza et al., 2005).

Cell Culture

Please reference Chapter II: General Methods

Electrophysiology

Please reference Chapter II: General Methods

Coimmunoprecipitation and Western Blotting

Please reference Chapter II: General Methods

Results

Clinical features of three patients with mutations of arginine 1872

The clinical features of three new cases are summarized in Table IIIa.1. All three patients were born after full-term pregnancies. Clinical exome sequencing identified the heterozygous mutation c.5615G>T resulting in the novel amino acid substitution p.Arg1872Leu in patients 1 and 2. Patient 3 carried the *SCN8A* mutation c.5615G>A resulting in the amino acid substitution p.Arg1872Gln. None of the mutations were present in either parent, demonstrating *de novo* origin. The features of these patients are consistent with the recently described clinical spectrum of *SCN8A* encephalopathy (Larsen et al., 2015) Two patients exhibited very early onset at 2 and

6 weeks of age. Sodium channel blockers were partially effective (Table IIIa.1). Detailed clinical histories are provided as an Appendix.

Patient (sex)	1 (F)	2 (F)	3 (M)
Amino acid substitution	p.Arg1872Leu	p.Arg1872Leu	p.Arg1872Gln
Seizure onset	2 weeks	6 weeks	4 months
Current age	17 years	1.5 years	2 years
Seizure types	GTC	GTC with apnea	GTC, A, T with bradycardia, SE
Development and motor abnormalities	Walking at 12-15 months, then regression with hypotonia progressing to hypertonia and quadriplegia	Sat 12 months, hypotonia	Speech arrest 10 months, sat 13 months, walked 16 months
Intellectual disability	Severe	Moderate	Severe
EEG	Generalized slowing, severe diffuse encephalopathy	Normal	Diffuse encephalopathy
MRI	Cerebella and cerebral atrophy	Normal	Bilateral flat insular cortex
Drug response	PHT and VNS partially effective	TPM and LEV temporarily effective, OXC, LTG, VPA, and CLN effective	ZNS and LEV temporarily effective, PHT and LEV effective

A, absence; CLN, clonazepam; GTC, generalized tonic-clonic; LEV, levetiracetam; LTG, lamotrigine; OXC, oxcarbazepine; PHT, phenytoin; SE, status epilepticus; T, tonic, TPM, topiramate; VNS, vagus nerve stimulator; VPA, valproate; ZNS, zonisamide.

Table IIIa.1. Clinical features of three new patients with amino acid substitution of arginine residue 1872.

Functional effects of mutations in arginine residue 1872

Arginine residue 1872 is located near the center of the cytoplasmic C-terminal domain of $Na_v1.6$ (Figure IIIa.1A). This site was implicated in direct interaction with the inactivation gate of the channel, mediated by interaction between positively and negatively charged residues (Lee and Goldin, 2008; Nguyen and Goldin, 2010). Loss of the positive charge of arginine residue 1872 is therefore predicted to impair channel inactivation.

Patient mutations substituting leucine, glutamine, or tryptophan for arginine 1872 were introduced into the full-length $Na_v1.6$ cDNA, which was transfected into the neuron-derived cell line ND7/23. Representative currents from ND7/23 cells transfected with wild-type (WT) and mutant $Na_v1.6$ channels are shown in Figure IIIa.2A. Peak current density was elevated for p.Arg1872Trp, but was not significantly changed for p.Arg1872Leu or p.Arg1872Gln (Figure IIIa.2B, Table IIIa.2). To determine the kinetics of open state inactivation, macroscopic current decay was fit to single exponential functions and the fast time constant (τfast) was plotted as a function of voltage. Transition from open state to the inactivated state was significantly delayed by all three mutations (Figure IIIa.2C), consistent with prediction. The slowing of fast

inactivation is evident when the peaks of the current traces are aligned so that inactivation kinetics can be compared directly (Figure IIIa.2D).

At 100 msec after stimulus, p.Arg1872Leu exhibited elevated persistent current normalized to the peak of the macroscopic current ($I_{persistent}/I_{peak}$) (Figure IIIa.2E, Table IIIa.2). Ramp currents evoked using a slow ramp stimulus did not differ from WT for any of the mutants (data not shown).

Analysis of steady-state kinetics demonstrates that p.Arg1872Leu and p.Arg1872Gln cause a small but significant hyperpolarizing shift in the voltage dependence of activation ($P < 0.05$) (Figure IIIa.2F, Table IIIa.2). In addition, p.Arg1872Gln caused a depolarizing shift in steady-state inactivation (Figure IIIa.2G, Table IIIa.2). The values for the slope (k) were unchanged.

Functional effects of the recurrent mutation p.Arg1617Gln

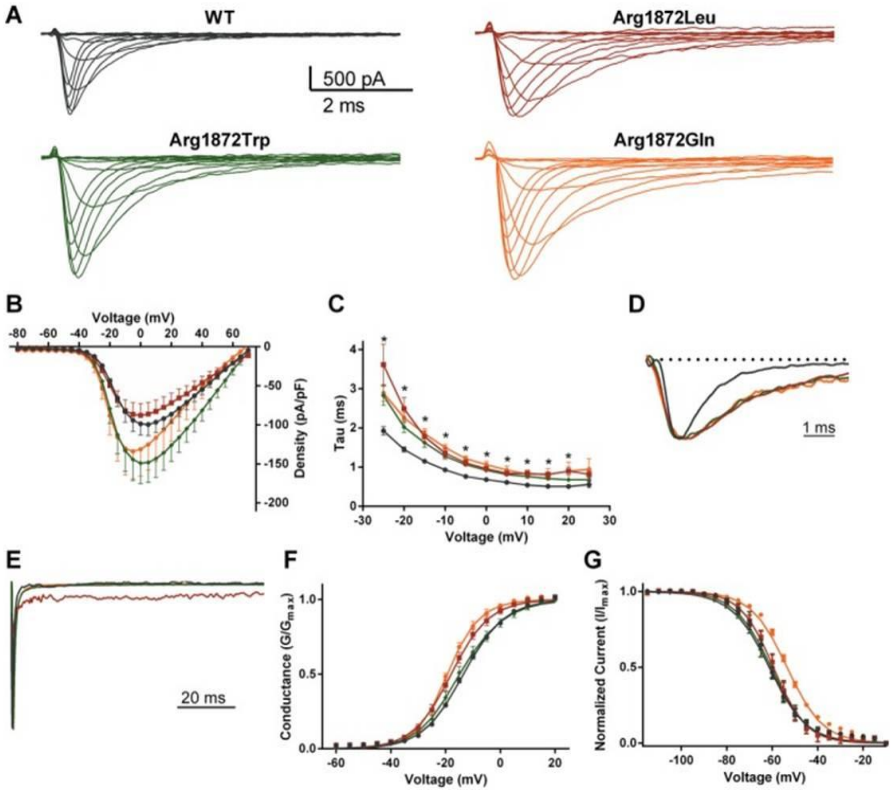

Figure IIIa.2. Biophysical effects of missense mutations at residue Arg1872 in $Na_v1.6$. (A) Representative traces of families of Na currents from ND7/23 cells transfected with the indicated $Na_v1.6$ cDNAs. (B) Averaged current–voltage (I-V) relation for cells expressing WT and mutant $Na_v1.6$. Peak currents were normalized to cell capacitance. (C) Average fast time constant obtained from single exponential fits to macroscopic current decays as a function of voltage (mV). (D) Representative traces of normalized currents evoked by a −20 mV stimulus from a holding potential of −120 mV illustrate delays in macroscopic current decay. (E) Representative normalized current traces recorded during a 100-msec depolarizing pulse from −120 mV to 0 mV illustrating the presence of elevated persistent sodium current for p.Arg1872Leu. (F) Voltage dependence of channel activation. (G) Voltage dependence of steady-state inactivation. Smooth lines correspond to the least squares fit when average data were fit to a single Boltzmann equation. Data are mean ± SEM. Statistical significance: *$P < 0.05$. Black, wild type; red, p.Arg1872Leu; orange, p.Arg1872Gln; green, p.Arg1872Trp.

Arginine residue 1617 is the outermost positively charged residue in the voltage-responsive transmembrane segment DIV-S4 and is implicated in coupling of channel activation with subsequent inactivation.

Representative currents from ND7/23 cells transfected with the p.Arg1617Gln mutant of $Na_v1.6$ are shown in Figure IIIa.3A. Peak current densities for p.Arg1617Gln were not different from WT (Figure IIIa.3B). A profound change in the kinetics of transition from open state to the inactivated state was observed. At voltages above -20 mV, the WT channel exhibits faster decay time constants with increasing depolarizing voltage steps, but this response is missing for p.Arg1617Gln (Figure IIIa.3C). Sample traces reveal the striking difference in current decay between WT and mutant channel (Figure IIIa.3D). The apparent uncoupling of activation to fast inactivation likely accounts for the large increase

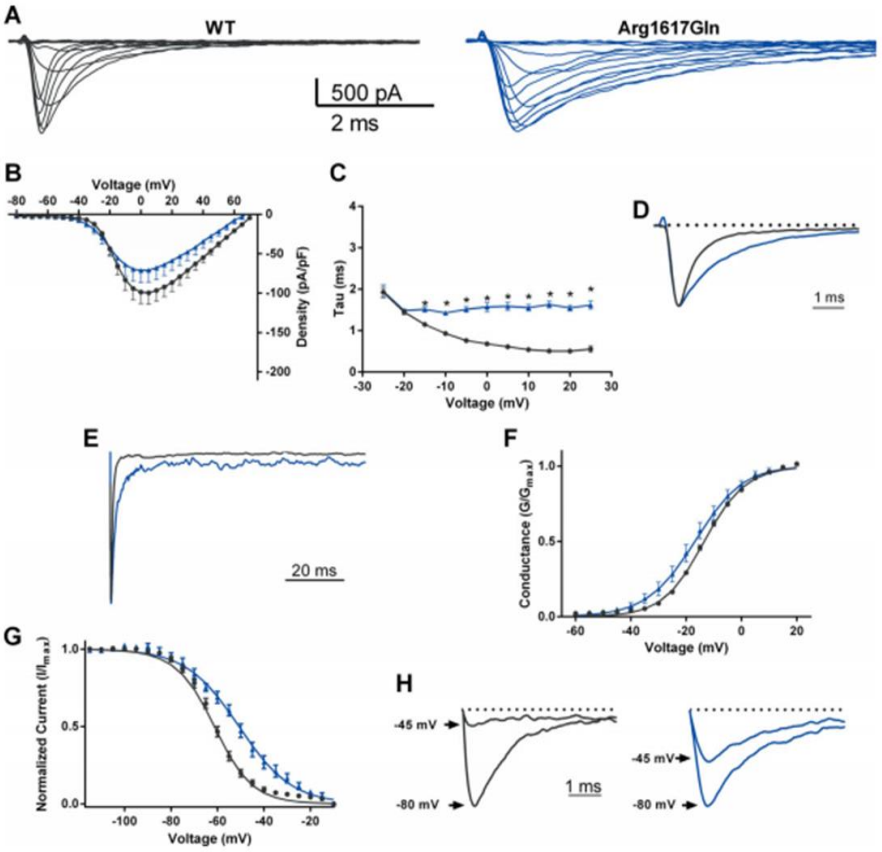

Figure IIIa.3. Biophysical effects of the missense mutation p.Arg1617Gln in $Na_v1.6$. (A) Representative traces of families of Na currents from ND7/23 cells transfected with the indicated $Na_v1.6$ cDNA. (B) Averaged current–voltage (I-V) relation for cells expressing WT and p.Arg1617Gln. Peak currents were normalized to cell capacitance. (C) Average fast time constant obtained from single exponential fits to macroscopic current decays as a function of voltage (mV). (D) Representative traces of normalized currents evoked by a depolarizing step to −20 mV from a holding potential of −120 mV illustrate significant delay in macroscopic current decay in p.Arg1617Gln (blue) compared to WT (black). (E) Representative normalized current traces recorded during a 100-msec depolarizing pulse from −120 mV to 0 mV illustrating the presence of elevated persistent sodium current. (F) Voltage dependence of channel activation. (G) Voltage dependence of steady-state inactivation. (H). Representative inactivation traces recorded after a 1-sec prepulse of −100 mV (larger amplitude) and −45 mV (smaller amplitude). Smooth lines in (F) and (G) correspond to the least squares fit when average data were fit to a single Boltzmann equation. Data are mean ± SEM. Statistical significance: *P < 0.05. Black, wild type; blue, p.Arg1617Gln.

in persistent current from 1% of peak transient current for the WT channels to 6% of peak transient current for the p.Arg1617Gln channels (Figure IIIa.3E). The elevation of persistent current is evident in the ratio of persistent current to peak current for p.Arg1617Gln (Table IIIa.2).

The inactivation parameters for p.Arg1617Gln were significantly shifted in the depolarizing direction and the value of the slope was increased, demonstrating disruption in the normal process of channel inactivation (Figure IIIa.3G, Table IIIa.2). The difference in the extent of inactivation at -45 mV is shown in Figure IIIa.3H. There was also a small hyperpolarizing shift in the voltage dependence of activation (Figure IIIa.3F, Table IIIa.2).

	Peak Current		Persistent		Activation (mV)			Inactivation (mV)		
	(pA/pF)	*n*	Ratio (Ip/Ipeak)	*n*	$V_{1/2}$	*k*	*n*	$V_{1/2}$	*k*	*n*
WT	−101 ± 15	30	1.8 ± 0.4	8	−13.3 ± 0.5	−7.3 ± 0.2	30	−61.5 ± 1.1	8.0 ± 0.4	19
Arg1872Leu	−89 ± 15	10	4.7 ± 1.5*	6	−17.9 ± 1.2***	−6.7 ± 0.4	10	−60.0 ± 1.3	7.5 ± 0.8	10
Arg1872Trp	−153 ± 27†	21	2.7 ± 0.4	11	−14.2 ± 1.4	−7.2 ± 0.4	21	−61.4 ± 1.6	8.6 ± 0.6	18
Arg1872Gln	−135 ± 35	8	1.6 ± 0.5	17	−19.2 ± 0.8***	−5.8 ± 0.5**	8	−53.5 ± 0.5***	7.9 ± 0.3	18
Arg1617Gln	−73 ± 15	10	5.5 ± 1.7*	5	−17.1 ± 2.0*	−7.8 ± 0.3	10	−52.6 ± 1.7***	12.5 ± 0.6***	8

Values represent mean ± SEM, *n* = number of cells, $V_{1/2}$, voltage of half-maximal activation or inactivation; *k*, slope factor. Significance was determined by unpaired Student's *t* test: **P* < 0.05 versus WT, ***P* < 0.005 versus WT, ****P* < 0.0005 versus WT, or Mann–Whitney test, †*P* < 0.05 versus WT.

Table IIIa.2. Biophysical properties of *SCN8A* mutations.

Protein interactions with the C-terminal domain of $Na_v1.6$

In addition to its role in channel inactivation, the C-terminal domain of $Na_v1.6$ interacts with several proteins that regulate channel trafficking or activity (Spampanato et al., 2004; Mantegazza et al., 2005; Laezza et al., 2009). To determine whether mutations at Arg1872 disrupt these interactions, we tested the effect of the p.Arg1872Trp mutation with substitution of the large uncharged tryptophan residue. HEK cells were cotransfected with cDNAs encoding the HA-tagged WT or mutant C-terminal fragment of $Na_v1.6$ and cDNAs encoding the G-protein subunits $G\beta_2$ and $G\gamma_3$. Lysates were incubated with anti-HA-coated beads and bound proteins were eluted and examined by western blotting. The yield of $G\beta_2$ was comparable with mutant and WT C-terminus (Figure IIIa.4A). Similarly, the mutation did not impair binding of the sodium channel β1 subunit (Figure IIIa.4B) and the fibroblast growth factor isoform FGF14b (Figure IIIa.4C).

Discussion

Unlike protein termination mutations, the pathogenic impact of missense mutations is difficult to predict without functional tests. Due in part to the multiple intramolecular interactions within the sodium channel α subunit, (Motoike et al., 2004; Payandeh et al., 2011) substitution of a single amino acid often has multiple effects on sodium channel function.

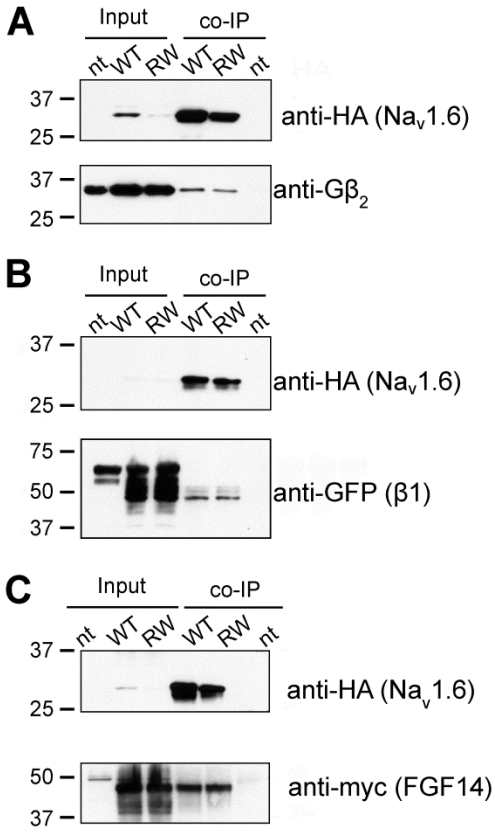

Figure IIIa.4. Substitution of tryptophan for Arg1872 of $Na_v1.6$ does not impair co-immunoprecipitation of interacting proteins. (A) $G\beta_2$ (B) GFP-tagged sodium channel subunit β1. (C) myc-tagged FGF14b.

Mutations at Arg1872 and Arg1617 impair channel inactivation by different intramolecular mechanisms

The three allelic mutations that eliminate the positively charged residue Arg1872 from the C-terminus of $Na_v1.6$ all result in a significant delay in transition from the open state to the inactivated state. This observation is consistent with previous studies demonstrating a direct role of the C-terminal domain in fast inactivation (Mantegazza et al., 2001; Nguyen and Goldin, 2010). Interaction of the C-terminus of sodium channel $Na_v1.5$ with its inactivation gate was shown to stabilize the inactivated state (Cormier et al., 2002; Motoike et al., 2004). Exchange of C-terminal domains between sodium channels $Na_v1.2$, $Na_v1.5$, and $Na_v1.6$ results in partial transfer of inactivation properties (Mantegazza et al., 2001; Lee and Goldin, 2008). The interaction between the C-terminus and the inactivation gate appears to involve electrostatic interactions, since inactivation of $Na_v1.2$ was slowed by reversing the charge of Glu1880 (corresponding to Glu1870 in $Na_v1.6$) by replacement with lysine (Nguyen and Goldin, 2010). These data support the view that loss of the positively charged residue arginine 1872 destabilizes interaction with the inactivation gate and delays entry into the inactivated state. This is predicted to increase the fraction of channels that can reopen during sustained depolarization, resulting in increased channel activity and

epileptogenic persistent current. The different effects on current density and channel kinetics of these allelic substitutions can be related to the chemical structure of the substituted residue. Substitution of the corresponding arginine residue of $Na_v1.2$ by leucine or glutamine also results in epileptic encephalopathy (Carvill et al., 2013; Baasch et al., 2014).

Replacement of arginine residue 1617 by glutamine appears to interfere with the initiation of fast inactivation from the open state. Arginine 1617 is the outermost charged residue in the S4 voltage sensor segment of DIV, which is thought to initiate channel inactivation through a conformational change (Chanda et al., 2004). In the crystal structure of the single domain bacterial channel NaChBac, the outermost arginine of S4 interacts with the negatively charged glutamate residue in segment S1 in the open state, and the negatively charged aspartate in segment S2 in the closed state (Yarov-Yarovoy et al., 2012). Loss of the positively charged arginine by p.Arg1617Gln would disrupt these electrostatic interactions, consistent with the observed defect in coupling of activation and inactivation (Figure IIIa.2C). We also observed a small depolarizing shift in the voltage dependence of inactivation due to p.Arg1617Gln. The alterations in $V_{1/2}$ and the slope of the steady-state inactivation curve are consistent with impaired allosteric interactions between the DIV-S1 sensor segment that initiates activation and the DIV-S4 sensor segment that initiates inactivation.

Comparison with previously described pathogenic mutations of SCN8A

Through different effects on intramolecular interactions, the recurrent mutations of Arg1617 and Arg1872 lead to disruption of channel inactivation in 15 independent patients. Along with the original mutation, p.Asn1768Asp, this work indicates that impaired inactivation of $Na_v1.6$ is the predominant pathogenic mechanism in EIEE13. A contrasting mechanism, premature channel activation, was observed for two mutations located in transmembrane segments of domain II, pThr767Ile and p.Asn984Lys (Estacion et al., 2014; Blanchard et al., 2015). The other two functionally characterized *SCN8A* mutations caused reduction in peak current density (p.Gly1451Ser) (Blanchard et al., 2015) and decreased protein stability (p.Arg223Gly) (de Kovel et al., 2014); the role of these effects in neuronal hyperexcitability is unclear.

Functional alterations of SCN8A and clinical severity

There is considerable heterogeneity in the clinical features of patients with mutation of Arg1872, even among patients with identical mutations. With respect to age of onset, intellectual disability, and motor function, the least severe course of disease was seen in patients with p.Arg1872Gln. More severe impairment, extending to inability to initiate purposeful movement and one case of SUDEP, was seen in the patients with p.Arg1872Leu and p.Arg1872Trp. p.Arg1872Gln led to bradycardia in patient 3, consistent with our recent observation of cardiac arrhythmia in a mouse model of EIEE13 (Frasier et al., 2016). The expression of $Na_v1.6$ in cardiomyocytes (Noujaim et al., 2012) may contribute to risk of SUDEP in EIEE13 patients.

The five previously described patients with the p.Arg1617Gln mutation also displayed considerable clinical heterogeneity, with seizure onset between 3 and 12 months of age, and variation in drug responses (Wagnon and Meisler, 2015). One patient became nonambulatory and one had SUDEP.

The features of patients with mutations of Arg1617 and Arg1872 exhibit considerable overlap, consistent with their shared effect on channel inactivation. Seizure onset within the first month is more common in patients with mutations of Arg1872, but there is no difference in the proportion of patients whose seizures are refractory to drug treatment, or in the frequency of nonambulatory status. The variation within each group appears as great as the difference between groups. Variation between patients with identical mutations may be accounted for by differences in genetic background, including genetic variation in other channel genes (Klassen et al., 2011), as well as stochastic variation during the development of the nervous system. The course of drug treatment itself may influence clinical outcome (Wagnon and Meisler, 2015).

Development of targeted therapy for EIEE13

Sodium channel blockers have some efficacy in this patient population, presumably by countering the effects of gain-of-function mutations causing channel hyperactivity (Tables IIIa.1). This beneficial response contrasts to the response of patients with Dravet syndrome (EIEE6), in which the effects of loss-of-function mutations of *SCN1A* are exacerbated by administration of sodium channel blockers. Unfortunately, response to antiepileptic drugs in EIEE13 is often transient. The development of $Na_v1.6$-specific channel blockers has been hampered by the structural similarity among members of the voltage-gated sodium channel gene family. A mouse epilepsy model with impaired inactivation of *Scn2a* was effectively treated with

the cardiac drugs ranolazine and GS967, which are somewhat selective inhibitors of persistent sodium current (Anderson et al., 2014). Activation of potassium channels to compensate for sodium channel hyperactivity is another potential approach. Recurrent missense mutations at *SCN8A* residues Arg1617 and Arg1872 result in elevated activity of $Na_v1.6$ as a result of impaired channel inactivation. This work confirms the important role of gain-of-function mutations in EIEE13 and demonstrates that impaired channel inactivation is a prominent pathogenic mechanism.

Appendix: Clinical Descriptions

Patient 1 experienced onset of generalized tonic–clonic seizures at 2 weeks of age that were refractory to treatment. A vagus nerve stimulator placed at 4 years of age reduced seizure frequency. Phenytoin reduced seizures, while carbamazepine, oxcarbazepine, lamotrigine, and topirimate were not effective. The patient was able to stand and walk with support at 12–15 months, but regressed and became nonambulatory, with generalized hypotonia at 5 years, contractures and spasticity at 13 years, and generalized hypertonia and spastic quadriplegia at 16 years. MRI revealed moderate cerebellar and mild cerebral atrophy. At 17 years, the patient is nonverbal with severe intellectual disability.

Patient 2 experienced three prolonged seizures between 6 and 8 weeks of age. No abnormalities were detected by MRI or prolonged EEG. She responded well to levetiracetam and topiramate for 2 months before the return of generalized tonic–clonic seizures with stiffening of the extremities, twitching, and eye fluttering. Seizures were often accompanied by apnea and oxygen desaturation that resolved after the seizure. The patient was transitioned from levetiracetam and topirimate to oxcarbazepine and lamotrigine with good response until seizure frequency increased at 11 months of age. With the addition of valproate and clonazepam, seizures were well controlled from 12 months to the current age of 18 months. Developmental delay was mild until 11 months, when increased seizure frequency resulted in acute developmental regression including loss of head and trunk control, loss of eye contact, and placement of a feeding tube. Control of seizures at 12 months of age resulted in improvement including regained eye contact and head control and the ability to sit with support.

Patient 3 experienced seizures beginning at 4 months of age, usually during sleep or on waking, accompanied by tonic posturing of the head and severe bradycardia, followed by flexing

of the arms and extension of the legs. Levetiracetam and zonisamide controlled seizures for 1 month before daily seizures reoccurred. Elevating zonisamide reduced seizures but caused severe (nonepileptic) encephalopathy, reversible upon lowering zonisamide. Addition of phenytoin reduced seizures to ≤1 per week. Gradual reduction of phenytoin resulted in increased seizure frequency. After an episode of status epilepticus at 19 months, seizure frequency stabilized at 5–10 per day, with development of asymmetric and absence seizures. Complete seizure control was obtained at 20 months with phenytoin and levetiracetam, and continued through the current age of 24 months. EEG was normal initially, but 6 weeks after seizure onset a hypofunctional area was detected in the left temporal lobe, from which abundant spike-and-wave configurations and polyspikes emerged. EEGs at 6 and 9 months showed severe diffuse encephalopathy and multifocal epileptic discharges without hypsarrhythmia. MRI at 12 months showed a slightly underdeveloped cortex. Development was normal prior to seizure onset. Speech arrested at 10 months of age. While seizures were partially controlled between 11 and 17 months of age, he began sitting and walking with support. After status epilepticus at 19 months there was regression, but by 24 months he recovered unassisted walking and improved social interaction without improvement in development of speech.

IIIb. Loss-of-Function Mutations of *SCN8A* Result in Intellectual Disability and Movement Disorders Without Seizures.

Rationale

In Chapter IIIb, we examine two mutations on the opposite end of the *SCN8A* encephalopathy spectrum. G964R and E1218K are loss-of-function *SCN8A* mutations from patients with intellectual disability and no seizures. Before this study, no previous loss-of-function *SCN8A* mutations from patients with intellectual disability and no seizures had been electrophysiologically characterized. The work in Chapter IIIb is significant because it demonstrates the range of the phenotypic spectrum that can be produced by mutations to the *SCN8A* gene. Additionally, this work argues that mutations to the *SCN8A* gene should be screened for in cases of idiopathic intellectual disability.

Introduction

Whole-exome sequencing has revealed a major role for *de novo* mutations in the etiology of sporadic intellectual disability (Vissers et al., 2015). Between one-third and one-half of sporadic cases may be accounted for by *de novo* mutations in genes required for neuronal development and synaptic transmission. The neuronal sodium channel *SCN8A* ($Na_v1.6$) is concentrated at the axon initial segment and at nodes of Ranvier of myelinated axons (O'Brien and Meisler, 2013). Exome analysis for *SCN8A* mutations has thus far focused on children with seizure disorders (Meisler et al., 2016). More than 150 missense mutations of *SCN8A* have been identified, and gain-of-function hyperactivity is the most common pathogenic mechanism for seizures.

By contrast, we previously described a loss-of-function, protein truncation allele of *SCN8A* that cosegregated with cognitive impairment in a family without seizures (Trudeau et al., 2006). To follow up on that observation, we have now examined the functional effects of 2 *SCN8A* missense mutations identified by exome sequencing in children with intellectual disability who also did not have seizures. Both mutations caused complete loss of channel

activity, confirming the role of loss-of-function mutations of *SCN8A* as a cause of isolated cognitive impairment.

Methods

Molecular Diagnostics

Exome sequencing for patient 1 was performed by GeneDX (Gaithersburg, MD). In addition to the *SCN8A* variant, a frameshift mutation in GJB2 (c.167delT, p.L56RfsX26) was inherited from an unaffected parent. Exome sequencing for patient 2 was performed at the laboratory for DNA Diagnostics in the University Medical Center Utrecht. In addition to the *SCN8A* variant, the PDHA1 variant (c.520G.A, p.Ala174Thr) was present in the child and an unaffected grandfather. Analysis of copy number variation and Fragile X expansion for patient 2 were negative. Procedures were approved by the institutional ethics standard committees.

Standard Protocol Approvals, Registrations, and Patient Consents.

Written consent for research was obtained from the guardians of both patients whose variants were studied.

Site-Directed Mutagenesis of $Na_v1.6$ Complementary DNA.

Mutations were introduced into the tetrodotoxin-resistant mouse complementary DNA (cDNA) $Na_v1.6R$ by site-directed mutagenesis with QuikChange II XL (Agilent Technologies, Santa Clara, CA) as described (Wagnon et al., 2015a). Two independent mutagenesis experiments generated cDNA clones A and B for each mutation. The 6-kb open reading frame was resequenced, and clones lacking other mutations were analyzed.

Electrophysiology

Please reference Chapter II: General Methods

Western Blot

Please reference Chapter II: General Methods

Results

Identification of novel missense variants of SCN8A

Patient 1 is a 7-year-old girl who experienced global developmental delay and hypotonia in early childhood. She walked and spoke her first words at 18 months.

She is receiving special education services at school and is repeating the first grade due to below average academic attainment. Psychoeducational testing revealed receptive-expressive language disorder and borderline intellectual functioning with a diagnosis of social communication disorder. She did not meet criteria for autism spectrum disorder.

Attention-deficit hyperactivity disorder was diagnosed at 6 years and has responded to methylphenidate. Exome sequencing revealed the *SCN8A* variant c.2890G.C (p.Gly964Arg; G964R) which arose *de novo* and was not present in either parent. Gly 964 is located in transmembrane segment 6 of domain II (D2S6) and is highly conserved through invertebrate and vertebrate evolution (Figure IIIb.1, A and C).

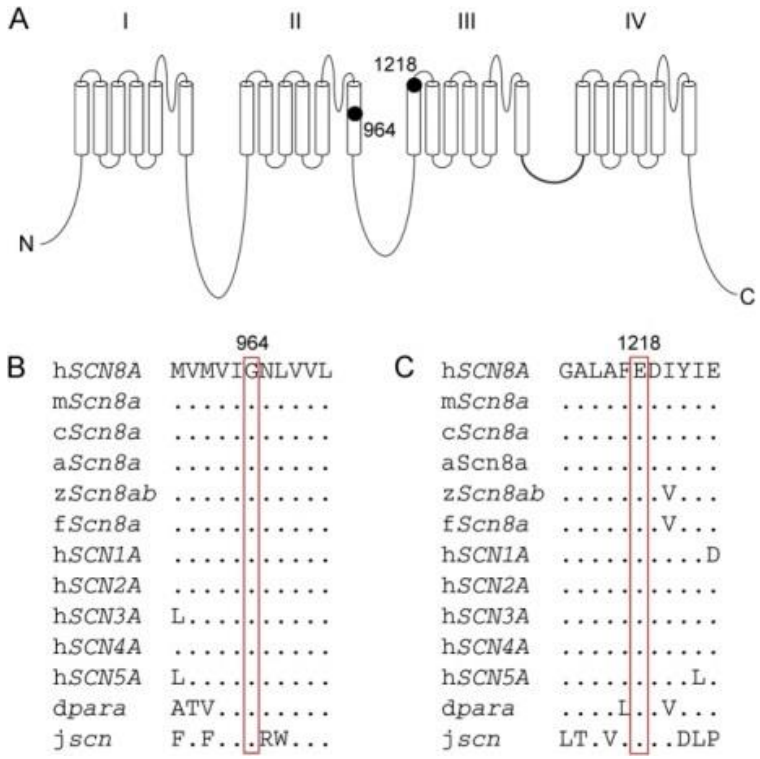

Figure IIIb.1. Location and evolutionary conservation of *SCN8A* mutations in individuals with intellectual disability (A) Four-domain structure of the voltage-gated sodium channel α subunit. p.Gly964Arg (G964R) is located in transmembrane segment 6 of domain II. p.Glu1218Lys (E1218K) is located in transmembrane segment 1 of domain III. (B) Evolutionary conservation of residue G964 in multiple species. (C) Conservation of residue E1218 in multiple species. a = anole; c = chicken; dpara = drosophila "paralytic"; f = fugu; h = human; jscn = jellyfish sodium channel; m = mouse; z = zebrafish. Amino acids are indicated by the single-letter code; dots represent identity to the human amino acid.

Patient 2 is a 10-year-old boy who was born after a pregnancy complicated by polyhydramnios. Development was delayed from birth. Early ataxic gait resolved with age. Behavioral problems included temper tantrums. Metabolism and brain MRI were normal. There were no dysmorphic features. Exome sequencing

and analysis of 770 genes identified the *SCN8A* variant c. 3652G.A (p.Glu1218Lys; E1218K) located at the distal terminus of transmembrane segment 1 in domain III (D3S1). This residue is highly conserved through evolution (Figure IIIb.1, A and B). The variant was not present in the maternal genome; the father was not available for testing.

Additional clinical features are detailed in Table IIIb.1. Both mutations were predicted to be deleterious by in silico prediction programs. Neither mutation was previously observed in patients or in the Exome Aggregation Consortium Database.

Table Clinical features of patients with intellectual disability and *SCN8A* mutations

	Patient 1	Patient 2
Sex	Female	Male
Age	7 y	10 y
Nucleotide change	c.2890G>C	c. 3652G>A
Inheritance	De novo	Unknown (father unavailable)
Protein change	G964R	E1218K
Channel domain	D2S6	D3S1
In silico predictions	Deleterious	Deleterious
CADD	25	32
PROVEAN	−7.4	−3.8
Polyphen 2	0.9	1.0
Channel activity observed	Inactive	Inactive
Protein	Stable	Unstable
Diagnosis	Language disorder borderline intellectual function	Intellectual disability
IQ	73	56
Social interaction	Social communication disorder; minimal interaction with peers; good eye contact	Temper tantrums
Development	Global delay walk, talk at 18 mo	Global motor delay, severe speech delay
EEG	Normal	Not done
Seizures	None	None
MRI	Not done	Normal
Metabolism	Not done	Normal
Motor development	Hypotonia; motor delay improved with time	Unstable gait, resolved
Other phenotypes	ADHD at 6-y special education, chronic headache, finger chewing	No other phenotypes
Treatment	ADHD responsive to methylphenidate	No medication

Abbreviation: ADHD = attention-deficit hyperactivity disorder.

Table IIIb.1. Clinical features of patients with intellectual disability and *SCN8A*

Electrophysiologic characterization of SCN8A mutations G964R and E1218K

ND7/23 cells were transfected with wild-type or mutant cDNAs, and sodium currents were recorded (Figure IIIb.2, A and B). The macroscopic Na current in nontransfected cells was -10.0 ± 1.8 pA/pF (n = 8). Cells transfected with wild-type $Na_v1.6$ exhibited a robust macroscopic Na current of -102 ± 12 pA/pF (mean ± SEM) (n = 30). The current in cells transfected with mutant cDNA did not differ from nontransfected cells: G964R, -5.2 ± 0.5 pA/pF (n = 30) and E1218K, -9.8 ± 1.5 pA/pF (n = 27). To confirm the loss of activity, site-directed mutagenesis was repeated and a second independent clone with each mutation was analyzed, with the same result. Both missense variants thus result in a complete loss of channel activity.

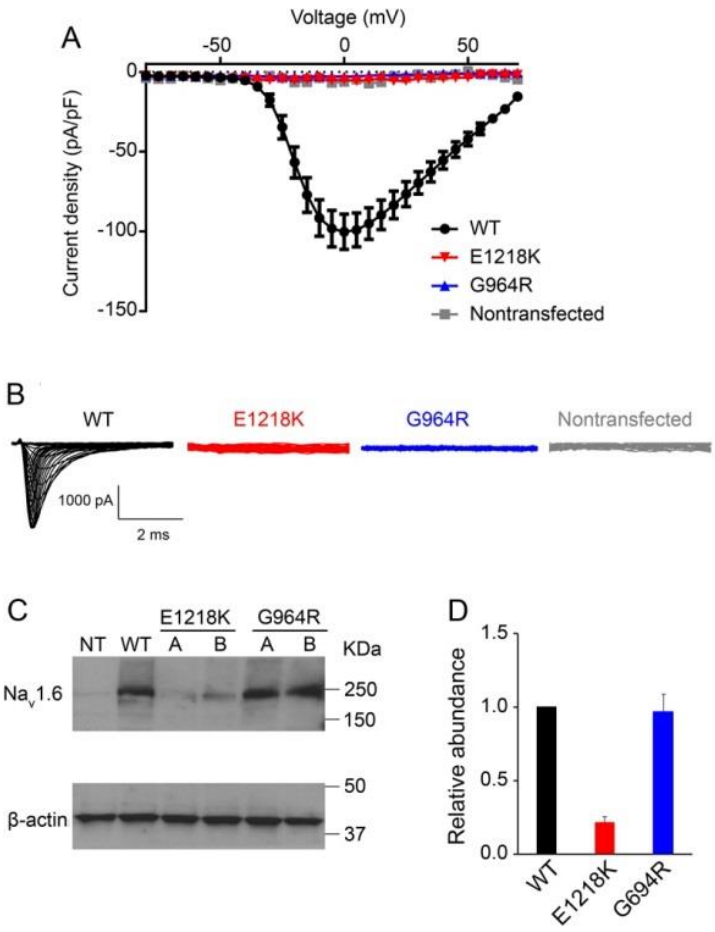

Figure IIIb.2. Mutations E1218K and G964R result in loss of $Na_v1.6$ function.

Expression of mutant protein

To evaluate the mechanism for loss of channel activity, we examined protein abundance in transfected HEK cells. Wild-type $Na_v1.6$ and G946R cDNAs generated a protein with the predicted molecular weight of 250 kDa, which was not present in nontransfected cells (Figure IIIb.2C). However, repeated transfections of the E1218K mutant cDNA detected only a low level of protein (Figure IIIb.2, C and D), indicating that this mutation reduces protein stability.

Discussion

The patients described exhibited developmental delay and cognitive impairment but no history of seizures. Each carried a pathogenic missense variant of *SCN8A* that altered a highly

conserved amino acid residue in a transmembrane segment of the channel, resulting in loss-of-function. *SCN8A* is one of the most conserved genes in the mammalian genome, with an unusually low rate of coding variation (Petrovski et al., 2013). The low frequency of frameshift and nonsense mutations among 60,000 individual exomes was used to calculate the probability of 1.0 that *SCN8A* is intolerant to haploinsufficiency (Lek et al., 2016). The population data support our conclusion that haploinsufficiency of *SCN8A* is responsible for cognitive impairment in these patients.

Impaired cognition in the patients is also consistent with the evidence that heterozygous loss-of-function mutations in mouse $Na_v1.6$ also result in cognitive and behavioral deficits without spontaneous seizures. Impaired learning in water maze and eyeblink conditioning tests (Woodruff-Pak et al., 2006; McKinney et al., 2008) and elevated anxiety in the open-field test (Levin et al., 2006) have been described.

At the cellular level, complete inactivation of mouse *Scn8a* reduces repetitive firing, resurgent current and persistent current in cerebellar Purkinje cells, prefrontal cortical pyramidal cells, and hippocampal CA1 cells (O'Brien and Meisler, 2013). These changes decrease the frequency of action potentials. Reduced neuronal activity is a likely consequence of the loss-of-function mutations of *SCN2A* and receptors involved in excitatory neurotransmission that have also been associated with intellectual disability. Chronic reduction of neuronal activity may alter the dynamics of synaptic plasticity during maturation and lead to aberrant cerebral circuitry and intellectual disability.

In contrast to the loss-of-function variants described here, we previously identified 8 gain-of-function variants resulting in channel hyperactivity resulting in epileptic encephalopathy (Meisler et al., 2016). We also found loss-of-function missense variants in 2 patients with seizures (de Kovel et al., 2014; Blanchard et al., 2015), indicating that genetic background influences clinical outcome. Both gain-of-function and loss-of-function variants of the related sodium channel *SCN2A* have also been associated with seizures (Wolff et al., 2017). A recent analysis of *de novo* mutations in more than 7,000 individuals with developmental disorders identified 5 missense variants of *SCN8A* in patients with seizures and 2 missense variants of *SCN8A* in patients with cognitive impairment but no seizures. We would suggest that the former variants are likely to cause channel hyperactivity and the latter to cause loss of function. Protein truncation variants of *SCN8A* are underrepresented in all populations studied to date, including

controls, patients with intellectual disability, and patients with seizures. It seems likely that these protein truncations are associated with distinct disorders not yet subjected to large-scale exome sequencing, such as neuromuscular and movement disorders.

The *de novo* mutation of *SCN8A* in patient 1 is consistent with the growing recognition of the role of *de novo* mutations in sporadic intellectual disability. In 3 earlier studies examining 142 individuals with intellectual disability, 1 *de novo* missense mutation of *SCN8A* was detected (Rauch et al., 2012; Gilissen et al., 2014; Hamdan et al., 2014). Better estimates of the quantitative contribution of *SCN8A* mutations to sporadic and inherited forms of isolated cognitive impairment will emerge from additional large-scale screening of patient populations.

IIIc. Evaluating the Efficacy of Phenytoin in an *in vitro* Model of *SCN8A* Encephalopathy.

Rationale

In Chapter IIIc we examine the efficacy of the sodium channel blocker phenytoin on a novel gain-of-function *SCN8A* mutation. In addition to electrophysiologically characterizing a new *SCN8A* mutation, this work is a significant contribution to the field because it is one the first basic science studies examining the mechanism and efficacy of a clinically available AED on a EIEE13 mutation. Though no statistics are currently available on the efficacy of AEDs in EIEE13 patients, it is believed that long term seizure control is difficult to achieve in a significant portion of patients. Additionally, there are limited studies examining which clinically available AEDs should be used first and which should be avoided. Here, we demonstrate that the sodium channel blocker phenytoin is effective in diminishing proexcitatory alterations induced by the I1327V mutations. This data is significant because it argues that sodium channel blockers, specifically phenytoin, may be the most effective clinically available treatment for patients with EIEE13.

Introduction

Since seizures in many EIEE13 patients are associated with a gain-of-function in Na channel activity, a rational approach to therapy would be to use anticonvulsants with Na channel blocking characteristics. However, the seizures in EIEE13 patients are difficult to control even with Na channel blockers and many patients remain refractory. A recent study of four children with EIEE13 demonstrated good seizure control with high doses of phenytoin (Boerma et al., 2015). One of these patient mutations included in the study has been examined functionally and shown to result in a hyperpolarizing shift in voltage-dependence of activation (Blanchard et al., 2015). In the current study, we determined the biophysical properties of another *SCN8A* mutation, p.Ile1327Val, located within the highly conserved region of transmembrane segment 5 adjacent to the cytosolic interface of the S4–S5 linker of domain II (Vaher et al., 2014). Our data show that I1327V is a gain-of-function mutation that is predicted to lead to increased neuronal activity and the generation of seizures. We demonstrate that phenytoin (100 μM) results in

greater tonic block and use dependent block of I1327V channels compared with WT channels. The preferential effect of phenytoin on the mutant channel may increase the effectiveness of phenytoin in treating refractory seizures associated with EIEE13.

Methods

Site-Directed Mutagenesis of the $Na_v1.6$ cDNA

The amino acid substitution I1327V was introduced into the tetrodotoxin (TTX)-resistant derivative of the full-length rNa_v1.6 cDNA clone (NM_014191.3, NP_055006.1) (Herzog et al., 2003), as previously described (Veeramah et al., 2012; Blanchard et al., 2015; Wagnon et al., 2015a). Site-directed mutagenesis was carried out with the QuikChange II XL kit (Agilent Technologies). The entire 6-kb open reading frame was sequenced to confirm the absence of other mutations.

Cell Culture

Please reference Chapter II: General Methods

Electrophysiology

Please reference Chapter II: General Methods.

Data Analysis

Please reference Chapter II: General Methods.

Results

Electrophysiological characterization of I1327V

Isoleucine residue 1327 is located in the highly conserved region of transmembrane segment 5 of domain III (D3S5) adjacent to the cytosolic S4–S5 linker of Na_v1.6 (Figure IIIc.1A). Representative currents from ND7/23 cells transfected with wildtype (WT) and I1327V Na_v1.6 are shown in Figure IIIc.1B. Peak current density for I1327V was not elevated compared to WT (Figure IIIc.1C). Analysis of steady-state kinetics demonstrates a small but significant

hyperpolarizing shift in the half maximal voltage dependence of activation for I1327V ($V_{1/2}$) of −2.5 mV (P< 0.05: Figure IIIc.1D, E). Slope factor (k) was also significantly decreased (P<0.005: Figure IIIc.1F, Table IIIc.1). To determine the kinetics of open state inactivation, macroscopic current decay was fit to single exponential functions and the fast time constant (τ) was plotted as a function of voltage. Transition from open state to the inactivated state was significantly delayed in I1327V channels at depolarizing voltages ranging between +15 mV to +35 mV (Figure IIIc.1G), consistent with the prediction of disrupted inactivation. The slowing of fast inactivation is evident when the peaks of the current traces at +35 mV are aligned so that inactivation kinetics can be compared directly (Figure IIIc.1H). When examined at a time point of 100 ms after the voltage stimulus, decay of macroscopic current was complete for both I1327V and WT, indicating the absence of

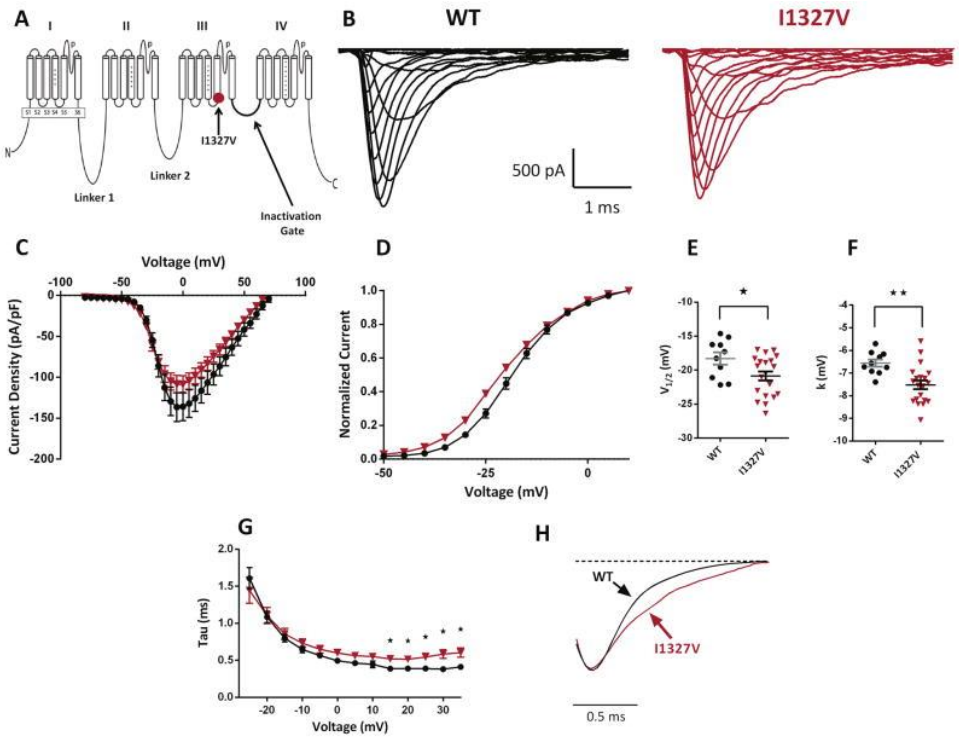

Figure IIIc.1. I1327V modulates steady state activation. (A) Four-domain structure of the voltage-gated Na channel α subunit shows that I1327V is located at the cytosolic interface of the S4–S5 linker and transmembrane segment 5 of domain III. (B) Representative traces of families of Na currents recorded from ND7/23 cells transfected with the indicated $Na_v1.6$ cDNAs. (C) Averaged current-voltage (I-V) relationship for cells expressing WT and I1327V. Peak currents were normalized to cell capacitance. (D) Voltage dependence of channel activation. Smooth lines correspond to the least squares fit when average data were fit to a single Boltzmann equation. (E) Scatter plot of voltage at half-maximal activation ($V_{1/2}$) for cells expressing WT and I1327V. (F) Scatter plot of the slope factor of activation (k). (G) Average fast time constants obtained from single exponential fits to macroscopic current decays as a function of voltage. (H) Representative traces of normalized currents evoked by a +35 mV stimulus from a holding potential of −120 mV illustrate delays in macroscopic current decay between WT (black) and I1327V (red). Data are means ± S.E.M. Statistical significance: * P <0.05; ** P<0.005. Black circles, WT; red triangles, I1327V.

increased persistent current in the mutant channel (data not shown).

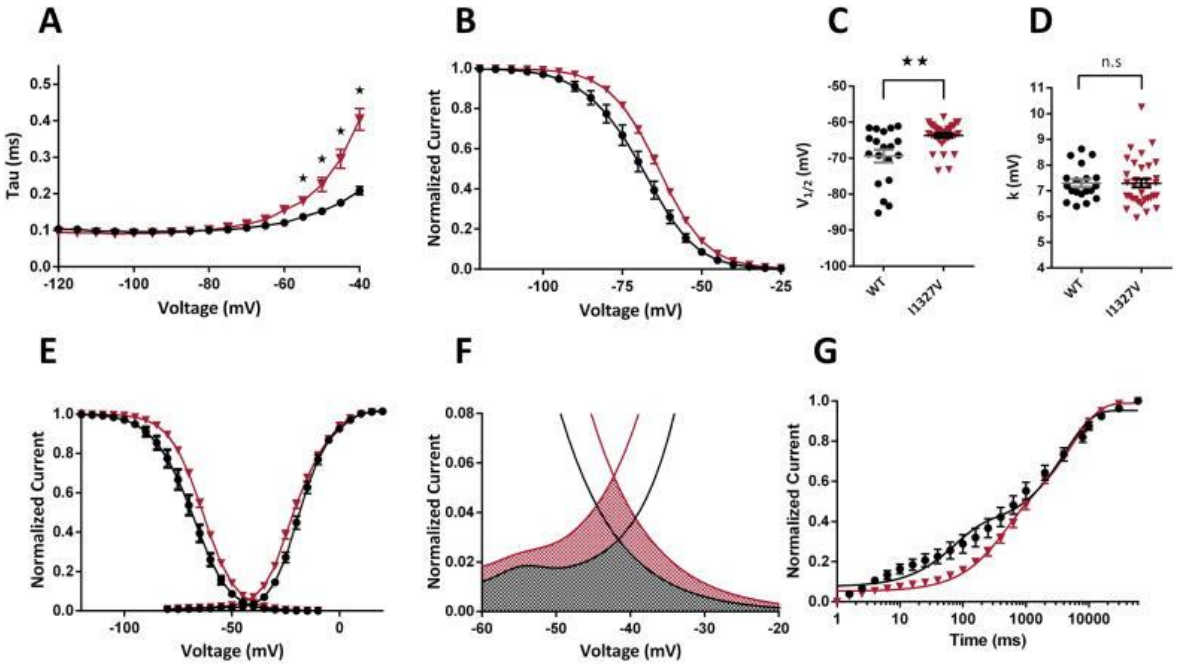

Figure IIIc.2. I1327V disrupts channel inactivation properties. (A) Average fast time constant obtained from single exponential fits to deactivation of WT and I1327V channels. (B) Voltage dependence of steady-state inactivation. Smooth lines correspond to the least squares fit when average data were fit to a single Boltzmann equation. (C) Scatter plot of voltage at half-maximal inactivation ($V_{1/2}$) for cells expressing WT and I1327V (D) Scatter plot of the slope factor (k) of inactivation. (E) The window current is obtained by overlapping the normalized activation and inactivation curves from WT and I1327V cells. (F) Enhanced view of overlapping activation and inactivation curves shows an increase in I1327V window current (red shaded area) compared to WT (gray shaded area). G) Recovery from inactivation at a post train level of −90 mV. Data are means ± S.E.M. Statistical significance: * P <0.05; ** P<0.005. Black circles, WT; red triangles, I1327V.

We next determined the effects of I1327V on the kinetics of channel deactivation. Compared to WT channels, I1327V significantly increased the time constant (τ) of deactivation over the range of voltages between −55 mV and −40 mV (Figure IIIc.2A), indicating a slower transition from the open state back to the closed state. Disruption in normal inactivation processes have been described for several *SCN8A* mutations (Wagnon et al., 2015a). In I1327V channels a significant depolarizing shift in the $V_{1/2}$ of steady-state inactivation was recorded (5.7 mV; P< 0.005: Figure IIIc.2B, C) with no change in slope values (Figure IIIc.2D). Window

currents can be determined by taking the area under the overlapping normalized activation and inactivation curves (Figure IIIc.2E). We determined the window current for I1327V and WT channels and found an increase in the window current for the mutant channel (Figure IIIc.2F). Lastly, we examined recovery from inactivation using a recovery voltage of −90 mV and found no significant difference between WT and I1327V transfected cells (Figure IIIc.2G; Table IIIc.1).

	Activation			Inactivation			Recovery			
	$V_{1/2}$	k	n	$V_{1/2}$	k	n	τ1	τ2	% Fast	n
WT	−18.3 ± 0.9	−6.6 ± 0.2	10	−69.4 ± 1.8	7.3 ± 0.2	19	390 ± 85.8	6614 ± 799	47.6 ± 0.1	19
I1327V	−20.8 ± 0.7*	−7.5 ± 0.2**	20	−63.7 ± 0.6**	7.3 ± 0.2	33	577 ± 50.8	6020 ± 380	45.2 ± 0.1	33

Table IIIc.1. Biophysical properties of I1327V and WT channels. Values represent means ± S.E.M, n = number of cells, $V_{1/2}$, voltage of half-maximal activation or inactivation; k, slope factor. Significance was determined by unpaired Student's T-Test.

Inhibition of I1327V by phenytoin

The anti-epileptic drug (AED) phenytoin (Dilantin®) is clinically used to treat epileptic seizures. The mechanism is thought to involve the inhibition of Na channels (Kuo and Bean, 1994). Phenytoin binds preferentially to the inactivated form of $Na_v1.6$ and the drug can block high frequency firing of action potentials, trapping channels in the inactivated state (Kuo and Bean, 1994). Since I1327V displayed disrupted inactivation parameters we sought to determine if phenytoin would inhibit currents evoked from a holding potential of −60 mV, a potential when many of the channels can cycle between the closed, open and inactivated states. At a concentration of 100 μM, tonic block by phenytoin was significantly greater for I1327V currents (53 ± 2.0%; n=10) than WT currents (43 ± 2.0%; n = 8: $P< 0.05$; Figure IIIc.3A and B). In addition to voltage dependent block, AEDs also exhibit use-dependent block as an important mechanism of action, permitting enhanced block of high frequency neuronal firing associated with epileptic seizures (Rogawski and Loscher, 2004). In a similar manner to tonic block, phenytoin (100 μM) produced a greater use dependent block of I1327V channels compared to WT (Figure IIIc.3C). In the absence of phenytoin, there was very little block of control (6.0 ± 1.0%; n = 23) and I1327V (7.0 ± 1.0%; n = 29) channel currents during the use dependent protocol. In the presence of phenytoin, WT channels were blocked by 11 ± 2.0% (n = 12) at

pulse 60. In contrast, phenytoin caused greater use-dependent block of I1327V channels, blocking the current by 21 ± 4.0 % (n = 9) (P< 0.05).

Phenytoin (100 μM) also caused a hyperpolarizing shift in the voltage dependence of activation for both WT channel ($V_{1/2}$ by −7.6 mV; P< 0.05; Figure IIIc.3D–E) and I1327V channels ($V_{1/2}$ by −16.9 mV; P< 0.05: Figure IIIc.3F–G). Phenytoin had no effect on the slope (k) in WT or I327V channels (Table IIIc.2). Inactivation parameters were significantly shifted in a hyperpolarized direction by phenytoin (100 μM) for both WT ($V_{1/2}$ by −15.4 mV; P<0.05; Figure IIIc.4A–C) and I1327V ($V_{1/2}$ by −13.0 mV; P< 0.005: Figure IIIc.4D–F). Slope factors (k) remained unchanged for both WT and I1327V (Table IIIc.2). Phenytoin did not significantly alter either the fast or slow time constants of recovery from inactivation at −90 mV in either I1327V or WT transfected cells (Table IIIc.2). Phenytoin did, however, significantly decrease the amplitude of the Na current recorded after a recovery interval of 60 s in WT (47.3% ± 3.4 Figure IIIc.4G) and I1327V (33.6% ± 11.3 Figure IIIc.4H).

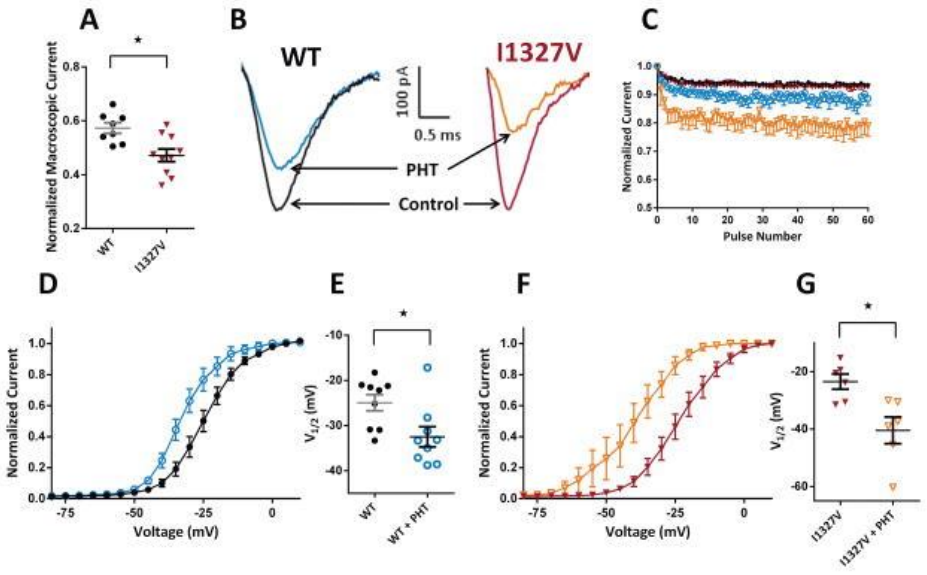

Figure IIIc.3. Phenytoin (PHT) inhibits Na channel currents evoked from WT and I1327V and modulates steady-state activation parameters. (A) Scatter plot showing normalized macroscopic current amplitude remaining following tonic block by phenytoin (100 μM). Currents were elicited by a depolarizing step to 0 mV for 12 ms from a holding potential of −60 mV. (B) Representative traces show greater tonic inhibition of I1327V currents over WT currents by phenytoin (100 μM) (C) Use-dependent block by phenytoin (100 μM). Cells were held at −120 mV and a voltage step to +20 mV was applied for 20 ms at a frequency of 10 Hz. (D) Shift in the voltage dependence of WT channel activation following treatment with phenytoin (100 μM). Smooth lines correspond to the least squares fit when average data were fit to a single Boltzmann equation. (E) Scatter plot of voltage at half-maximal activation ($V_{1/2}$) (F) Shift in the voltage dependence of I1327V channel activation following treatment with phenytoin (100 μM). Smooth lines correspond to the least squares fit when average data were fit to a single Boltzmann equation. (G) Scatter plot of voltage at half-maximal activation ($V_{1/2}$). Data are means ± S.E.M. Statistical significance: *P <0.05. Black filled circles, WT; blue open circles, WT + phenytoin, red filled triangles, I1327V; orange open triangles, I1327V + phenytoin.

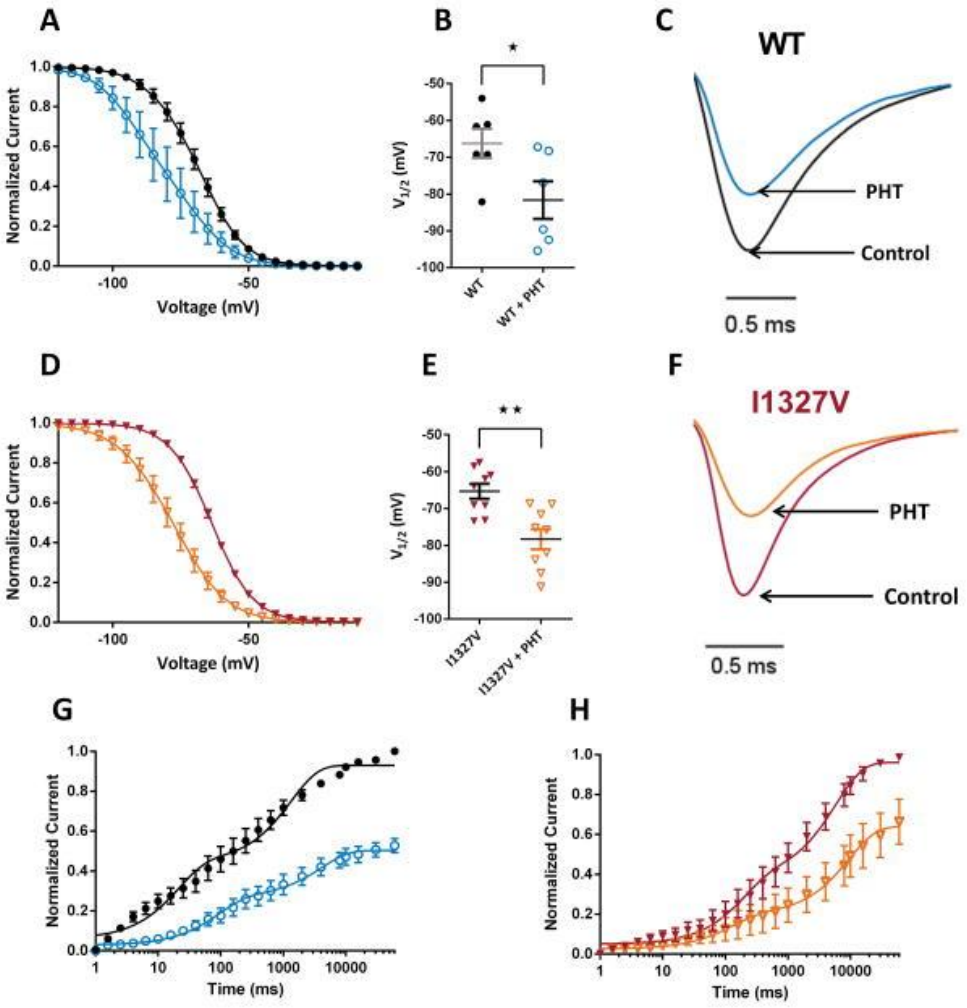

Figure IIIc.4. Phenytoin (PHT) modulates steady state inactivation properties in cells expressing WT and I1327V channels. (A) Shift in the voltage dependence of WT channel inactivation following treatment with phenytoin (100 μM). Smooth lines correspond to the least squares fit when average data were fit to a single Boltzmann equation. (B) Scatter plot of voltage at half-maximal inactivation ($V_{1/2}$). (C) Representative WT traces elicited following a pre-pulse to −75 mV demonstrating the shift in inactivation following application of phenytoin (100 μM). Traces were normalized to the pre-phenytoin peak current. (D) Shift in the voltage dependence of I1327V channel inactivation following treatment with phenytoin (100 μM). Smooth lines correspond to the least squares fit when average data were fit to a single Boltzmann equation. (E) Scatter plot of voltage at half-maximal inactivation ($V_{1/2}$). (F) Representative I1327V traces following a pre-pulse to −75 mV demonstrating the shift in inactivation following the application of phenytoin (100 μM). Recovery from inactivation before and after the application of phenytoin (100 μM) in WT (G) and I1327V (H) cells. Data are means ± S.E.M. Statistical significance *P <0.05; **P<0.005. Black filled circles, WT; blue open circles, WT + phenytoin; red filled triangles, I1327V; orange open triangles, I1327V + phenytoin.

Discussion

The *de novo* mutation I1327V was identified in two unrelated patients with early onset encephalopathy (Vaher et al., 2014; Singh et al., 2015). Residue Ile1327 is located within the highly conserved region of transmembrane segment D3S5 adjacent to the cytosolic interface with the S4–S5 linker. Mutation studies indicate that residues located along the S4–S5 linker of domain III are critical to fast inactivation since they provide an interaction site for the fast inactivation gate (Smith and Goldin, 1997). Since isoleucine and valine are relatively similar in structure and both are non-polar, hydrophobic amino acids, the mechanisms behind disrupted inactivation are not obvious. We hypothesize that substituting the bulky isoleucine side chain with methyl and ethyl groups, for the smaller valine side chain, composed only of methyl groups, may disrupt the hydrogen bonds that form between the inactivation gate and the S4–S5 linker of domain III, disrupting the normal activation process.

Consistent with the gain-of-function mechanism, I1327V resulted in a hyperpolarizing shift in activation parameters, enabling mutant channels to open at voltages more negative than WT channels. This shift, coupled with a depolarizing shift in the voltage dependence of inactivation, would extend the voltage range where channels would be available for activation and have a finite probability of opening. This range of voltages is commonly referred to as the window current and an enhancement in this current would reduce action potential thresholds, facilitating action potential firing and potentially initiating seizure generation and spread. Increases in window currents have been associated with increased persistent sodium current activity and epileptogenesis in animal models (Ketelaars et al., 2001; Ellerkmann et al., 2003). A delay in the decay of the macroscopic current at depolarized voltages further supports the view that a valine for isoleucine substitution at position 1327 results in a major disruption of the normal inactivation process in the mutant channel, specifically delaying entry into the inactivated state. A slowing in channel deactivation would increase the availability of Na channels by delaying the transition of open channels back into the closed state during short depolarizations, further increasing the probability that channels remain in the open state configuration for longer periods of time.

There is considerable heterogeneity among the 10 *SCN8A* mutations that have now been characterized through electrophysiology studies. One common pathogenic mechanism is a

disruption in the inactivation process. In some cases, including the current mutation I1327V, this is due to a depolarizing shift in the inactivation curve that delays channel inactivation (Estacion et al., 2014), while other mutations have an increase in persistent Na channel current after prolonged depolarization (Veeramah et al., 2012). Many of these mutations are located at sites involved in channel inactivation, including domain III, IV and the C-terminus (Wagnon and Meisler, 2015). In contrast, two mutations located within transmembrane segments of domain II have normal inactivation parameters, but establish a gain-of-function phenotype via hyperpolarizing activation curves, thereby increasing channel availability at more negative membrane potentials and consequently increasing window currents (Estacion et al., 2014; Blanchard et al., 2015).

AEDs that inhibit Na channels as a mechanism of action have been used in treating seizures in EIEE13 patients. However, it is unclear which AEDs should be considered first choice for these patients. Furthermore, mechanistic studies demonstrating the response of mutant channel currents to AEDs are lacking. In a recent study of four patients with seizures that were refractory to many AEDs, good seizure control was obtained with high dose phenytoin (Boerma et al., 2015). Withdrawal of phenytoin resulted in seizure reoccurrence in all four patients. This work suggests that phenytoin may be more effective for *SCN8A* encephalopathy than other clinically available AEDs. The mode of action of phenytoin includes inhibition of Na channels, but it also affects calcium channels (Twombly et al., 1988; Kuo and Bean, 1994). Phenytoin has little effect on Na channels in their resting or closed state, but at more depolarized potentials, such as those observed during high frequency firing, the block by phenytoin is pronounced (Kuo and Bean, 1994; Lenkowski et al., 2007). This greater affinity for the inactivated state of the channel over the closed state of the channel is an important characteristic of many AEDs (Macdonald and Kelly, 1994). When tested on the mutation I1327V, tonic block and use dependent block by phenytoin was more pronounced for the mutant channel than WT channels. A likely explanation is that phenytoin binds slowly to open and inactivated channels (Kuo and Bean, 1994). The mutant channel displayed impaired deactivation kinetics and slowed transition from the open state to the inactivated state at depolarized voltages, allowing channels to remain longer in non-closed conformation. Increased proportion of channels in open and inactivated states would increase the time available for phenytoin to bind tightly and trap the mutant channels in a non-conducting conformation, preventing them from contributing to action

potential initiation. This feature is referred to as the modulated receptor hypothesis (Hille, 1977). Phenytoin also reversed the depolarizing shifts in inactivation recorded with I1327V and caused further hyperpolarizing shifts in activation curves. In view of these findings, patients with the I1327V mutation may achieve good seizure control with phenytoin in a similar manner to the patients reported in the study by Boerma et al (Boerma et al., 2015).

The mutation described here has been observed in two patients to date. The first patient was a male child who experienced seizures immediately after birth and continued to experience refractory epilepsy until his death at the age of 1 year and 5 months (Vaher et al., 2014). It is unclear whether this patient was treated with phenytoin. The second patient was a male child who appeared to experience seizures in utero, perceived as "drumming" sensations during the later stages of pregnancy (Singh et al., 2015). Although several AEDs were unsuccessful at providing seizure control in this patient, a high dose of phenytoin (18–20 mg/L) did provide temporary seizure control. Both patients had severe, early-onset movement disorders. Our study demonstrates that these patients had a gain-of-function mutation of *SCN8A* which likely accounted for their epileptic encephalopathy. The effectiveness of phenytoin at inhibiting the mutant channel currents provides additional evidence that phenytoin may be a useful treatment for *SCN8A* encephalopathy.

	Activation			Inactivation			Recovery			
	$V_{1/2}$	k	n	$V_{1/2}$	k	n	τ1	τ2	% Fast	n
WT	−24.9 ± 1.8	−6.3 ± 0.2	9	−66.2 ± 4.1	7.2 ± 0.3	6	181 ± 95	4405 ± 1196	56.4 ± 0.1	7
WT + PHT	−32.5 ± 2.2*	−5.8 ± 0.5	9	−81.6 ± 5.1*	7.9 ± 0.4	6	145 ± 57	4942 ± 1757	51.6 ± 0.1	7
I327V	−23.5 ± 2.6	−7.3 ± 0.2	6	−65.3 ± 2.0	7.4 ± 0.4	9	423 ± 205	8668 ± 122	44.4 ± 0.1	5
I1327V+ PHT	−40.4 ± 4.6*	−6.2 ± 0.5	6	−78.3 ± 2.7**	8.6 ± 0.4	9	1044 ± 647	11858 ± 2902	45.4 ± 0.1	5

Table IIIc.2. Phenytoin (100 μM) modulates the biophysical properties of I1327V and WT channels. Values represent means ± S.E.M, n = number of cells, V1/2, voltage of half-maximal activation or inactivation; k, slope factor. Significance was determined by paired Student's T-Test. *P<0.05 to pre-phenytoin condition, **P<0.005 to pre-phenytoin condition.

IV. Aberrant Sodium Channel Currents and Hyperexcitability of Medial Entorhinal Cortex Neurons in a Mouse Model of SCN8A Encephalopathy.

Rationale

In Chapter IV, we electrophysiologically characterize the mEC layer II excitatory neurons from a novel *SCN8A* encephalopathy mouse model. In this study, layer II mEC neurons from both heterozygote (D/+) and homozygote (D/D) mice were studied to determine how a gain-of-function *SCN8A* mutation alters neuronal physiology. This work is a major contribution to the field as it is one of the first studies to examine neuronal hyperexcitability in D/+ mice and the first study to do so in D/D mice. Additionally, we are the first group to describe increases in resurgent sodium current (I_{NaR}) in brain slice neurons from both D/+ and D/D mice. With the help of this novel mouse model, the work in Chapter IV expands our knowledge of *SCN8A* encephalopathy beyond what is possible using cultured cell assays alone. Additionally, the experiments in Chapter IV lay the foundation for future *in vitro* and *in vivo* experiments that will further improve our understanding of *SCN8A* encephalopathy and the ways to treat the disease.

Introduction

In this study, we evaluated the effects of the $Na_v1.6$ N1768D mutation in layer II stellate neurons of the medial entorhinal cortex (mEC) and extended the studies to include both heterozygous and homozygous mutant mice. mEC layer II stellate neurons provide excitatory input to the dentate gyrus and CA3 neurons and elevate circuit excitability in animal models of temporal lobe epilepsy (Kobayashi et al., 2003; Hargus et al., 2011).We observed increased rates of AP firing and proexcitatory changes in Na channel properties of mEC neurons, with larger effects in homozygous mice than in heterozygotes. Changes were observed in neurons from heterozygous mice 1 month before seizure onset. These studies provide insight into the mechanisms by which a gain-of-function mutation in $Na_v1.6$ leads to increased neuronal excitability. Our studies provide support for the region specificity of alterations and suggest that the profound proexcitatory changes observed in mEC neurons increase network drive into the hippocampus, contributing to the development of spontaneous recurrent seizures.

Methods

Animals

Scn8a^{N1768D} knock-in mice were generated as described previously (Jones and Meisler, 2014; Wagnon et al., 2015b). All animal experiments were conducted in accordance with the guidelines established by the National Institutes of Health's Guide for the Care and Use of Laboratory Animals and were approved by the University of Virginia's Institute of Animal Care and Use Committee. The line was maintained by backcrossing to C57BL/6J WT mice (The Jackson Laboratory). Experiments were performed on male and female homozygous D/D mice (*Scn8a*$^{N1768D/N1768D}$), heterozygous D/+ mice (*Scn8a*$^{N1768D/+}$), and WT +/+ littermates at 3 weeks of age. The genotyping assay (Wagnon et al., 2015b) was performed as follows. DNA was isolated from tail biopsies by digestion with 1 mg/ml proteinase K in buffer containing 50 mM KCl, 10 mM Tris-HCl, pH 8.0, and 0.1% Triton X-100. Genotyping used the introduced HincII site in the mutant allele (Jones and Meisler, 2014). A 327 bp genomic fragment of *Scn8a* containing the mutation was amplified by PCR with the primers Tar-F (5-TGACT GCAGC TTGGA CAAGG AGC-3) and Tar-R (5-TCGAT GGTGT TGGGC TTGGG TAC-3). PCR products were digested with HincII and analyzed on 2% agarose gels stained with ethidium bromide. The WT allele generates a single fragment of 327 bp and the mutant allele generates two fragments of 209 and 118 bp.

Brain Slice Preparation and AP Recordings

Please reference Chapter II: General Methods.

Brain Slice Na Channel Electrophysiology

Please reference Chapter II: General Methods.

Immunohistochemistry

WT, D/+, and D/D mice (minimum 3 mice for each genotype) were anesthesized with isoflurane, decapitated, and brains rapidly removed and placed in chilled (4°C) ACSF. Horizontal 500-µm-thick sections were prepared using a Vibratome and transferred to a chamber

containing oxygenated ACSF at 37°C and incubated for 35 min. Slices were then embedded in optimal cutting temperature compound in cryomolds, snap-frozen on dry-ice-chilled isopentane, and kept on dry ice. Cryostat sections (16 μm) were prepared and thawmounted onto Superfrost Plus slides (Fisher Scientific) and stored at 80°C for no longer than 3 days before further processing. Slices were fixed in an ice-cold acetone–ethanol mixture for 5 min, air-dried, washed with KPBS, and then placed for 60 min in KPBS blocking solution (5% fish skin gelatin, 5% normal goat serum, 0.25% Triton X-100, and 0.65% w/v BSA), followed by incubation in blocking solution containing the pair of primary antibodies for 48 h at 4°C (rabbit anti-$Na_v1.6$, 1:500, Alomone Laboratories), and monoclonal mouse anti-Ankyrin G (1:500, NeuroMab). The slides were then washed with KPBS, incubated in blocking solution containing a pair of secondary antibodies (Alexa Fluor 488-conjugated goat anti-mouse IgG and Alexa Fluor 555-conjugated goat anti-rabbit IgG, both at 1:500, both Invitrogen). Slides were washed in KPBS, incubated in nuclear blue (1 drop/ml; Invitrogen), washed, air-dried, and coverslipped in Polymount (Polysciences).

Confocal images were captured of mEC layer II neurons using a Zeiss LSM 710 confocal microscope with a 63x oil-immersion objective and ZEN Zeiss LSM Imaging software. The settings of the laser intensities and image capture were initially optimized but then not changed during the scanning of the slides. Quantification and analysis was performed using ImageJ software. For analysis of $Na_v1.6$ and Ankyrin G immunofluorescence intensity, a line scan representing the length of the AIS as determined by Ankyrin G labeling was drawn and the relative optical density (R.O.D) was determined along the duration of the AIS. To compare the localization of $Na_v1.6$ in the AIS between genotypes, plots of R.O.D along the duration of the AIS for $Na_v1.6$ and Ankyrin G were compared. $Na_v1.6$ expression was compared between genotypes by normalizing $Na_v1.6$ immunofluorescence against that of Ankyrin G for each AIS and the average $Na_v1.6$/Ankyrin G ratio was calculated to determine channel density.

Data Analysis

Please reference Chapter II: General Methods.

Results

Aberrant spike frequency in mEC layer II stellate neurons

Membrane properties were recorded from visually identified mEC layer II stellate neurons (Figure IV.1). In comparison with WT littermates, AP firing frequencies were significantly elevated in D/D and D/+ neurons at current injection steps of 110 pA and 120 pA (Figure IV.1D,E). For example, at 110 pA, the AP firing rate was increased by 3-fold in D/+ neurons (7.6 ± 1.1 Hz, n = 20: P< 0.05) and by 4-fold in D/D neurons (9.6 ± 1.2 Hz, n = 27: P< 0.05) compared with WT neurons (2.2 ± 1.2 Hz, n = 20). At the higher depolarizing current injection steps, we recorded spike frequency adaptation in D/+ and D/D neurons, but not in WT neurons. For example, at 470 pA, the AP firing frequency was 35.9 ± 3.3 Hz (n = 20) in WT neurons and was reduced to 26.9 ± 3.2 Hz (n = 27: P< 0.05) in D/+ and 17.2 ± 1.9 Hz (n = 20: P< 0.05) in D/D neurons (Figure IV.1D–F). Firing frequencies between D/D and D/+ neurons were only significantly different at current injection steps of 460 and 470 pA (P< 0.05; Figure IV.1F).

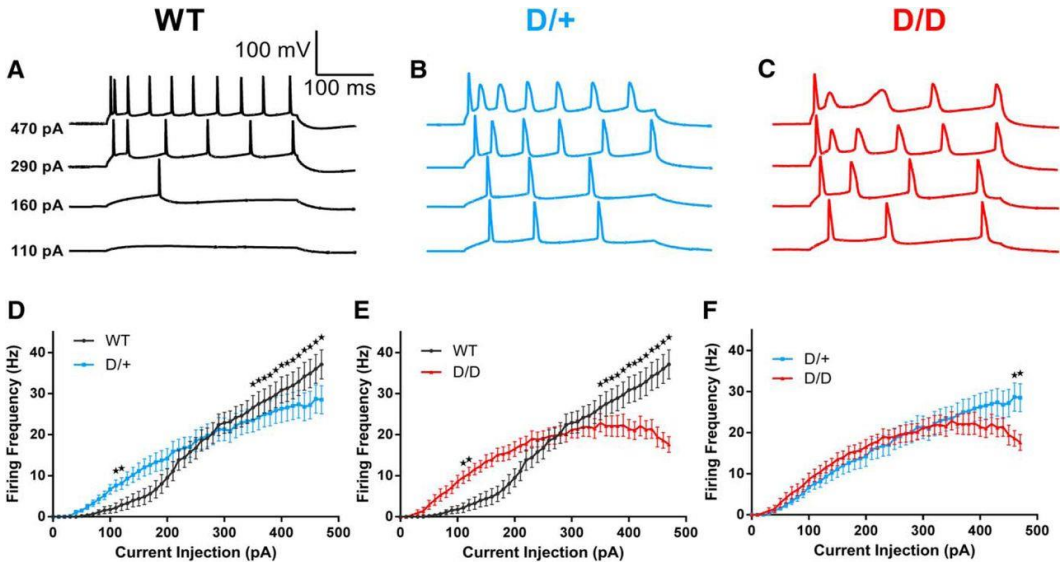

Figure IV.1. Neuronal hyperexcitability of mEC layer II stellate neurons from *Scn8a*^{N1768D} mice. (A–C) Representative traces of spikes elicited by 300 ms current injection steps of increasing current from a holding potential of −65 mV. (D, E) Higher firing rates of D/+ (n = 20) and D/D (n = 21) neurons compared with WT (n = 20) at stimulation <300 pA. (F) Firing rate of D/+ neurons is greater than that of D/D neurons at stimulation >460 pA. Data are shown as means ± SEM. *p < 0.05, two-way ANOVA with *post hoc* Tukey's test for multiple comparisons.

Altered neuronal membrane properties

AP spikes elicited from D/+ and D/D neurons appeared distinct from WT neurons. To quantify the apparent differences in the elicited APs, we measured the membrane properties of

the first three APs evoked at 290 pA, a stimulation intensity that evoked a similar frequency of APs (~21 Hz) in all genotypes (Figure IV.2A_i–C_i). We measured the maximal negative repolarizing voltage between AP spikes (Figure IV.2E). In WT neurons, the maximal hyperpolarizing voltages between AP spikes trended toward more negative voltages after the initial AP spike. For D/+ and D/D neurons, a greater depolarized interspike voltage was recorded immediately after the first spike and remained significantly elevated for all subsequent spikes compared with WT ($P < 0.05$). In addition, D/D neurons showed a significantly depolarized interspike voltage compared with D/+ neurons ($P < 0.05$). These data suggest an increase in depolarizing current in mutant neurons that likely accounts for the increase in firing frequency seen with somatic current injection.

RMP and R_i did not differ between genotypes (Table IV.1). The threshold potential for the first AP was not affected by genotype, but that for the second and third APs was significantly depolarized in D/D neurons compared with WT. Within both the D/+ and D/D genotypes, the AP threshold was significantly depolarized in the second and third APs compared with first AP. In contrast, thresholds in WT neurons did not change with successive APs.

The amplitude of the first AP was elevated in D/+ and D/D neurons compared with WT (Figure IV.2D, Table IV.1), but was reduced in the second AP for the mutant neurons. The amplitude of the third AP remained significantly reduced in D/D neurons compared with WT neurons. Within each genotype, WT neurons showed no significant changes in AP amplitude between the successive APs (Table IV.1). D/+ and D/D neurons showed a significant reduction in AP amplitude when comparing the first AP with the second and third AP spikes. However, when comparing the second and third AP spikes from mutant neurons, AP amplitudes of the third AP were significantly ($P < 0.05$) increased, likely due to the increase in interspike intervals, allowing recovery of some inactivated Na channels. The duration of all three APs measured at 50% (APD_{50}) and 90% (APD_{90}) was significantly increased in the mutant neurons compared with WT ($P < 0.05$: Figure IV.2D, Table IV.1). In addition, APD_{50} and APD_{90} were significantly ($P < 0.05$) increased in D/D neurons compared with D/+ neurons for the second and third elicited APs. Within the D/+ and D/D genotypes, the durations of the second and third AP spikes were more prolonged than the first AP (Figure IV.2B_{ii},C_{ii}, Table IV.1). Again, no significant changes in AP duration for successive APs were detected in WT neurons.

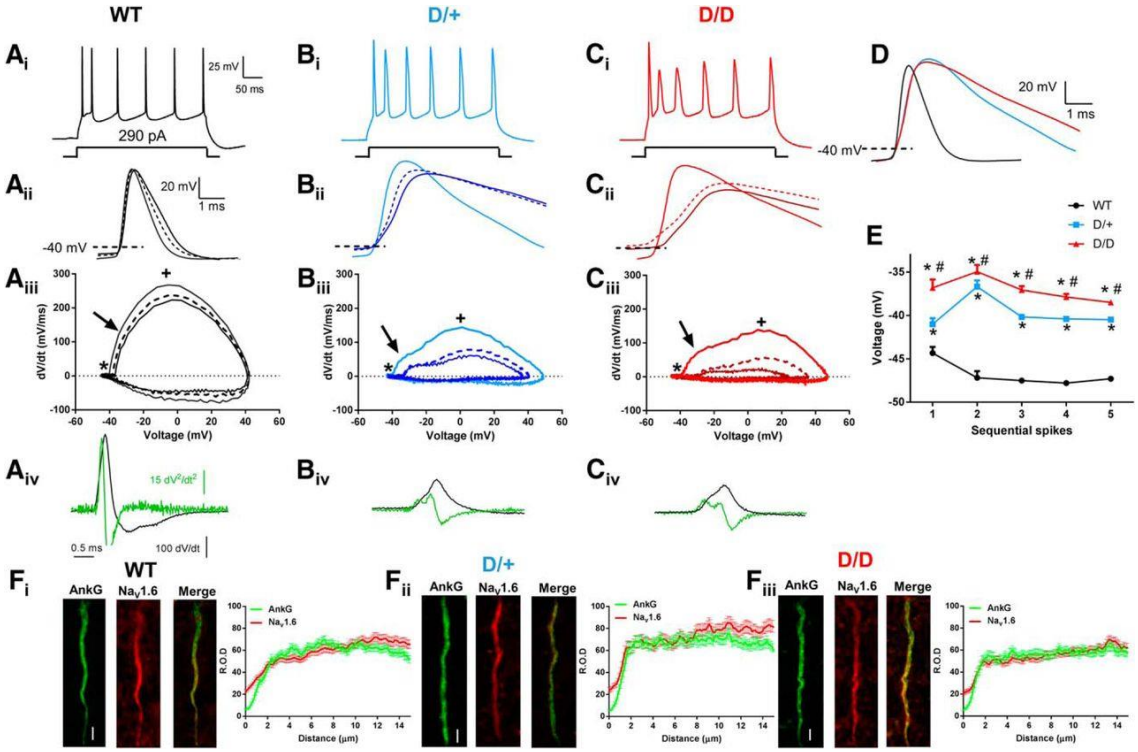

Figure IV.2. Aberrant AP morphology in mutant mEC neurons. (A_i–C_i) AP morphology elicited by a 300 ms depolarizing current injection of 290 pA. (D) Superimposition of the first AP spike elicited by a depolarizing step to 290 pA from WT, D/+, and D/D neurons demonstrating the increase in AP duration in mutant neurons compared with WT. Note the delay in rising and falling phase of the AP in D/+ and D/D neurons. (A_{ii}–C_{ii}) Superimposed traces of the first three AP spikes elicited by injection of 290 pA. The duration of spikes 2 and 3 is extended in the mutant neurons. Solid trace is the first AP, darker traces are the second AP, and broken lines are the third AP. (A_{iii}–C_{iii}) Phase plots of dV/dt vs voltage for the first three AP spikes. *AP thresholds. Arrow indicates inflection of the rising phase of the phase plot indicative of AIS spike initiation; +, maximal conduction velocity as the spike invades the soma. The abrupt rise of dV/dt seen in WT neurons is less pronounced for the first spike in mutant neurons and further slowed for the second and third spikes. (A_{iv}–C_{iv}) First derivative (dV/dt) derived for the first AP spike. The peak of the first derivative is reduced in mutant neurons, indicating a slower upstroke velocity of the AP. Latency between spike initiation at the AIS and invasion into the soma was lengthened in mutant neurons, suggesting slower spike conduction. Second derivatives of the APs (superimposed, green) are also shown. The peaks are clearly discernable for the mutant neurons and are separated by a more pronounced latency. (E) Plot of maximal hyperpolarizing voltages between AP spikes evoked by a 290 pA current injection (WT, n = 20; D/+, n = 20; D/D, n = 21). (F_i–F_{iii}, Left) $Na_v1.6$ expression along the AIS of WT, D/+, and D/D neurons (AnkG, green; $Na_v1.6$, red; Merge; yellow). Right, Graphs showing the localization and R.O.D of AnkG and $Na_v1.6$ (WT, n = 124 from 4 animals; D/+, n = 83 from 3 animals; D/D, n = 100 from 4 animals) staining along the length of the AIS for WT, D/+, and D/D neurons. Scale bars, 2 µm. Data are shown as mean ± SEM. *p < 0.05, one-way ANOVA with *post hoc* Tukey's test for multiple comparisons compared with WT; # p < 0.05 one-way ANOVA with *post hoc* Tukey test for multiple comparisons when D/+ were compared with D/D neurons.

A surprising finding was the slower upstroke velocities for the mutant APs compared with WT (Figure IV.2B_{ii},C_{ii}). When comparing within genotypes, the second and third AP spike upstroke velocities were significantly reduced compared with the first AP. Downstroke velocities in mutant neurons were also dramatically slower compared with WT cells for all three elicited

APs (Figure IV.2B_{ii},C_{ii}). For all genotypes, downstroke velocity was significantly decreased in the second and third APs compared with the first AP.

Phase plots of the first three APs are shown in Figure IV.2, A_{iii}–C_{iii}. The inflections along the rising segment of the phase plots (arrows) result from the axonally initiated spike, which is followed by invasion into the soma and the activation of additional channels there (indicated with a plus sign). In WT neurons, the first inflection representing the AIS spike was less obvious and was continuous with the somatic inflection, suggesting an initiation site close to the soma and a smooth rapid invasion of the spike into the soma. In contrast, AIS inflections were more pronounced in D/+ and D/D neurons, suggesting disrupted backpropagation into the soma (Figure IV.2A_{iii}–C_{iii}). Analysis of the first and second derivatives of the first AP evoked by current injection into the soma further emphasizes the presence of two prominent, but smaller peaks representing the AIS and somatic spikes in D/+ and D/D neurons (Figure IV.2B_{iv}–C_{iv}). The latency between the two peaks (τ_{del}) was measured from the second derivative and was significantly longer in both D/+ neurons (0.35 ± 0.02 ms, $P < 0.05$; n = 16) and D/D neurons (0.42 ± 0.03 ms, $P < 0.05$; n = 17) compared with WT neurons (0.05 ± 0.01 ms; n = 15). A delay in the axosomatic spike has been suggested previously to indicate a change in the spike initiation site to more distal sites from the soma (Royeck et al., 2008). To determine whether $Na_v1.6$ expression along the AIS was different in the mutant neurons compared with WT, immunofluorescence experiments were performed (Figure IV.2F_i–F_{iii}). Robust $Na_v1.6$ staining was observed at the AIS and was colocalized with Ankyrin G staining, a marker for the AIS. No

	RMP, mV	R_i, MΩ	Threshold, mV	Amplitude, mV	APD_{50}, ms	APD_{90}, ms	Upstroke velocity, mV/ms	Downstroke velocity, mV/ms	*n*
1st AP									
WT	−65.8 ± 1.1	111.8 ± 10.9	−40.4 ± 1.4	42.1 ± 1.7	0.8 ± 0.1	2.5 ± 0.1	268.0 ± 9.1	−77.5 ± 3.5	20
D/+	−66.1 ± 1.2	112.6 ± 11.2	−41.3 ± 4.2	47.3 ± 1.4[a]	2.5 ± 0.2[a]	7.1 ± 0.7[a]	190.2 ± 19.4[a]	−34.6 ± 2.2[a]	20
D/D	−65.7 ± 2.1	110.7 ± 13.2	−41.6 ± 1.2	46.4 ± 1.3[a]	3.3 ± 0.2[a,b]	9.6 ± 1.2[a]	168.6 ± 5.8[a,b]	−21.4 ± 2.7[a,b]	21
2nd AP									
WT			−37.4 ± 0.9	40.9 ± 0.9	1.4 ± 0.1	2.9 ± 0.1	218.0 ± 10.2[c]	−48.6 ± 2.5[c]	20
D/+			−36.5 ± 1.1[c]	33.6 ± 2.9[a,c]	4.8 ± 0.8[a,c]	8.7 ± 0.7[a,c]	100.2 ± 22.0[a,c]	−19.2 ± 2.9[a,c]	20
D/D			−32.8 ± 1.8[a,c]	25.4 ± 0.9[a,b,c]	7.7 ± 0.5[a,b,c]	14.4 ± 1.2[a,b,c]	55.6 ± 7.1[a,b,c]	−12.8 ± 2.6[a,b,c]	21
3rd AP									
WT			−37.9 ± 0.9	41.4 ± 2.7	1.3 ± 0.8	2.9 ± 0.2	229.7 ± 11.8[c]	−59.3 ± 1.2[c]	20
D/+			−35.9 ± 1.7[c]	38.3 ± 1.8[c,d]	5.2 ± 0.6[a,c]	9.7 ± 1.7[a,c]	98.5 ± 17.9[a,c]	−19.0 ± 1.9[a,c]	20
D/D			−31.1 ± 1.1[a,b,c]	32.9 ± 1.1[a,b,c,d]	8.2 ± 1.7[a,b,c]	14.1 ± 1.8[a,b,c]	53.7 ± 7.1[a,b,c]	−13.0 ± 3.5[a,b,c]	21

Table IV.1. Membrane properties of WT, D/+, and D/D mEC layer II stellate neurons. Values represent mean ± SEM. n = number of cells. [a]$p < 0.05$ versus WT neurons. [b]$p < 0.05$ D/+ versus D/D. [c]$p < 0.05$ 1st AP versus 2nd and 3rd APs within the same genotype. [d]$p < 0.05$ 2nd versus 3rd AP within the same genotype.

differences in staining pattern were detected between any of the genotypes along the AIS, suggesting a similar expression profile of $Na_v1.6$ in all three genotypes.

Synaptically evoked AP bursting in N1768D mutant mice

Brief stimulation of the deep layers of the mEC evoked a single AP spike in mEC layer II stellate neurons of all three genotypes (1T; Figure IV.3A–C). However, increasing the stimulation intensity above AP threshold to twofold (2T) or threefold (3T) evoked multiple AP spikes in D/+ neurons (n = 21) and D/D neurons (n = 20), but not in WT neurons (n = 20; Figure IV.3A–D). Significantly more spikes were evoked in D/D neurons than in D/+ neurons (P< 0.05).

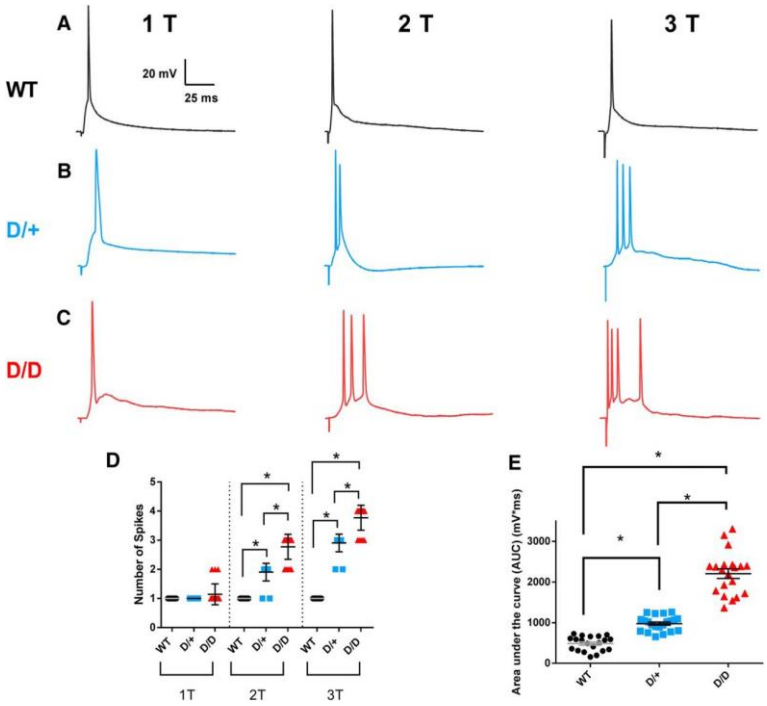

Figure IV.3. Synaptic stimulation of mutant mEC neurons elicits burst firing and prolonged depolarization. (A–C) mEC deep layers were briefly stimulated at the AP threshold (1T), at twice the threshold value (2T), and at three times the threshold (3T). AP firing was measured in WT (n = 20), D/+ (n = 21), and D/D neurons (n = 22). Bursts of APs were elicited in the mutant neurons in response to 2T and 3T stimulation. (D) AP frequency in response to increasing stimulation intensity. (E) AUC for APs evoked at 1T stimulation is greater for D/D neurons than for D/+ or WT neurons. Data are shown as mean ± SEM. *p < 0.05, one-way ANOVA with *post hoc* Tukey's test for multiple comparisons.

In addition to bursting, synaptically evoked responses produced longer depolarizations in D/+ and D/D neurons than in WT neurons. Analysis of evoked APs revealed an increase in the duration of the depolarizing event from 59.6 ± 5.9 ms (n = 20) in WT neurons to 110.7 ± 6.1 ms (n = 21: P< 0.05) in D/+ neurons and further to 176.1 ± 11.5 ms (n = 20: P< 0.05) in D/D neurons. The evoked responses in D/D neurons had significantly longer durations than those in D/+ neurons. Analysis of the area under the evoked response curve (AUC) at T1 revealed a 2-fold to 4-fold increase in D/+ neurons (n = 21: P< 0.05) and D/D neurons (n = 20: P< 0.05) compared with WT (n = 20) (Figure IV.3E). D/D neurons also had a significant increase in AUC at T1 stimulation compared with D/+ cells (P<

0.05). Similar increases in mutant neurons were also seen at T2 and T3 stimulation (data not shown).

I_{NaP} and I_{NaR} currents are elevated in mutant neurons

I_{NaP} currents are thought to be major contributors to the generation of high-frequency AP firing. Elevated I_{NaP} has been recorded in neurons from human patients and animal models of epilepsy (Vreugdenhil et al., 2004; Stafstrom, 2007; Hargus et al., 2011, 2013) and the N1768D channel generates elevated persistent current in transfected cells (Veeramah et al., 2012) and in hippocampal neurons (Lopez-Santiago et al., 2017). To determine whether I_{NaP} currents were increased in mEC layer II stellate neurons from the N1768D mutant mice, voltage ramps were applied in brain slice preparations. Ramp voltage recordings displayed an inward current that was completely abolished by the application of 1 μM TTX (Figure IV.4A–C). The peak I_{NaP} current amplitude was determined by subtracting traces obtained in the presence of TTX from those obtained in its absence. I_{NaP} currents in WT littermates had

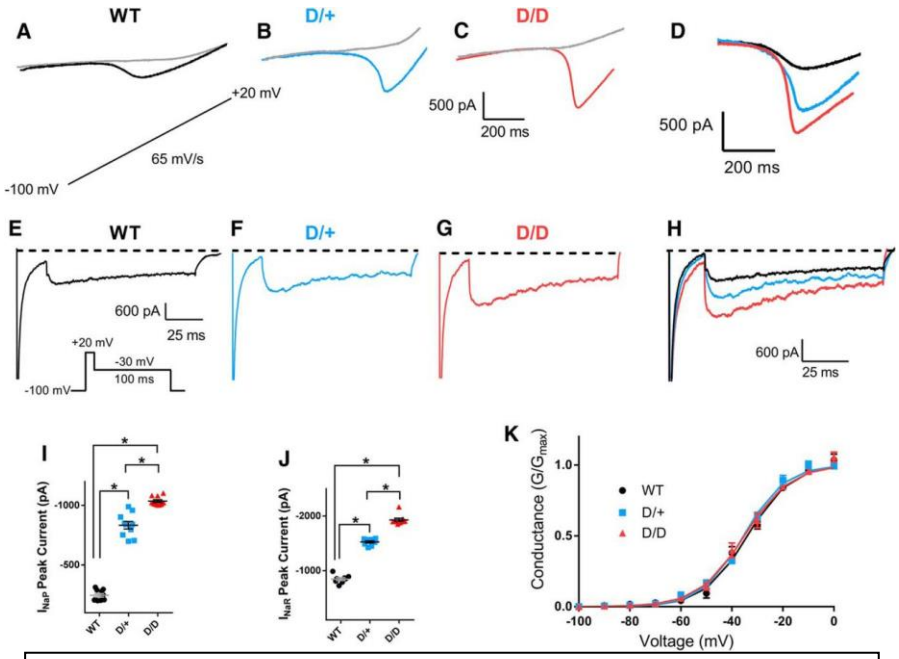

Figure IV.4. I_{NaP} and I_{NaR} Na channel currents are increased in N1768D mutant mEC layer II stellate neurons. Using recording solutions designed to reduce other types of inward and outward currents, voltage ramps were applied at a rate of 65 mV/s (inset) to elicit I_{NaP} currents. All I_{NaP} currents were abolished in the presence of 1 μm TTX (gray traces). Amplitudes of I_{NaP} currents were obtained by taking the original trace and subtracting from it the trace recorded in the presence of TTX (1 μm). (A–C) I_{NaP} recordings from WT, D/+, and D/D mEC neurons. (D) Superimposition of TTX subtracted I_{NaP} amplitudes for the three genotypes. (E–G) I_{NaR} recordings from WT, D/+, and D/D mEC neurons. I_{NaR} currents were recorded using the indicated voltage protocol. Traces shown were obtained after subtracting traces recorded in the presence of TTX (1 μm). (H) Superimposition of I_{NaR} of the three genotypes. (I) Peak I_{NaP} currents in WT (n = 10), D/+ (n = 10), and D/D (n = 10) mEC neurons. (J) Peak I_{NaR} currents in WT (n = 8), D/+ (n = 9), and D/D (n = 9) mEC neurons. (K) Voltage dependence of I_{NaR} activation revealed no significant shifts in $V_{1/2}$ or k. Smooth lines correspond to the least-squares fit when average data were fit to a single Boltzmann equation. Data are shown as mean ± SEM. *p < 0.05, one-way ANOVA with *post hoc* Tukey's test for multiple comparisons.

amplitudes of -247 ± 14 pA (n = 10). Amplitudes were significantly higher in both D/+ neurons (-834 ± 6 pA; n = 10: P< 0.05) and D/D neurons (-1037 ± 12 pA; n = 10: P< 0.05). I_{NaP} currents were larger in D/D than in D/+ neurons (P< 0.05) (Figure IV.4D,I). Conductance plots of I_{NaP} currents revealed no significant differences in activation parameters (data not shown).

I_{NaR} currents are slow inactivating depolarizing currents that can contribute to increased AP frequency and burst firing (Raman and Bean, 1997). Peak I_{NaR} currents were significantly elevated in D/+ neurons (-1522 ± 22 pA; n = 9: P< 0.05) and D/D neurons (-1936 ± 34 pA; n = 9: P< 0.05) compared with WT (-847 ± 27 pA; n = 10; Figure IV.4E–H,J). In a similar manner to I_{NaP} currents, I_{NaR} current amplitudes were also larger in D/D than in D/+ neurons (P< 0.05; Figure IV.4H,J), demonstrating the greater deleterious effect of two copies of the mutant channel and the absence of WT channel. The properties of I_{NaR} activation were not altered in any of the mice (Figure IV.4K).

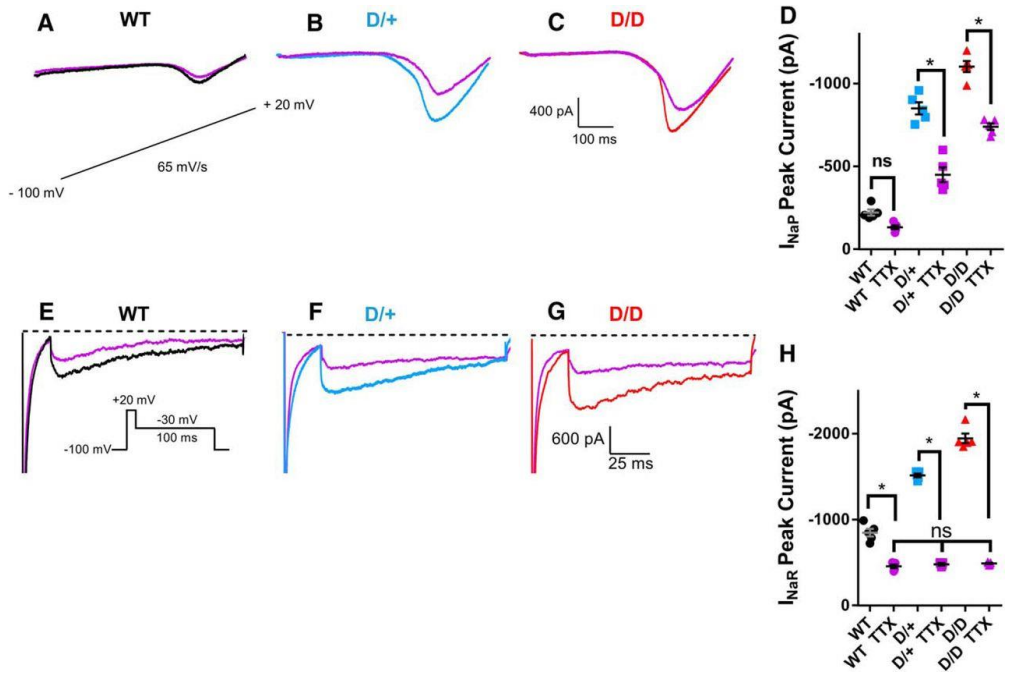

Figure IV.5. TTX (30 nm) decreases I_{NaP} and I_{NaR} currents. (A–C) I_{NaP} currents were elicited by applying a voltage ramp at a rate of 65 mV/s before (WT, black; D/+, blue; D/D, red) and after application of TTX (30 nm; purple traces for all genotypes). Traces shown are those obtained after subtracting traces recorded in the presence of TTX (1 μm). (D) Scatter plot of I_{NaP} peak amplitudes before and after the application of TTX (30 nm) (WT, n = 5; D/+, n = 5; D/D, n = 5). (E–G) I_{NaR} measured before (WT, black; D/+, blue; D/D, red) and after the application of TTX (30 nm; purple traces for all the genotypes). (H) Scatter plot of I_{NaR} current peak amplitude before and after the presence of TTX (30 nm) (WT, n = 6; D/+, n = 6; D/D, n = 5). Data are shown as mean ± SEM. *p < 0.05, one-way ANOVA with *post hoc* Tukey's test for multiple comparisons.

Effects of TTX (30 nM) on I_{NaR} and I_{NaP} currents

Elevated I_{NaR} and I_{NaP} currents could account for increased firing frequencies, AP burst firing upon synaptic stimulation and greater depolarized inter spike voltages observed in D/+ and

D/D neurons. Low concentrations of TTX have been shown to reduce spike afterdepolarized potentials (ADPs) without affecting properties of the fast spike (Yue et al., 2005). To test the specific contributions of I_{NaR} and I_{NaP} to the aberrant AP morphology observed in mutant neurons, we first determined the effects of 30 nM TTX on I_{NaR} and I_{NaP} currents (Figure IV.5) and then determined the effects of reducing I_{NaR} and I_{NaP} currents on AP spikes (Figure IV.6). TTX (30 nM) caused a small decrease in I_{NaP} peak current in WT neurons, but this did not reach significance (Figure IV.5A,D). In contrast, TTX (30 nM) caused a significant reduction in both D/+ (by 47%) and D/D (by 35%) I_{NaP} peak currents (Figure IV.5B–D). In the presence of TTX, I_{NaP} currents remained significantly ($P< 0.05$) increased in D/+ and D/D neurons compared with WT and between D/+ and D/D neurons ($P< 0.05$). For I_{NaR} currents, TTX (30 nM) significantly reduced I_{NaR} peak currents in all three

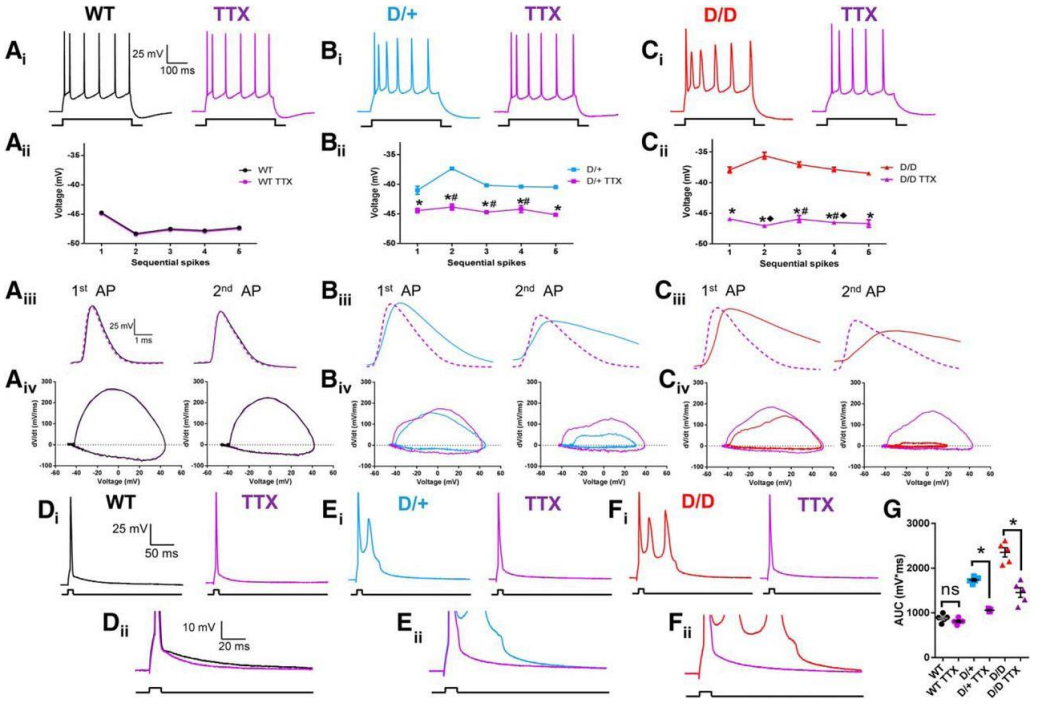

Figure IV.6. TTX (30 nm) increases upstroke velocity and decreases AP duration in D/+ and D/D neurons. (A_i–C_i) APs elicited by a 300 ms current injection pulse of 290 pA before (WT, black; D/+, blue; D/D, red) and after application of TTX (30 nm; purple traces for all genotypes). (A_{ii}–C_{ii}) Plot of maximal hyperpolarizing voltages between AP spikes evoked by a 290 pA current injection before and after the application of TTX (30 nm) (WT, n = 10; D/+, n = 11; D/D, n = 13). (A_{iii}–C_{iii}) Superimposed traces of the first two AP spikes elicited by injection of 290 pA (WT, black; D/+, blue; D/D, red) and after application of TTX (30 nm; purple traces for all genotypes). (A_{iv}–C_{iv}) Superimposed phase plots of the first two elicited APs before (WT, black; D/+, blue; D/D, red) and after application of TTX (30 nm; purple traces for all genotypes). (D_i–F_i) AP spikes elicited by a brief (4 ms) injection of suprathreshold current injection before (WT, black; D/+, blue; D/D, red) and after application of TTX (30; purple traces for all genotypes). (D_{ii}–F_{ii}) Superimposed traces of AP spikes shown in D_i–F_i.(G) Scatter plot showing the AUC for AP spikes elicited by a brief (4 ms) current injection pulse before and after the application of TTX (30 nm) (WT, n = 5; D/+, n = 5; D/D, n = 5). Data are shown as mean ± SEM. *p < 0.05, one-way ANOVA with *post hoc* Tukey's test for multiple comparisons comparing with the pre-TTX condition. ♦p < 0.05, one-way ANOVA with *post hoc* Tukey's test for multiple comparisons comparing D/D + TTX with D/+ + TTX. #p < 0.05, one-way ANOVA with *post hoc* Tukey's test for multiple comparisons comparing WT + TTX.

genotypes ($P < 0.05$; Figure IV.5E–H). In the presence of TTX, I_{NaR} currents were not significantly different between WT and mutant neurons.

Effects of TTX (30 nM) on AP spikes

To determine the effects of reducing I_{NaP} and I_{NaR} currents on AP spike properties, we applied low concentrations of TTX (30 nM) and examined APs evoked at a current injection step of 290 pA, a level in which all three genotypes fire spikes at the same frequency. TTX (30 nM) had no effect on AP firing frequency in WT or D/+ neurons, but did significantly increase firing frequency of D/D neurons at current injection steps at 460 and 470 pA, reducing the extent of spike frequency adaptation (data not shown). TTX also had no effect on WT AP spike properties (Table IV.2). In contrast, TTX resulted in a more negative maximal repolarizing voltage potential between AP spikes of D/+ and D/D neurons, but many voltage potentials remained significantly more depolarized than WT (Figure IV.6B_{ii},C_{ii}). Furthermore, TTX increased the upstroke and downstroke velocities of the first and second AP spikes elicited in D/+ and D/D mEC neurons, reducing AP duration (Figure IV.6B_{iii}–C_{iii}, Table IV.2). AP amplitudes were also increased in the second AP spike for both D/+ and D/D neurons. Phase plots of the effects of TTX on all three genotypes are shown in Figure IV.6, A_{iv}–C_{iv}, where a small, but significant rescue of AP morphology can be seen in D/+ and D/D neurons. Low-concentration TTX has been shown to reduce ADPs that drive spike bursting in CA1 neurons (Yue et al., 2005). We evoked AP spikes using a brief, 4 ms suprathreshold current injection pulse (Figure IV.6D–F). In WT neurons, the brief pulse elicited a single AP spike. In contrast, the brief pulse elicited burst firing in D/+ and D/D neurons. TTX (30 nM) had no effect on AP spikes in WT neurons, but eliminated burst firing in D/+ and D/D neurons, resulting in only a single AP being elicited in response to stimulation. Analysis of the AUC for spikes evoked showed significant decreases after application of TTX (30 nM; Figure IV.2G), further supporting a major role for Na channel currents in driving burst epileptiform activity in these neurons.

Altered Na channel physiology

Previous evaluation of N1768D in transfected cells overexpressing the mutant channel revealed altered Na channel gating properties (Veeramah et al., 2012). To determine whether these alterations are seen when the mutant channel is expressed at a physiological level in

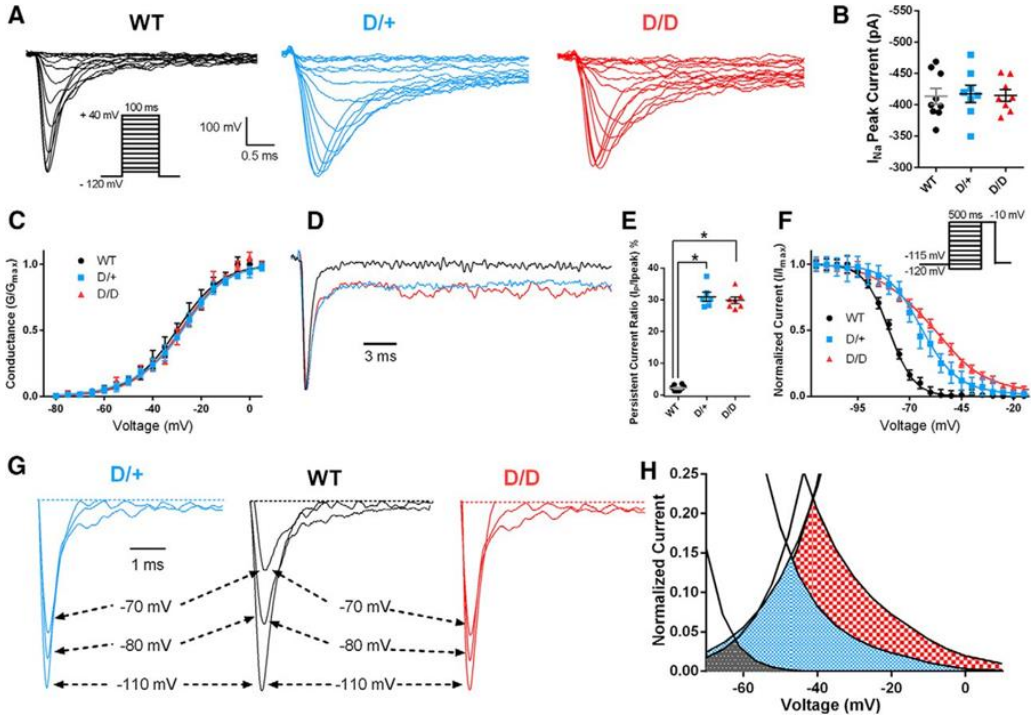

Figure IV.7. Altered Na channel currents in mutant mEC neurons. (A) Representative current traces recorded using the outside-out patch-clamp configuration for WT, D/+, and D/D mEC layer II stellate neurons. (B) Scatter plot of peak I_{Na} current from WT (n = 9), D/+ (n = 8), and D/D (n = 8) mEC neurons. (C) Voltage dependence of channel activation for WT (n = 9), D/+ (n = 7), and D/D (n = 6) mEC neurons. Lines correspond to the least-squares fit when average data were fit to a single Boltzmann equation. (D) Representative normalized current traces recorded during a 100 ms depolarizing pulse from a holding potential of −120 mV to −10 mV demonstrates elevated persistent Na current in mutant neurons. (E) Ratio of $I_{Persistent}/I_{peak}$ current 100 ms after stimulation in WT (n = 9), D/+ (n = 7), and D/D (n = 6) mEC neurons. (F) Voltage dependence of channel inactivation for WT (n = 7), D/+ (n = 7), and D/D (n = 9) neurons. Lines correspond to the least-squares fit when average data were fit to a single Boltzmann equation. (G) Representative steady-state inactivation traces elicited after prepulses to −110 mV, −80 mV, and −70 mV. Note the delay in channel inactivation for D/+ and D/D neurons compared with WT, indicating severe impairment of channel inactivation. (H) Window current obtained by overlapping normalized activation and inactivation curves. Window current is elevated in D/+ (blue shaded area) and D/D (red checkered area) compared with WT (black shaded area) neurons. The voltage range for the window current is also shifted in a depolarizing direction. Data are shown as mean ± SEM. *p < 0.05, one-way ANOVA with *post hoc* Tukey's test for multiple comparisons.

neurons, Na channel currents were recorded using outside-out patches from visually identified mEC layer II stellate neurons in brain slice preparations (Figure IV.7). Representative macroscopic Na currents are shown in Figure IV.7A. Na channel current densities from outside-out recordings were not significantly different between genotypes (Figure IV.7B). Analysis of I–V curves revealed no significant shifts in the voltage at half maximal activation ($V_{1/2}$) or the slope factor (k) (Figure IV.7C, Table IV.3). A frequent feature of $Na_v1.6$ gain-of-function mutations is the presence of a persistent/noninactivating Na current after prolonged depolarizations (Veeramah et al., 2012; Wagnon and Meisler, 2015; Wagnon et al., 2015a;

Meisler et al., 2016). Both D/+ and D/D neurons had significantly elevated persistent/noninactivating Na channel currents after a prolonged depolarization step from -100 mV to -10 mV for 100 ms (Figure IV.7D,E, Table IV.3). In contrast to the normal activation gating parameters, a significant depolarizing shift in the $V_{1/2}$ of steady-state inactivation was detected in D/+ (12.9 mV) and D/D (17.3 mV) neurons compared with WT (Figure IV.7F,G, Table IV.3). k was also significantly increased in D/+ and D/D neurons (Table IV.3). Window currents were determined from the area under the overlapping normalized activation and inactivation curves (Figure IV.7H). Window currents for D/+ and D/D neurons were increased by 7-fold and 12-fold, respectively, and were persistent over a greater voltage range than WT.

	RMP, mV	R_i, MΩ	Threshold, mV	Amplitude, mV	APD_{50}, ms	APD_{90}, ms	Upstroke velocity, mV/ms	Downstroke velocity, mV/ms	*n*
1st AP									
WT	−66.9 ± 1.1	113.8 ± 11.2	−41.3 ± 1.3	43.5 ± 1.8	1.1 ± 0.2	2.4 ± 0.5	266.0 ± 7.0	−78.1 ± 1.2	10
+TTX	−65.3 ± 2.1	109.8 ± 10.2	−42.0 ± 1.0	44.0 ± 1.7	1.2 ± 0.1	2.3 ± 0.2	262.9 ± 2.8	−75.3 ± 1.9	10
D/+	−65.1 ± 1.0	110.4 ± 10.2	−42.6 ± 5.5	46.3 ± 1.5	2.8 ± 0.5	7.8 ± 0.2	185.5 ± 5.5	−40.5 ± 1.2	11
+TTX	−65.4 ± 1.0	114.6 ± 12.1	−43.5 ± 1.2	45.5 ± 0.8	1.9 ± 0.1[a]	4.5 ± 0.5[a]	199.0 ± 2.1[a]	−51.2 ± 1.0[a]	11
D/D	−64.8 ± 1.2	111.8 ± 12.2	−40.9 ± 1.0	47.1 ± 2.1	4.0 ± 1.0	10.8 ± 0.1	156.8 ± 1.3	−20.1 ± 1.7	13
+TTX	−65.8 ± 1.2	109.7 ± 9.2	−42.0 ± 2.1	46.9 ± 2.1	2.7 ± 0.1[b]	6.5 ± 1.0[b]	198.1 ± 1.1[b]	−41.1 ± 1.0[b]	13
2nd AP									
WT			−38.2 ± 1.0	41.0 ± 0.9	1.6 ± 0.5	3.0 ± 1.2	210.2 ± 5.2	−44.9 ± 1.0	10
+TTX			−38.5 ± 1.5	41.2 ± 1.9	1.5 ± 0.2	3.1 ± 0.3	209.9 ± 7.2	−43.8 ± 1.2	10
D/+			−35.5 ± 2.6	30.9 ± 1.0	4.0 ± 0.5	9.5 ± 1.3	99.1 ± 12.0	−18.3 ± 0.5	11
+TTX			−37.5 ± 1.9	38.9 ± 1.0[a]	2.7 ± 0.1[a]	7.0 ± 1.1[a]	150.1 ± 8.0[a]	−29.0 ± 0.8[a]	11
D/D			−30.8 ± 1.2	22.1 ± 1.8	6.5 ± 1.3	16.8 ± 1.4	45.9 ± 1.9	−10.9 ± 0.5	13
+TTX			−36.8 ± 1.0[b]	38.1 ± 2.3[b]	3.5 ± 0.3[b]	8.5 ± 0.4[b]	142.9 ± 2.6[b]	−20.9 ± 0.3[b]	13

Table IV.2. Effects of TTX (30 nm) on AP spikes. Values represent mean ± SEM. n = number of cells. [a]$p < 0.05$ D/+ versus D/+ in presence of 30 nm TTX. [b]$p < 0.05$ D/D versus D/D in presence of 30 nm TTX.

Discussion

In this study, we investigated the mechanisms by which the $Na_v1.6$ gain-of-function mutation N1768D leads to neuronal hyperexcitability, the hallmark of spontaneous seizures. Our studies reveal several new findings. First, we show that mEC layer II stellate neurons in D/+ and D/D mice are hyperexcitable, firing a greater number of AP spikes upon current injection than WT littermates, which is not the case for hippocampal or neocortical neurons (Lopez-Santiago et al., 2017). For D/+ mice, the increase in excitability of mEC neurons precedes the onset of seizures by >1 month.

Second, AP spike morphology was strikingly aberrant in D/+ and D/D mEC neurons, a finding that was not observed when the mutation was overexpressed in cultured hippocampal neurons (Veeramah et al., 2012) or in CA3 and cortex layer 2/3 neurons of D/+ mice (Lopez-Santiago et al., 2017). The most obvious abnormality was the increased spike width and slower upstroke velocity in mutant neurons. Sodium entry occurs mainly during the upstroke of the AP, with much less entry during the repolarization phase (Carter and Bean, 2009). The incomplete Na channel inactivation during the falling phase of the AP in mutant neurons would have three effects: (1) continued Na entry into the cell, increasing as the membrane potential moved further from the equilibrium potential for Na and thus providing a sustained depolarizing current during spike trains; (2) opposition to repolarizing potassium currents, thus lengthening the refractory period; and (3) accumulation of inactivated Na channels with subsequent spikes as a result of a greater depolarized interspike voltages. We report here that AP duration was significantly increased in both D/+ and D/D mEC neurons compared with WT, a finding that was also seen in CA1 neurons, but not in CA3 or neocortex neurons (Lopez-Santiago et al., 2017). Application of low-concentration TTX (30 nM) significantly reduced the interspike repolarization voltages, increased upstroke velocity, and reduced AP duration in mutant neurons. A likely explanation for these observations is that block of Na channel currents, particularly I_{NaP} and I_{NaR} currents, reduces persistent depolarizing current, hyperpolarizes the interspike voltage potentials, and allows recovery of Na channels inactivated after the first spike. These channels would be available and contribute to increasing upstroke velocity of the second and third spikes. A reduction in the depolarizing Na current due to TTX inhibition would also provide less opposition to repolarizing potassium currents, further enhancing repolarization and reducing AP duration.

Third, we show for the first time that neuronal resurgent (I_{NaR}) currents are increased as a result of the gain-of-function mutation in $Na_v1.6$. I_{NaR} currents are slow-inactivating currents that contribute to enhanced firing frequency and the generation of burst firing. I_{NaR} currents generate

	Activation			Inactivation			Persistent current	
	$V_{1/2}$	k	n	$V_{1/2}$	k	n	Ratio ($I_{persistent}/I_{peak}$)%	n
WT	-30.4 ± 1.4	-7.3 ± 0.2	9	-75.5 ± 1.5	6.1 ± 0.3	7	1.1 ± 0.5	9
D/+	-31.0 ± 2.3	-7.8 ± 0.7	7	-62.6 ± 2.3^{a}	13.5 ± 1.3^{a}	7	31.1 ± 0.5^{a}	7
D/D	-30.5 ± 1.4	-7.9 ± 0.4	6	$-58.2 \pm 1.9^{a,b}$	$17.6 \pm 1.3^{a,b}$	9	32.1 ± 0.1^{a}	6

Table IV.3. Na channel physiology in WT, D/+, and D/D mEC layer II stellate neurons. Values represent mean ± SEM. n = number of cells. [a]$p < 0.05$ versus WT. [b]$p < 0.05$ D/+ versus D/D neurons.

strong regenerative depolarizing currents that contribute to elevated spike frequency (Raman and Bean, 1997; Yue et al., 2005). Increased I_{NaR} currents are predicted to provide excessive depolarizing current that would significantly increase the firing frequency of mutant neurons and the excitatory drive into neuronal circuits (Yamada-Hanff and Bean, 2013). An increase in I_{NaR} currents was recently reported in cultured cells expressing two missense mutations of $Na_v1.6$, including N1768D (Patel et al., 2016), further supporting the importance of this current in epilepsy.

We evoked APs either by somatic depolarization or stimulation of presynaptic inputs. Somatic depolarization caused premature mature AP initiation and increased frequency of AP firing at lower current injection steps in mutant neurons. At greater depolarizations, a reduction in AP frequency was observed in the mutant neurons, likely due to an accumulation of noninactivating Na channels and the impaired recovery of completely inactivated channels as interspike membrane voltages remained depolarized. In support of this, low concentrations of TTX (30 nM) increased firing frequencies of D/D neurons at high stimulation intensities (460 and 470 pA). A surprising finding was the similar firing frequency of D/+ and D/D neurons except at very high current injection levels, where adaptation was more pronounced in D/D neurons. This was unexpected because I_{NaP} and I_{NaR} currents recorded from the soma were larger in D/D than in D/+ neurons and the greater rightward shift in the inactivation curve produced larger window currents in D/D neurons. Together, these events significantly increase the availability of a depolarizing current for spike initiation at earlier depolarizing steps in D/D neurons. However, a consequence of sustained depolarizations at greater depolarizing steps is the increase in the proportion of completely inactivated Na channels that would limit Na channel availability for spike initiation at high firing frequencies. In contrast, synaptically evoked responses were significantly different, with D/D neurons evoking longer depolarizing events and greater bursts of AP spikes than D/+ neurons. WT neurons fired only single spikes even at high stimulation intensities. The presence of mutant $Na_v1.6$ channels in dendrites (Caldwell et al., 2000) may account for these differences. Activation of the inactivation deficient mutant channel along dendrites would amplify synaptic events, initiating regenerative spikes and increasing the probability of reaching spike threshold at the AIS.

A striking feature of neurons expressing the $Na_v1.6$ gain-of-function mutation is the profound increase in I_{NaP} and I_{NaR}, both of which are important in the regulation of firing

frequency and burst firing (Raman and Bean, 1997; Yue et al., 2005). Increases in I_{NaP} and I_{NaR} have been reported in neurons from human patients (Vreugdenhil et al., 2004) and animal models of acquired epilepsy (Hargus et al., 2011, 2013). Several studies of EIEE13 mutations in cultured cells reported increased noninactivating persistent Na current after prolonged depolarizations (Veeramah et al., 2012; Estacion et al., 2014; Wagnon et al., 2015a). Increased persistent currents were recently reported in hippocampal inhibitory and excitatory neurons of D/+ mice (Lopez-Santiago et al., 2017). We observed a clear, sustained increase in persistent current after prolonged depolarization of mutant neurons. An increase in I_{NaP} and I_{NaR} currents could cause proexcitatory changes in AP morphology, driving intrinsic bursting and sustaining neuronal hyperexcitability in mutant mice. Low concentrations of TTX inhibited both I_{NaP} and I_{NaR} and ameliorated abnormal AP morphology in D/+ and D/D neurons, as well as inhibiting AP burst firing elicited by brief stimulation pulses. These findings further support the importance of these currents in driving spike bursting (Yue et al., 2005).

We focused on mEC layer II stellate neurons because of their role in the excitation of hippocampal neurons. They have also been implicated in the initiation and propagation of epileptic seizures in models of temporal lobe epilepsy (Kobayashi et al., 2003). We observed profound proexcitatory alterations in mEC neurons, including increased spike amplitudes, slower upstroke velocities, and depolarizing shifts in Na channel inactivation parameters, all of which were not reported in hippocampal or neocortical neurons (Lopez-Santiago et al., 2017), further supporting brain region- and circuit-level specificity of the effects of this gain-of-function mutation. The properties of four classes of excitatory neurons from the D/+ mouse are compared in Table IV.4. Because mEC neurons relay excitatory inputs to the dentate gyrus and CA3 via the perforant and temporoammonic pathways (Witter et al., 1989), increased spiking frequency of mEC neurons would provide excessive

	mEC	CA1	CA3	Cortex 2/3
I_{NaP}	↑	↑	↑	ND
I_{NaR}	↑	ND	ND	ND
Inactivation $V_{1/2}$	↑	=	=	=
Maximum firing frequency	↑	↓	=	=
Synaptic evoked	↑	ND	ND	ND
Spontaneous firing	=	↑	↑	=
Upstroke velocity	↓	=	=	=
AP amplitude	↑	=	=	=
AP threshold	↓	=	=	=
AP duration	↑	↑	=	=

Figure IV.4. Different effects of the *SCN8A*-N1768D mutation in three classes of excitatory neurons

excitatory input into the dentate gyrus and CA3 and further exacerbate an already hyperexcitable hippocampal circuit (Kobayashi et al., 2003).

The axon initial segment is the site of AP initiation (Rasband, 2010). During early mouse development, the AIS is first occupied by $Na_v1.2$, which is replaced by $Na_v1.6$ between 2 and 3 weeks of age (Boiko et al., 2001). This developmental profile may account for the onset of seizures in D/D mice at 3 weeks of age. Seizure onset in patients with *SCN8A* mutations ranges from 0 to 18 months and in utero seizures have been reported, suggesting that human $Na_v1.6$ may populate the AIS before birth (Singh et al., 2015).

A surprising finding was the observation of proexcitatory alterations in mEC neurons from D/+ mice more than a month before the onset of seizures. The delay may be explained by a requirement for activation of additional neurons and circuits that require additional time to mature into an epileptic state. Alternatively, seizure onset may require the higher levels of I_{NaP}, I_{NaR}, and window currents in mEC neurons that occur earlier in D/D mice to prime the epileptic circuit for seizure initiation. Further studies to explore epileptogenic circuits and key sites of seizure onset in this model of EIEE13 will be informative.

The N1768D mutation was identified in a heterozygous individual with EIEE13 and was first characterized using ND7/23 cells and cultured hippocampal neurons (Veeramah et al., 2012). We demonstrate that mutant neurons from the knock-in mouse model exhibit several of the abnormalities described in the transfected cells, including impaired channel inactivation, increased persistent current, and elevated firing rates. Our studies also provide new mechanistic information. The significant increases in two major Na channel currents critical in controlling neuronal excitability, I_{NaP} and I_{NaR}, add to the accumulating evidence of the importance of these currents in the pathology of the disease. We provide evidence of early proepileptiform behavior of mEC layer II stellate neurons in EIEE13. Because these proexcitatory changes precede the onset of spontaneous seizures in heterozygous mice, we propose that early neuronal hyperexcitability gradually increases the excitability of key cerebral circuits, culminating in the initiation of spontaneous seizures in this model of *SCN8A* encephalopathy.

V. Proexcitatory Alterations in Sodium Channel Activity Facilitate Subiculum Neuron Hyperexcitability in Temporal Lobe Epilepsy

Rationale

In Chapter V, we examine how $Na_v1.6$ contributes to neuronal hyperexcitability in acquired, rather than genetic, epilepsy. Specifically, we demonstrate how proexcitatory alterations to sodium channel physiology cause hyperexcitability in TLE subiculum neurons. This work is a significant contribution to the field as relatively sparse literature focusing on the subiculum in TLE exists. Additionally, we believe we are one of few studies to show altered sodium channel physiology in the region in TLE and the first to implicate $Na_v1.6$ as a main facilitator of subiculum neuronal hyperexcitability. The work in Chapter V also demonstrates that studying $Na_v1.6$ is relevant across a variety of epileptic disorders and it argues that the development of a selective $Na_v1.6$ blocker could potentially benefit an array of epilepsy patients.

Introduction

The importance of sodium channels in facilitating increases in subiculum neuron excitability in epilepsy has yet to be thoroughly determined. In the current study we investigated if sodium channel function was altered in subiculum neurons in TLE using the continuous hippocampal stimulation (CHS) rat model. Additionally, we wanted to see if persistent (I_{NaP}) and resurgent (I_{NaR}) sodium channel currents were increased in TLE. I_{NaP} currents are slow inactivating currents that arise in subthreshold voltage ranges and are capable of amplifying a neuron's response to synaptic input (Stafstrom, 2007). I_{NaR} currents occur from channel re-opening during the repolarization phase of the AP and both I_{NaR} and I_{NaP} have been shown to facilitate bursting APs and high frequency AP firing (Raman and Bean, 1997; Yue et al., 2005; van Drongelen et al., 2006; Stafstrom, 2007; Lewis and Raman, 2014). Here we show that bursting subiculum TLE neurons are hyperexcitable and display increased persistent (I_{NaP}) and resurgent (I_{NaR}) sodium currents. Proexcitatory alterations in sodium channel activation and inactivation gating were also detected. Using a tetrodotoxin metabolite, 4,9-anhydro-TTX to inhibit mainly $Na_v1.6$ channels (Rosker et al., 2007), we show that inhibition of I_{NaP} and I_{NaR}

currents leads to attenuation of subiculum neuronal hyperexcitability and burst firing associated with TLE. We propose that increases in I_{NaP} and I_{NaR} currents and pro-excitatory changes in sodium channel physiology, together with synaptic network changes, contribute to the hyperexcitability of subiculum neurons in TLE, which aid in seizure initiation and seizure spread throughout the temporal lobe.

Methods

Animals

All animal experiments were conducted in accordance with the guidelines established by the National Institutes of Health guide for the Care and Use of Laboratory Animals and were approved by the University of Virginia's Institute of Animal Care and Use Committee. Adult male Sprague–Dawley rats (250–300 g) received a bipolar twisted pair of stainless steel electrodes to either hemisphere unilaterally in the posterior ventral hippocampus for stimulation and recording (coordinates from bregma AP ~ −5.3 mm, ML ~ 4.9 mm, DV ~ 5.0 mm, bite at ~−3.5 mm) (Paxinos and Watson, 2006). Electrodes were attached to Amphenol connectors and secured to the skull with jeweler's screws and dental acrylic. One week following surgery, rats were stimulated through the hippocampal electrode to induce limbic status epilepticus using a protocol previously described (Lothman et al., 1989). In brief, animals were stimulated for 90 min with 10-s trains of 50 Hz, 1 ms biphasic square waves with a maximum intensity of 400 μA peak to peak delivered every 11 s. Following the induction of and recovery from limbic status epilepticus, rats were placed in standard laboratory housing. Three months after the induction of status epilepticus, animals were evaluated for the presence and frequency of spontaneous temporal lobe seizures (Bertram and Cornett, 1994). During the monitoring phase, rats were placed in specially designed cages, which allowed full mobility of the animals, good visualization for video monitoring, and a stable recording environment. Animals had free access to food and water, as well as a standard 12 h light–dark cycle. Seizures were recorded and documented using a commercial computerized EEG program (Harmonie, Stellate Systems). All data were reviewed at an offline reading station connected to the vivarium computers via a local area network. The time of occurrence, behavioral severity (Racine 5 point scale) and duration for all seizures were noted.

Seizure Determination

Electrographic seizures in the rats were characterized by the paroxysmal onset of high frequency (> 5 Hz) increased amplitude discharges that showed an evolutionary pattern of a gradual slowing of the discharge frequency and subsequent post-ictal suppression. Seizure duration was measured from the onset of the high frequency activity or initial spike to the cessation of the terminal regular electrographic clonic activity.

Brain Slice Preparation and Action Potential Recordings

Please reference Chapter II: General Methods.

Sodium Channel Electrophysiology

Please reference Chapter II: General Methods.

Immunohistochemistry

TLE and aged matched WT rats (4 rats for each group, 350–450 g) were euthanized with isoflurane, decapitated, and brains rapidly removed and placed in chilled (4 °C) ACSF. Horizontal 500 μm thick sections were prepared using a Vibratome, and transferred to a chamber containing oxygenated ACSF at 37 °C and incubated for 35 min. Slices were then embedded in OCT compound in cryomolds and snap-frozen on dry ice-chilled isopentane, and kept on dry ice. Cryostat sections (16 μm) were prepared and thaw-mounted onto Superfrost Plus slides (Fisher Scientific) and stored at −80 °C for no > 3 days prior to further processing. Slices were fixed in ice-cold acetone-ethanol mixture for 5 min, air-dried, washed with KPBS and then placed for 60 min in KPBS blocking solution (5% fish skin gelatin, 5% normal goat serum, 0.25% Triton × 100, and 0.65% w/v BSA), followed by incubation in blocking solution containing the pair of primary antibodies for 48 h at 4 °C (rabbit anti-$Na_v1.6$, 1:500, Alomone labs and monoclonal mouse anti Ankyrin G, 1:500, NeuroMab). The slides were then washed with KPBS, incubated in blocking solution containing a pair of secondary antibodies (Alexa 488-conjugated goat anti-mouse IgG and Alexa 555- conjugated goat anti-rabbit IgG, both at 1:1000, Invitrogen (Molec. Probes). Slides were washed in KPBS, incubated in Nuclear Blue (1 drop/ml, Invitrogen), washed, air-dried, and cover slipped in Polymount (Polysciences Inc.).

Confocal images were captured of subiculum neurons using a Zeiss LSM 710 confocal microscope (Zeiss, Oberkochen, Germany) with a 63× oil immersion objective and ZEN Zeiss LSM Imaging software. The settings of the laser intensities and image capture were initially optimized but then not changed during the scanning of the slides. Quantification and analysis was performed using Image J software. For analysis of $Na_v1.6$ expression, a line scan representing the length of the AIS, as determined by Ankyrin G staining, was drawn, and the mean relative optical density (R.O.D) determined. The mean R.O.D for Ankyrin G was unaltered between WT and TLE preparations and allowed for standardization of the immunolabeling as a ratio of $Na_v1.6$ to Ankyrin G staining for each AIS.

Data Analysis

Please reference Chapter II: General Methods.

Results

Subiculum bursting neurons are hyperexcitable in TLE

Subiculum bursting neurons were found to be in high density in the distal pyramidal layer just adjacent to the presubiculum, and WT neurons were distinguished by their propensity to produce a burst of APs at the onset of depolarization, followed by more tonic spiking (Figure V.1A; WT) (Mattia et al., 1993; Stewart and Wong, 1993; Taube, 1993; Staff et al., 2000; Petersen et al., 2017). In contrast, subiculum neurons from TLE animals were hyperexcitable, firing more than a single burst of APs at lower current injection steps compared to WT (Figure V.1A; TLE). Over a series of depolarizing current injection steps (50 pA to 470 pA) TLE neurons fired a significantly greater number of APs than WT ($P < 0.05$, Figure V.1A–B). We measured the maximal negative repolarizing voltage between APs for those evoked by a current injection step of 270 pA (Figure V.1C). In TLE subiculum neurons the maximal negative voltage attained after the completion of repolarization was significantly depolarized compared with WT neurons ($P < 0.01$ for APs 1, 3 and 4 and $P < 0.05$ for APs 2 and 5; Figure V.1C). These data indicate the presence of an increased sustained depolarizing current in TLE neurons that would drive neurons to spiking thresholds, accounting for the earlier AP initiation in TLE neurons. Analysis of AP properties revealed a significantly hyperpolarized threshold, a significant

increase in input resistance (R_i) and AP width in TLE neurons compared to WT. No significant differences were seen in resting membrane potential (RMP), AP amplitude or AP upstroke velocity (Table V.1).

Brief stimulation of the pyramidal layer of CA1 consistently evoked AP bursts in both control and TLE subiculum neurons (Figure V.1D & E). In TLE neurons, the average number of APs evoked was 3.2 ± 0.1 (n = 8). In contrast, WT neurons were less excitable and evoked 2.1 ± 0.1 APs, (n = 8; P < 0.01). Synaptically evoked bursts in TLE neurons were also longer lasting than those recorded in WT neurons (Figure V.1D & F). To better quantify this increase in burst duration, we measured the area under the curve (AUC) for AP trains evoked by synaptic stimulation in both WT and TLE subiculum neurons. Compared to WT neurons, TLE neurons showed a significant increase in AUC (P < 0.01; Figure V.1F) further suggesting the presence of a greater depolarizing current in TLE neurons.

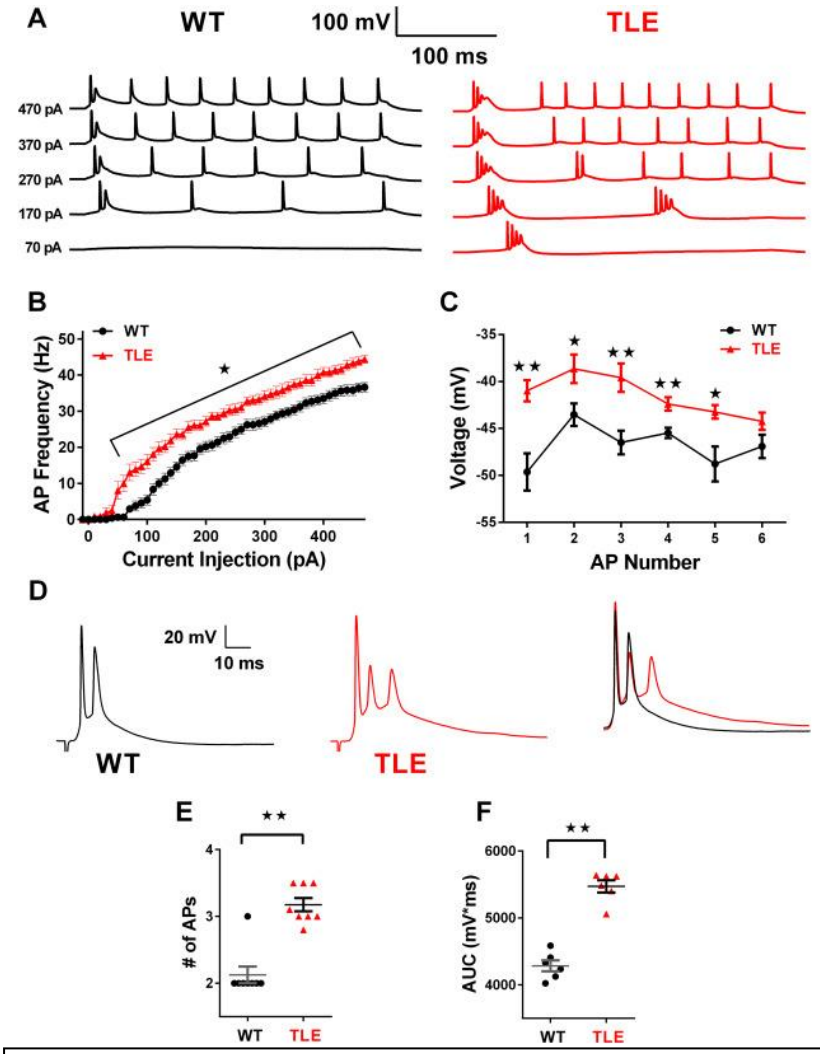

Figure V.1. Subiculum neurons are hyperexcitable in TLE. (A) Representative traces of APs elicited by 300 ms current injection steps of increasing amplitude from a holding potential of − 65 mV. (B) AP frequency versus injected current plot shows higher neuronal firing frequency in TLE (n = 12) neurons compared to control (n = 16). (C) Plot of maximal hyperpolarizing voltages reached between APs evoked by a 270 pA depolarizing current injection step. (D) Brief stimulation of the CA1 pyramidal layer elicited synaptically evoked AP bursts in WT (n = 8) and TLE neurons (n = 8). Right; superimposed traces of WT, black and TLE, red synaptically evoked responses shows increased response duration and spiking in TLE subiculum neurons compared with WT. (E) Scatter plot showing AP spiking frequency in response to synaptic stimulation. (F) Scatter plot showing area under the curve (AUC) for synaptically evoked APs. Data represent mean ± S.E.M. Statistical significance: *P < 0.05; **P < 0.01 Student's t-test with Welch's correction.

Proexcitatory shifts in sodium channel activation and inactivation gating in subiculum TLE neurons

To explore if proexcitatory alterations in sodium channel physiology play a significant role in increased subiculum hyperexcitability in TLE, sodium channel currents were recorded using outside-out patches from visually identified subiculum pyramidal neurons in brain slice preparations. Representative macroscopic sodium currents from WT and TLE subiculum neurons are shown in Figure V.2A. Sodium channel current densities from outside-out recordings were not significantly different between genotypes (Data not shown). Analysis of current-voltage (I-V) curves revealed a significant 6.3 mV hyperpolarizing shift in the $V_{1/2}$ of activation in TLE neurons (n = 14) compared to WT (n = 19, P < 0.05; Figure V.2B & C; Table V.2). Slope factor (k) was also increased in TLE subiculum neurons compared with WT (P < 0.05, Figure V.2D, Table V.2). In addition to alterations in activation parameters, inactivation parameters were also altered in TLE neurons with a 5.7 mV depolarizing shift in the $V_{1/2}$ (n = 18) compared to WT neurons (n = 12, P < 0.05; Figure V.2E & F, Table V.2). Slope factor (k) was not changed (Figure V.2G, Table V.2). Window currents were estimated from the area under the overlapping normalized activation and inactivation curves. Predicted window currents for TLE subiculum neurons were increased 2.6-fold

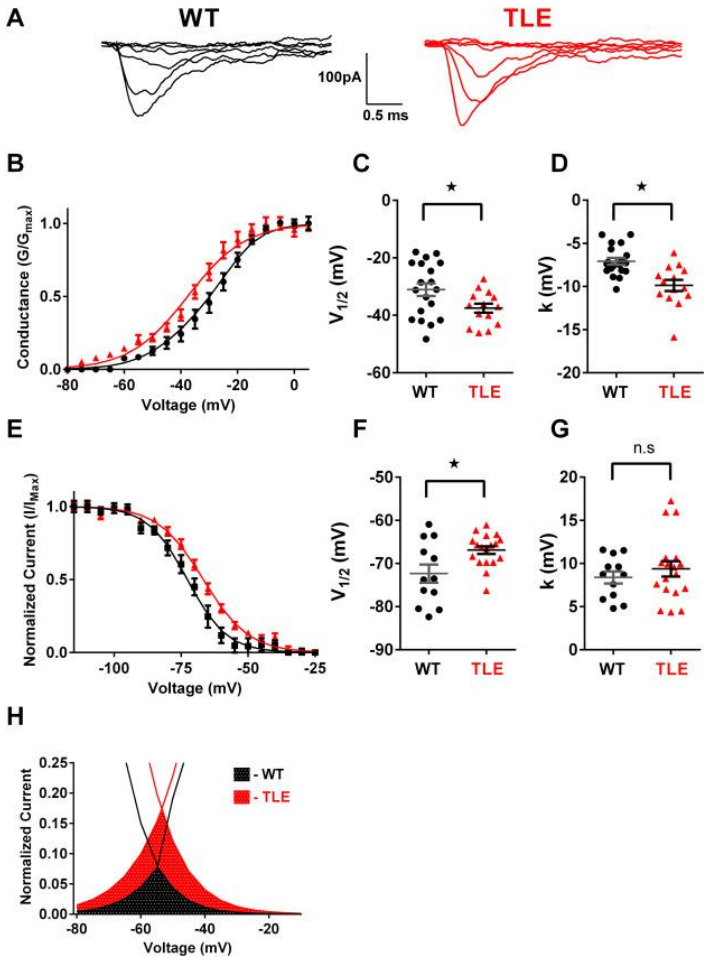

Figure V.2. TLE subiculum neurons exhibit proexcitatory alterations in sodium channel physiology. (A) Representative current traces recorded using the outside-out patch clamp configuration for WT and TLE subiculum neurons. (B) Voltage dependence of channel activation for WT (black, n = 19) and TLE (red, n = 14) subiculum neurons. Lines correspond to the least-squares fit when average data were fit to a single Boltzmann equation. (C) Scatter plot of voltage at half-maximal activation ($V_{1/2}$) for WT and TLE subiculum neurons. (D) Scatter plot of the slope factor (k) of activation in WT and TLE subiculum neurons. (E) Voltage dependence of channel inactivation for WT (black, n = 12) and TLE (red, n = 18) subiculum neurons. Lines correspond to the least-squares fit when average data were fit to a single Boltzmann equation. (F) Scatter plot of voltage at half-maximal inactivation ($V_{1/2}$) for WT and TLE subiculum neurons. (G) Scatter plot of the slope factor (k) of inactivation. (H) Window current predicted by overlapping normalized activation and inactivation curves. Estimated window current is elevated in TLE subiculum neurons (red checkered area) compared to WT (black checkered area). Data represent mean ± S.E.M. Statistical significance: *P < 0.05 Student's t-test with Welch's correction.

and were persistent over a greater voltage range than WT cells (Figure V.2H).

	RMP, mV	R_i, MΩ	Threshold, mV	Amplitude, mV	AP width (ms)	Upstroke velocity, mV/ms	Rheobase (pA)	N
WT	−61.3 ± 0.2	66.0 ± 2.9	−45.7 ± 0.3	96.6 ± 0.8	0.87 ± 0.0	359.0 ± 18.5	94.4 ± 5.0	16
TLE	−61.5 ± 0.2	86.8 ± 5.1**	−50.4 ± 0.6**	98.9 ± 1.4	0.95 ± 0.0**	315.8 ± 27.2	50.8 ± 5.3**	12
WT + 4,9-ah-TTX (100 nM)	−59.3 ± 0.3††	48.9 ± 2.7††	−41.6 ± 0.3††	90.0 ± 1.6††	0.99 ± 0.0††	346.2 ± 16.0	188 ± 10.8††	7
TLE + 4,9-ah-TTX (100 nM)	−59.6 ± 0.2††	76.8 ± 9.7	−42.9 ± 0.4††	95.0 ± 2.9	1.1 ± 0.3††	243.1 ± 20.3†	100 ± 7.3††	6

Table V.1. Values represent mean ± S.E.M, n = number of cells. RMP; Resting membrane potential. R_i; input resistance. Student's t-test with Welch's correction. ** $P < 0.01$ compared to WT. †$P < 0.05$ compared to no 4,9-ah-TTX. ††$P < 0.01$ compared to no 4,9-ah-TTX.

Subiculum bursting TLE neurons have increased persistent (I_{NaP}) and resurgent (I_{NaR}) currents

Persistent sodium currents (I_{NaP}) are thought to be a major contributor to the generation of AP bursts and have been recorded from a portion of isolated subiculum neurons from TLE patients (Vreugdenhil et al., 2004). I_{NaP} currents were recorded using slow voltage ramps using brain slice preparations. Ramp recordings displayed a robust inward current that was abolished by application of 1 μM TTX. The peak I_{NaP} was calculated by subtracting traces obtained in the presence of TTX from those obtained in the absence of the toxin. In TLE subiculum neurons, we observed a significant increase in I_{NaP} currents compared to WT cells (Figure V.3A–C). I_{NaP} currents from WT subiculum neurons had a peak amplitude of −160 ± 35 pA (n = 7). In contrast, peak I_{NaP} currents from TLE neurons were increased 7.5 fold to −1206 ± 104 pA (n = 6, $P < 0.01$; Figure V.3A–C). No significant differences were seen in the voltage-dependence or time course of activation of I_{NaP} (data not shown).

Resurgent sodium currents (I_{NaR}) are depolarizing currents that play a significant role in enhancing firing frequency or bursting activity (Raman and Bean, 1997). It is believed that I_{NaR} occurs from channel reopening during the repolarization phase of the AP that arises from the electrostatic repulsion of an open-channel blocker (Lewis and Raman, 2014; Patel et al., 2016). Peak I_{NaR} currents were elevated by 92% in TLE subiculum neurons (−1208 ± 122 pA, n = 6) compared with WT (−629 ± 62 pA, n = 9, $P < 0.01$; Figure V.3D-F). Similar to I_{NaP}, no significant differences were seen in the voltage-dependence or time course of activation of I_{NaR} (data not shown).

The $Na_v1.6$ isoform is considered to be one of the most significant contributors to both I_{NaR} and I_{NaP} (Raman and Bean, 1997; Hargus et al., 2013). The observed increase in both I_{NaR} and I_{NaP} in TLE subiculum bursting neurons could be accounted for by proexcitatory alterations

in $Na_v1.6$ physiology that could facilitate neuronal hyperexcitability. To test this hypothesis, we used the TTX metabolite 4,9 anhydro-tetrodotoxin (4,9-ah-TTX), which has a greater affinity for $Na_v1.6$ over other sodium channel isoforms, making the toxin a valuable tool for studying $Na_v1.6$ in neuronal physiology (Rosker et al., 2007; Hargus et al., 2013). Previous studies have shown that at a concentration of 100 nM, 4,9-ah-TTX inhibits approximately 50% of $Na_v1.6$ channels stably expressed in HEK 293 cells without any effect on $Na_v1.2$ channels (Hargus et al., 2013). We tested the effects of 100 nM 4,9-ah-TTX on both I_{NaR} and I_{NaP} currents. 4,9-ah-TTX (100 nM)

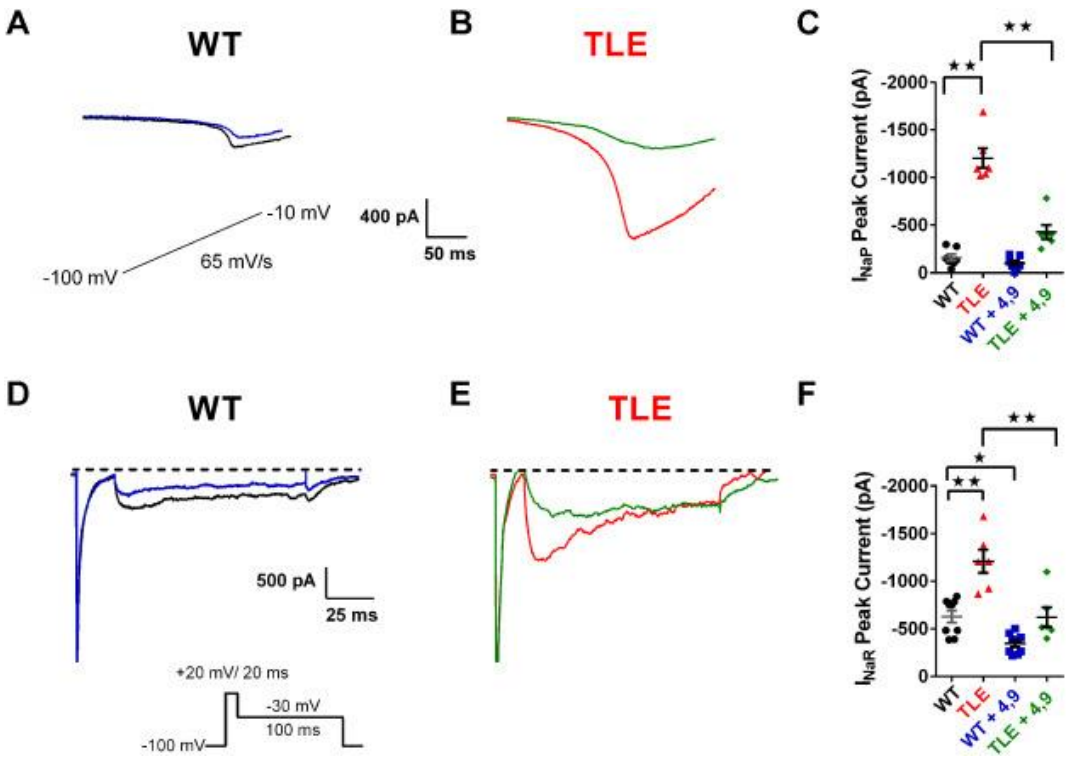

Figure V.3. TLE subiculum neurons show increased persistent (I_{NaP}) and resurgent (I_{NaR}) sodium currents that are attenuated by 4,9-anhydro-tetrodotoxin. I_{NaP} currents were elicited by applying a voltage ramp at a rate of 65 mV/s (inset of A). Recordings were repeated in the presence of TTX (1 μM). Traces shown are those obtained after subtracting traces recorded in the presence of TTX. (A) I_{NaP} currents in WT subiculum neurons are reduced by 4,9-ah-TTX (100 nM: WT, black; WT + 4,9-ah-TTX, blue). (B) I_{NaP} currents in TLE subiculum neurons are increased compared with WT and significantly attenuated by 4,9-ah-TTX (100 nM: TLE, red; TLE + 4,9-ah-TTX, green). (C) Scatter plot of I_{NaP} peak amplitudes pre and post application of 4,9-ah-TTX in WT and TLE subiculum neurons (WT, black, n = 7; TLE, red, n = 6; WT + 4,9-ah-TTX, blue, n = 7; TLE + 4,9-ah-TTX, green, n = 6). I_{NaR} currents recorded from subiculum neurons using the voltage protocols shown. Traces shown were obtained after subtraction of recordings obtained in the presence of TTX (1 μM). (D) I_{NaR} currents in WT neurons were reduced by 4,9-ah-TTX (100 nM: WT, black; WT + 4,9-ah-TTX, blue). (E) I_{NaR} currents in TLE neurons were larger than those recorded in WT neurons and significantly attenuated by 4,9-ah-TTX (100 nM: TLE, red, TLE + 4,9-ah-TTX (100 nM), green). (F) Scatter plot of I_{NaR} peak amplitudes before and after bath application of 4,9-ah-TTX (100 nM) for WT (WT, black, n = 9; WT + 4,9-ah-TTX (100 nM), blue, n = 9) and TLE neurons (TLE, red, n = 6; TLE + 4,9-ah-TTX (100 nM), green, n = 6). Data represent mean ± S.E.M. Statistical significance: *P < 0.05; **P < 0.01 Student's t-test with Welch's correction.

significantly reduced I_{NaP} in TLE subiculum neurons by 64.5% (from −1206 ± 104 pA, n = 6 to −428 ± 74 pA, n = 6, P < 0.01; Figure V.3B & C). In WT subiculum neurons, 4,9-ah-TTX (100 nM) caused a small decrease in I_{NaP}, by 37.5% (from 160 ± 35 pA, n = 7 to −100 ± 25 pA, n = 7, Figure V.3A & C). 4,9-ah-TTX had no effect on I_{NaP} activation parameters (data not shown).

In a similar manner to effects observed with I_{NaP} currents, 4,9-ah-TTX (100 nM) also reduced I_{NaR} currents in TLE subiculum neurons by 48.5% (from −1208 ± 122 pA, n = 6 to −622 ± 103 pA, n = 6, P < 0.01; Figure V.3E & F). I_{NaR} currents were also reduced in WT neurons by 4,9-ah-TTX (100 nM; from −629 ± 62.6 pA, n = 9 to −344.5 ± 34.4 pA, n = 9, P < 0.05; Figure V.3D & F). Once again, 4,9- ah-TTX had no effects on I_{NaR} activation parameters (data not shown).

	Activation			Inactivation		
	$V_{1/2}$ (mV)	k (mV)	n	$V_{1/2}$ (mV)	k (mV)	n
WT	− 31.3 ± 2.2	− 7.1 ± 0.4	19	− 72.6 ± 2.1	8.4 ± 0.7	12
TLE	− 37.5 ± 1.6*	− 9.9 ± 0.6*	14	− 66.9 ± 0.9*	9.4 ± 0.9	18

Table V.2. Sodium channel physiology in WT and TLE subiculum neurons. Values represent mean ± S.E.M, n = number of cells. $V_{1/2}$, voltage of half-maximal activation or inactivation; k, slope factor. *P < 0.05 vs WT, Student's t-test with Welch's correction.

Inhibition of $Na_v1.6$ suppresses neuronal excitability

Both I_{NaR} and I_{NaP} currents are important for controlling neuronal excitability and reductions in I_{NaR} and I_{NaP} currents by 4,9-ah-TTX should modulate neuronal excitability. To test this hypothesis we determined the effects of 4,9-ah-TTX (100 nM) on APs evoked by both somatic current injection and by synaptic stimulation. 4,9-ah-TTX (100 nM) significantly reduced AP frequency in both WT and TLE subiculum bursting neurons (Figure V.4A,C & E). At a current injection step of 470 pA, 4,9-ah-TTX (100 nM) decreased AP frequency in TLE neurons by 49.1% (from 44.4 ± 1.0 Hz, n = 12 to 22.6 ± 1.0 Hz, n = 6, P < 0.05; Figure V.4C & E). In WT subiculum neurons 4,9-ah-TTX (100 nM) decreased AP frequency by 37.4% (from 36.6 ± 1.3 Hz, n = 16 to 22.9 ± 1.2 Hz, n = 8, P < 0.05; Figure V.4A & E).

Morphology of the first AP elicited by a depolarizing current injection step was characterized by phase plots of dV/dt vs voltage in WT and TLE neurons before and after the administration of 4,9-ah-TTX (100 nM; Figure V.4B & D; Table V.1). In WT neurons, AP thresholds were depolarized in the presence of 4,9-ah-TTX.

In TLE subiculum neurons, 4,9-ah-TTX (100 nM) also depolarized AP thresholds and reduced upstroke velocity. Measurement of the maximal negative repolarizing voltage between APs at a current injection of 270 pA revealed a decreasing trend in both WT and TLE neurons, most likely the effect of inhibiting I_{NaP} and I_{NaR} currents. In WT, 4,9-ah-TTX (100 nM) significantly hyperpolarized inter AP voltages for the 2nd AP ($P < 0.05$**;** Figure V.4F). For

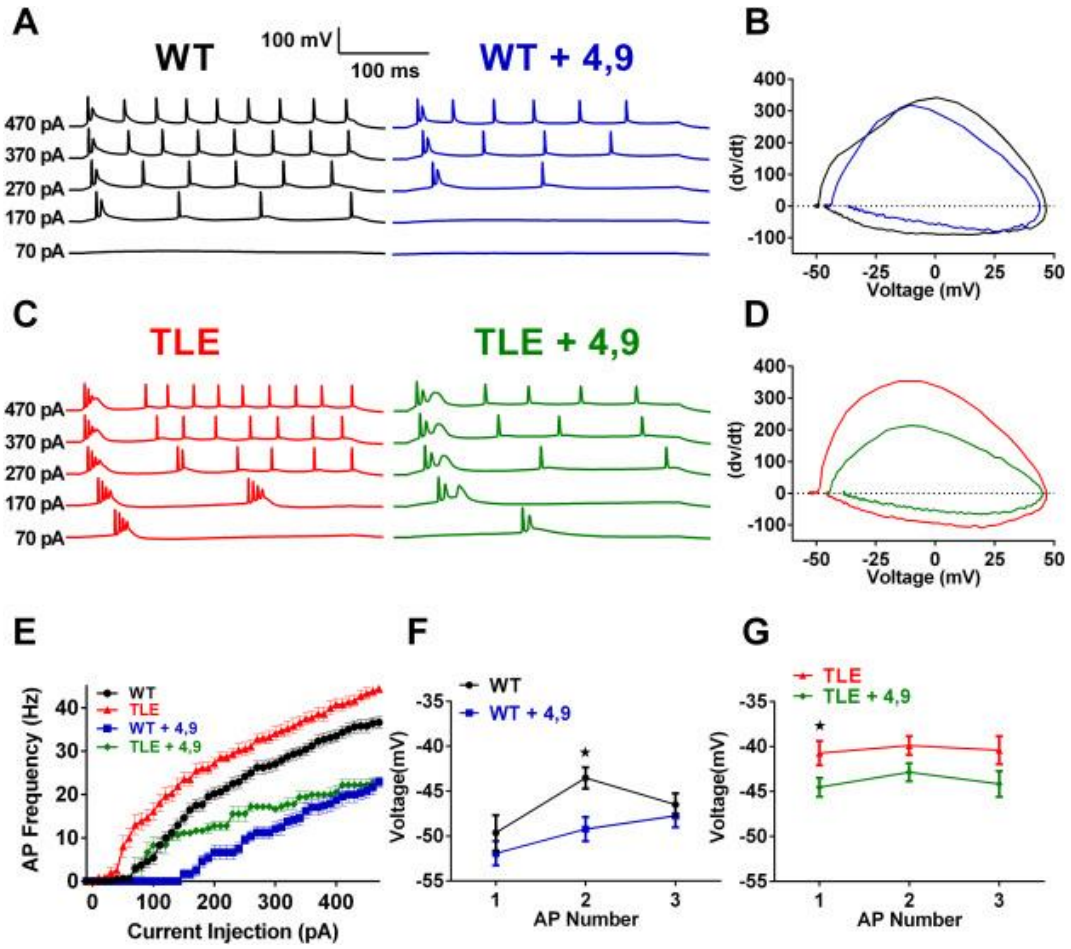

Figure V.4. Inhibition of Nav1.6 currents by 4,9-ah-TTX decreases neuronal excitability in subiculum bursting neurons. (A) Representative traces of APs elicited by 300 ms current injection steps of increasing current amplitude in WT neurons (A) (WT, black, WT + 4,9-ah-TTX (100 nM), blue). (B) Representative phase plot analysis of the first elicited AP in WT neurons before and after the application of 4,9-ah-TTX (WT, black; WT + 4,9-ah-TTX (100 nM), blue). (C) Representative traces of APs elicited by 300 ms current injection steps of increasing current amplitude in TLE neurons (TLE, red; TLE + 4,9-ah-TTX (100 nM), green). (D) Representative phase plot analysis of the first elicited AP in TLE neurons before and after the application of 4,9-ah-TTX (TLE, red; TLE + 4,9 ah-TTX (100 nM), green). (E) Effects of 4,9-ah-TTX (100 nM) on AP frequency for WT and TLE subiculum neurons (WT, black, n = 16; WT + 4,9-ah-TTX, blue, n = 7; TLE, red, n = 12; TLE + 4,9-ah-TTX, green, n = 6). Effects of 4,9-ah-TTX (100 nM) on maximal hyperpolarizing voltages between the first 3 APs evoked by a 270 pA current injection in WT (F) and TLE subiculum neurons (G). Data represent mean ± S.E.M. Statistical significance: *P < 0.05 Student's t-test with Welch's correction.

TLE neurons, 4,9-ah-TTX (100 nM) significantly hyperpolarized inter AP voltages for the 1st AP ($P < 0.05$; Figure V.4G).

We determined the role of $Na_v1.6$ on synaptically evoked APs (Figure V.5). Application of 4,9-ah-TTX (100 nM) significantly reduced synaptically evoked firing in TLE subiculum neurons from 3.2 ± 0.1 to 1.3 ± 0.2 APs in the presence of the toxin ($n = 8$, $P < 0.01$; Figure V.5C & E). In WT subiculum neurons, synaptically evoked APs were also reduced by 4,9-ah-TTX (100 nM), reducing firing from 2.1 ± 0.1 to 1.5 ± 0.3 APs after application of the toxin ($n = 7$; Figure V.5A & E). However, the reduction in spiking did not reach significance ($P < 0.06$). In addition to decreasing AP number, 4,9-ah-TTX (100 nM) significantly reduced the area under the curve (AUC) for TLE subiculum neurons, but not for WT cells (Figure V.5F).

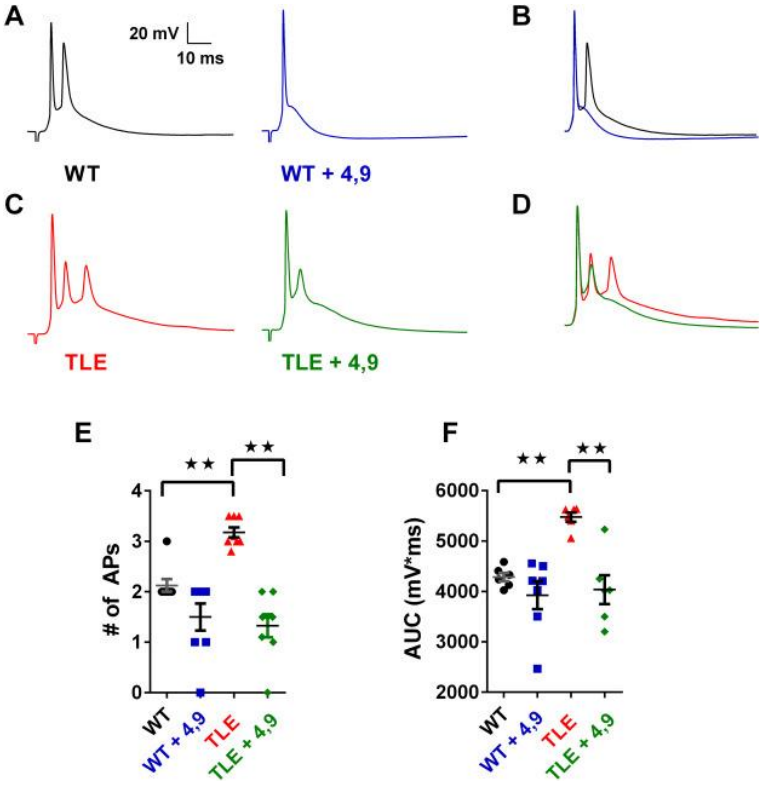

Figure V.5. Inhibition of $Na_v1.6$ currents by 4,9-ah-TTX attenuates synaptically evoked burst firing in TLE subiculum neurons. (A) Application of 4,9-ah-TTX (100 nM) reduces synaptically evoked AP bursts in WT and (C) TLE subiculum neurons. Superimposed traces for WT (B) and TLE (D) subiculum neurons illustrate effects of 4,9 ah-TTX (100 nM) on evoked responses. (E) Scatter plot showing AP frequency in response to synaptic stimulation before and after application of 4,9-ah-TTX (100 nM: WT, black, $n = 8$; WT + 4,9-ah-TTX, blue, $n = 8$; TLE, red, $n = 8$; TLE + 4,9-ah-TTX; green, $n = 8$). (F) Scatter plot showing area under the curve (AUC) for synaptically evoked APs. Data represent mean ± S.E.M. Statistical significance: **$P < 0.01$ Student's t-test with Welch's correction.

$Na_v1.6$ staining levels are not increased in TLE subiculum neurons

Increased staining for $Na_v1.6$ has been observed in TLE mEC neurons, suggesting an increase in $Na_v1.6$ expression levels (Hargus et al., 2013). To determine if $Na_v1.6$ staining was increased in subiculum neurons, immunofluorescence experiments were performed. Robust $Na_v1.6$ staining was observed at the AIS and was co-localized with Ankyrin G (Ank G) staining, a marker for the AIS (Figure V.6). Surprisingly, we saw no differences in the staining pattern for $Na_v1.6$ between WT and TLE subiculum neurons along the AIS.

Discussion

In this study, we investigated the importance of sodium channels in facilitating subiculum neuron hyperexcitability in TLE, the hallmark of seizures. The principal findings of this study are that subiculum neurons from TLE rats are: 1) hyperexcitable, firing bursts of APs, 2) exhibit proexcitatory shifts in sodium channel activation and inactivation gating parameters, leading to an increase in the estimated sodium channel window current, 3) have increased resurgent (I_{NaR}) and persistent (I_{NaP}) sodium currents, two currents known to facilitate AP bursts, 4) pharmacological reduction of $Na_v1.6$ reduces both I_{NaR} and I_{NaP} sodium channel currents and attenuates neuronal firing frequency and AP bursts after synaptic stimulation. These findings provide new knowledge regarding the importance of sodium channels, particularly $Na_v1.6$, as a mechanism, in part, for the increases in neuronal excitability observed in epileptic subiculum bursting neurons.

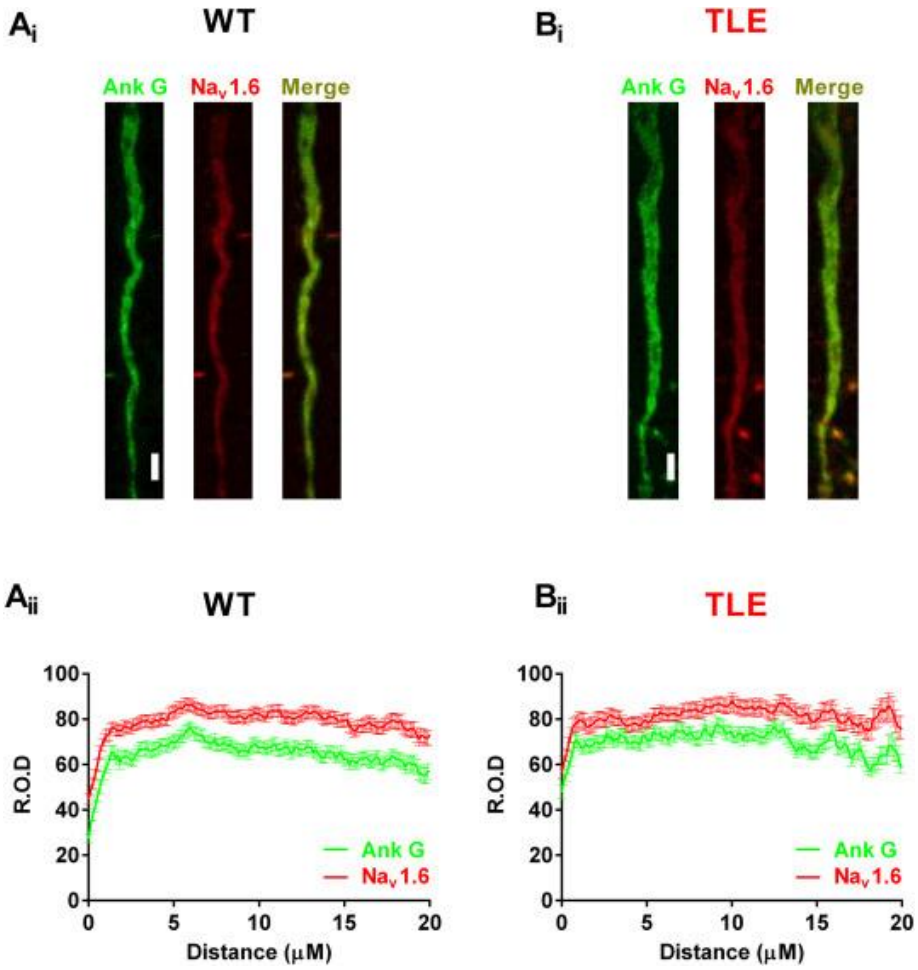

Figure V.6. $Na_v1.6$ AIS staining is not increased in TLE subiculum neurons compared to WT. $Na_v1.6$ staining along the AIS of WT (A_i) and TLE (B_i) subiculum neurons (Ank G, green; $Na_v1.6$, red; Merge; yellow). Graphs showing the localization and relative optical density (R.O.D) of Ank G and $Na_v1.6$ staining along the length of the AIS for WT (A_{ii}) and TLE (B_{ii}) subiculum neurons (WT, n = 191 AIS from 4 animals; TLE, n = 140 AIS from 4 animals). Scale bars represent 2 μm. Data represent mean ± S.E.M.

In this study, we investigated the importance of sodium channels in facilitating subiculum neuron hyperexcitability in TLE, the hallmark of seizures. The principal findings of this study are that subiculum neurons from TLE rats are: 1) hyperexcitable, firing bursts of APs, 2) exhibit proexcitatory shifts in sodium channel activation and inactivation gating parameters, leading to an increase in the estimated sodium channel window current, 3) have increased resurgent (I_{NaR}) and persistent (I_{NaP}) sodium currents, two currents known to facilitate AP bursts, 4) pharmacological reduction of $Na_v1.6$ reduces both I_{NaR} and I_{NaP} sodium channel currents and attenuates neuronal firing frequency and AP bursts after synaptic stimulation. These findings provide new knowledge regarding the importance of sodium channels, particularly $Na_v1.6$, as a mechanism, in part, for the increases in neuronal excitability observed in epileptic subiculum bursting neurons.

The dramatic increases in I_{NaR} and I_{NaP} currents were a striking feature of epileptic subiculum neurons. I_{NaP} currents are non-inactivating currents that play a significant role in

generating burst and high frequency AP firing. (Yue et al., 2005; van Drongelen et al., 2006; Stafstrom, 2007). Non-inactivating currents recorded after the rapid transient sodium current and labeled as I_{NaP} currents, have been recorded from subiculum neurons in patients with intractable TLE (Vreugdenhil et al., 2004). Increases in I_{NaP} currents would significantly impact AP frequencies, providing a persistent depolarizing current on which APs would be initiated. In addition, greater I_{NaP} currents would contribute to lower firing thresholds and increased AP widths reported in TLE neurons, all of which were modulated by 4,9-ah-TTX. Although input resistances was also increased in TLE neurons, contributing to increased excitability, it is unlikely that increases in I_{NaP} currents played a major role since the addition of 4,9-ah-TTX caused a small, but non-significant reduction in R_i (Crill, 1996), suggesting involvement of additional ion channels.

Resurgent sodium currents (I_{NaR}) are depolarizing currents thought to play a significant role in enhancing firing frequency or bursting activity (Raman and Bean, 1997). It is believed that I_{NaR} occurs from channel re-opening during the repolarization phase of the AP that arises from the electrostatic repulsion of an open-channel blocker (Lewis and Raman, 2014; Patel et al., 2016). Our studies revealed large increases in I_{NaR} currents in TLE neurons, which in combination with increased I_{NaP} currents, would facilitate AP bursting in epilepsy. Increases in these two current types may provide a common mechanism by which a sustained and continuous depolarization could be achieved, leading to AP initiation. Reducing I_{NaP} and I_{NaR} currents with 4,9-ah-TTX suppressed neuronal excitability and hyperpolarized the inter AP repolarizing voltage potentials. Since 4,9-ah-TTX at a concentration of 100 nM inhibits approximately 50% of $Na_v1.6$ channels (Hargus et al., 2013), these findings suggest a role for $Na_v1.6$, and particularly I_{NaP} and I_{NaR} currents in generating AP bursts (Rush et al., 2005). I_{NaR} and I_{NaP} currents were also increased in medial entorhinal cortex neurons of TLE rats and likely accounted for the increased AP frequency and neuronal hyperexcitability observed in that study (Hargus et al., 2013). Furthermore, increases in I_{NaR} currents are also an important feature for missense gain-of-function mutations of $Na_v1.6$, known to be responsible for epileptic encephalopathy in patients (Patel et al., 2016), speculating a causative role for this unique current in epilepsy.

The $Na_v1.6$ isoform is believed to be the main contributor of I_{NaR} and I_{NaP} (Rush et al., 2005) and CA1 pyramidal neurons from *Scn8a*^{med} mice show significant reductions in I_{NaR} and

I_{NaP} currents (Royeck et al., 2008). In agreement with those studies, inhibiting both I_{NaP} and I_{NaR} currents with 4,9-ah-TTX suppressed neuronal firing frequency and AP bursting in subiculum neurons. 4,9-ah-TTX is a TTX metabolite and has been reported to exhibit a < 200 fold greater selectivity against $Na_v1.6$ over other TTX-sensitive isoforms when tested on sodium channels expressed in *Xenopus* oocytes (Rosker et al., 2007). However, in mammalian expression systems 4,9-ah-TTX is less selective for $Na_v1.6$ (Hargus et al., 2013). Using a concentration of 4,9-ah-TTX that is likely to inhibit approximately 50% of $Na_v1.6$ channels (100 nM) we found that 4,9-ah-TTX suppressed neuronal excitability to a greater degree in TLE subiculum neurons than WT neurons. The reductions in firing rates in TLE neurons were accompanied by significant depolarization of the resting membrane potential and AP threshold, an increase in AP width, and a decrease in AP upstroke velocity.

Our studies revealed proexcitatory alterations in TLE subiculum neuron sodium channel physiology. Hyperpolarizing shifts in activation gating were coupled with depolarizing shifts in inactivation gating extending the voltage range where channels would be available for activation and have a finite probability of opening. The current established over this range is commonly referred to as the window current and an enhancement in this range, or "window," would increase the probability of channel opening, resulting in a reduction in AP thresholds, facilitating AP firing and potentially initiating seizure generation and spread. Increases in window currents have been associated with increased persistent sodium current activity and epileptogenesis in animal models of TLE (Ketelaars et al., 2001; Ellerkmann et al., 2003). In agreement, the voltage range of I_{NaP} currents reported in this study is consistent with the voltage range for the estimated window current.

A surprising finding was a lack of difference in $Na_v1.6$ staining intensity along the AIS between WT and TLE subiculum neurons. Previous studies in mEC neurons detected increases in $Na_v1.6$ staining, initiating as early as 7 days post-status epilepticus and continuing after 3 months, a time point where animals are in the chronic stage of epilepsy (Hargus et al., 2011, 2013). These differences between studies suggest heterogeneity between neurons in TLE. It is possible that post translational modifications of $Na_v1.6$ in subiculum TLE neurons accounts for the increases in I_{NaR} and I_{NaP} currents and also alterations in activation and inactivation gating parameters. Downregulated phosphorylation coupled with increased methylation resulted in a 3-fold increase in $Na_v1.2$ channel current in a kainic acid model of TLE (Baek et al., 2014).

Sodium channels are modulated by auxiliary subunits β subunits that not only modulate surface expression, but also channel gating (Patino and Isom, 2010). The β4 subunit specifically plays a significant role in the generation of I_{NaR} current (Grieco et al., 2005). Modifications in β4 subunit expression or activity could occur in TLE, affecting I_{NaR} current physiology.

The subiculum receives inputs from CA1 pyramidal neurons as well as neurons from the entorhinal cortex layers II/III (Witter et al., 2000a, 2000b; Stafstrom, 2005b). Conversely, the subiculum projects to a wide array of cortical and subcortical structures including recurrent projections back into the trisynaptic circuit via synapses with the entorhinal cortex (Swanson and Cowan, 1977; Witter and Groenewegen, 1990; O'Mara et al., 2001; Shao and Dudek, 2005; Tang et al., 2016). With its role as the output of the hippocampus and the presence of a large population of endogenously bursting neurons, the subiculum is perfectly predisposed to play a significant role in initiating and propagating epileptiform activity in TLE hippocampal circuitry (Staff et al., 2000; Harris and Stewart, 2001). In a study examining seizure initiation in a rat pilocarpine model of TLE, the subiculum was commonly the site of seizure initiation, and the site where ictal activity dissipated (Toyoda et al., 2013). Epileptiform activity originating in the subiculum can propagate to the CA1, driving hyperexcitability in hippocampal circuitry (Harris and Stewart, 2001). In human TLE patients, spontaneous rhythmic APs and epileptiform field potentials often originated in the subiculum before propagating into the hippocampus proper. This epileptiform activity persisted even when the subiculum was isolated, further supporting an intrinsic capability of the structure (Cohen et al., 2002).

In human patients and animal models of TLE, subiculum neurons are spared and become hyperexcitable leading to increased excitability within key hippocampal circuitry. As the output of the hippocampus, a hyperexcitable subiculum has the potential to both initiate and propagate epileptiform activity out of the temporal lobe leading to generalized ictal activity. Our findings support a role for sodium channels in facilitating subiculum neuronal hyperexcitability in TLE. We show that proexcitatory shifts in sodium channel activation and inactivation parameters, as well as increases in I_{NaR} and I_{NaP} currents are prevalent in epileptic subiculum neurons. We suggest an important role for $Na_v1.6$ in facilitating these proexcitatory alterations. Future intervention strategies that selectively target the $Na_v1.6$ isoform may be advantageous over current anticonvulsant therapies for seizure suppression.

VI. Conclusions and Future Directions

The voltage-gated sodium channel isoform $Na_v1.6$ is a key regulator of normal neuronal functioning in the CNS. With is prime location at the distal AIS (Hu et al., 2009), $Na_v1.6$ plays a crucial role in the initiation and propagation of APs. Previous studies have highlighted the importance of $Na_v1.6$ in normal neuronal behavior. Mice homozygous for a complete loss of *Scn8a* function develop motor defects by P14 and do not survive beyond P21 (Burgess et al., 1995; Kohrman et al., 1995; O'Brien and Meisler, 2013). Additionally, $Scn8a^{med}$ mice, which lack $Na_v1.6$ subunits, show reduced neuronal excitability and a significant elevation in spike threshold (Royeck et al., 2008). While loss of $Na_v1.6$ function is physiologically disrupting, proexcitatory alterations to $Na_v1.6$ can be equally devastating to CNS circuitry and the neurons that compose it. In this dissertation, we examine how proexcitatory, gain-of-function alterations in $Na_v1.6$ facilitate neuronal hyperexcitability in genetic and acquired epilepsy.

In Chapter III, *in vitro* cultured cell assays are utilized to electrophysiologically characterize both gain-of-function and loss-of-function mutations from patients with *SCN8A* encephalopathy. In IIIa, recurrent gain-of-function mutations at CpG dinucleotide mutation hotspots arginine 1872 and 1617 are studied, as these mutations account for up 20% of all known to date. Experiments in IIIa revealed that, while each mutation has slight differences, common pathogenic mechanisms can be found in the varying mutations. These similarities include proexcitatory shifts in the properties of inactivation and a significant increase in the persistent sodium current.

In Chapter IIIb, two loss-of-function *SCN8A* mutations from patients with intellectual disability and no seizures were characterized. Both mutations, G964R and E1218K, demonstrated a complete loss of channel function with no detectable inward sodium current. While the E1218K seems to disrupt protein stability, the mechanisms by which the G964R mutation eliminates channel function remains unknown.

Patients with EIEE13 often suffer from intractable epilepsy and patients that do achieve seizure control are often on an AED polytherapy. Research describing the efficacy of clinically available AEDs is sparse and as a result it is often unclear which drugs should be used first and which should be avoided. In Chapter IIIc, we first describe a novel gain-of-function *SCN8A* mutation, I1327V, which displays proexcitatory shifts in the properties of both activation and

inactivation. To expand on this characterization we also wanted to start to test the efficacy of clinically available AEDs on ameliorating the pathogenic physiology seen in the I1327V mutation. Recent studies have demonstrated that high doses of phenytoin significantly improved seizure control in 4 patients with gain-of-function *SCN8A* mutations (Boerma et al., 2015). To expand on this study, we tested phenytoin *in vitro* on the I1327V mutation with the hopes of better understanding how this drug alters mutant $Na_v1.6$ physiology. We discovered that phenytoin has preferential tonic and use-dependent block of I1327V channels over WT, and that phenytoin can reverse proexcitatory shifts in the properties of inactivation. We believe our work makes a strong argument for sodium channel blockers, specifically phenytoin, as the first treatment option for patients with gain-of-function *SCN8A* mutations.

Moving forward, there are experiments that would greatly expand on the data presented in Chapter III. First, the continuing electrophysiological characterization of gain-of-function *SCN8A* mutations is crucial for developing a better understanding of the disease. The phenotypic profile of an EIEE13 patient is hardly uniform, as each patient presents with a unique combination of symptoms that vary in severity. For example, a patient carrying the V1592L mutations displays a relatively more mild phenotype with complete seizure control, whereas a patient with the R1617Q mutation displayed severe intellectual disability and intractable seizures until the occurrence of SUDEP at age 3 (Larsen et al., 2015). The more we study the physiology of EIEE13 mutations, the better we'll understand the phenotypic spectrum seen in these patients. This will in turn allow clinicians to provide more efficacious, precise medicine that will improve seizure control and hopefully decrease the incidence of SUDEP. In addition to further mutant characterization, experiments testing the efficacy of clinical and experimental AEDs in *in vitro* culture cell assays will be imperative moving forward. Understanding how clinical AEDs alter mutant sodium channel physiology is the first step in figuring out which drugs are most efficacious in EIEE13 patients. Additionally, testing experimental AEDs in *in vitro* assays will lay the foundation for the development of new, more promising therapeutic treatments for patients as well as provide crucial data for future clinical trials.

In Chapter IV, we study hyperexcitability and aberrant sodium channel physiology in the mEC of a mouse model of *SCN8A* encephalopathy. To generate this novel mouse model, TALEN technology was used to knock-in the N1768D mutation. Mice heterozygous (D/+) and homozygous (D/D) for the mutant allele both recapitulate phenotypes seen in human patients

including seizures and SUDEP. In D/+ mice seizures begin in ~50% of mice at 8-16 weeks of age with the median age of death in seizing animals occurring around 14 weeks of age. In D/D mice a single, terminal seizure happens at around 3 weeks of age with motor impairments occurring leading up the event (Wagnon et al., 2015b). At 3 weeks of age, we discovered that mEC layer II neurons from both D/+ and D/D mice display abnormal AP morphology and are hyperexcitable in response to somatic current injection steps and synaptic stimulations. Driving this hyperexcitably in D/+ and D/D mEC neurons is proexcitatory alterations in sodium channel physiology. Specifically, we report a significant, dose-dependent increase in both persistent and resurgent sodium currents in D/+ and D/D mice in mEC layer II neurons. Additionally, we see proexcitatory shifts in sodium channel physiology, including a significant depolarizing shift in the properties of channel inactivation.

Future experiments stemming from Chapter IV could occupy an entire dissertation alone. To start, further electrophysiological analysis of other brain regions and cell types are needed to fully grasp how the N1768D mutation produces pathological neural networks. Specifically, further studies could focus on how interneurons are altered in both D/+ and D/D mice or respiratory regions of brain stem could be studied as these areas have been hypothesized to play a significant role in the occurrence of SUDEP. Another question that needs to be answered in the future is why do both D/+ and D/D mice display neuronal hyperexcitability and altered sodium channel physiology at 3 weeks, when D/+ mice typically don't start seizing until 8-16 weeks of age. The dose-dependent increase in both persistent and resurgent sodium currents seen in D/+ and D/D mice may provide a possible answer. An increase in these currents past a certain threshold could potentially prime neuronal circuits to be permissive to the occurrence of spontaneous recurrent seizures. Interestingly, preliminary experiments studying persistent and resurgent sodium currents from 8 week old D/+ mice show that current amplitude is not significantly different from 3 week old D/D animals (Ottolini et al., unpublished data). Lastly, future pharmacological experiments utilizing the D/+ mice could vastly improve our knowledge of the efficacy of AEDs in EIEE13. *In vivo* experiments using D/+ mice could give us answers as to which AEDs, clinical or experimental, are most efficacious in decreasing seizure frequency and preventing SUDEP. *In vitro* brain slice experiments will shed light on which drugs can effectively attenuate neuronal hyperexcitability and decrease persistent and resurgent sodium currents.

In Chapter V we move away from the genetically acquired EIEE13, and examine the role of $Na_v1.6$ in the acquired TLE. TLE is one of the most common forms of adult epilepsy and can be induced from a variety of etiologies. The DG and CA regions of the hippocampus have long been the primary areas of focus of research studying alterations in neuronal physiology and circuitry in the epileptic brain. In many ways this focus is warranted, as these regions are highly affected in TLE in terms of neuronal death and synaptic reorganization. While the DG and CA regions receive the majority of the research attention, other regions of the temporal lobe are often overlooked. The subiculum is one of these often understudied regions. As an output area of the temporal lobe, the subiculum is poised to play the crucial role of gatekeeper for synaptic transmission out of the hippocampus. Additionally, the subiculum is comprised of a large population of endogenously bursting neurons that is believed to help increase the reliability of synaptic conduction and AP backpropagation (Staff et al., 2000). These two features of the region make the subiculum vulnerable to epileptogenic induced hyperexcitability that will allow ictal activity to propagate out of the temporal lobe and into cortical and subcortical structures.

In Chapter V we show that subiculum TLE neurons become hyperexcitable, showing a more robust bursting phenotype and an increase in response to somatic current injection steps and synaptic stimulation. Additionally, subiculum neuron membrane properties are altered in a manner that is conducive to hyperexcitability. We hypothesized that alterations to sodium channel physiology play a crucial role in driving subiculum neuron hyperexcitability and that $Na_v1.6$ in particular was a significant contributor to increased neuronal activity. In agreement with this hypothesis, TLE subiculum neurons show increased persistent and resurgent sodium channel currents. This alteration would enable a more prominent bursting phenotype in conjunction with an increase in AP firing frequency. We also observed pathogenic, proexcitatory shifts in sodium channel physiology in subiculum bursting neurons. Specifically, we reported significant proexcitatory shifts in both the properties of activation and inactivation from TLE subiculum neurons. To test if $Na_v1.6$ is responsible for facilitating subiculum hyperexcitability, we applied 4,9-ah-TTX to subiculum TLE neurons. Our results showed that inhibiting $Na_v1.6$ in TLE subiculum neurons causes a significant decrease in neuronal excitability as well as attenuates the current amplitude of both persistent and resurgent sodium channel currents. We believe that this work is a significant contribution to the field because we believe we are one of few groups to thoroughly characterize subiculum neuron hyperexcitability

in TLE. Additionally, we are first to implicate $Na_v1.6$ directly in facilitating this increased neuronal excitability caused by TLE.

Future experiments for Chapter V should aim to better understand alterations to the subiculum in TLE as well as further delineate the significance of $Na_v1.6$ in driving network hyperexcitability in the disease. Additional *in vitro* experiments could be used to study alterations to other voltage-gated ion channels in the subiculum in TLE. Recent work has demonstrated the important role of T-type calcium channels, specifically $Ca_v3.1$, in the endogenous bursting phenotype of subiculum neurons (Joksimovic et al., 2017). Additionally, work in the neighboring CA1 shows that T-type calcium channels play a role in driving epileptogenesis and increasing the number of burst firing cells in TLE (Yaari et al., 2007). We hypothesize that similar proexcitatory alterations to T-type calcium channels occur in the subiculum. Furthermore, we believe that increased sodium channel and T-type calcium channel activity work in conjunction to drive neuronal and network hyperexcitability, similar to the "ping-pong mechanism of bursting" previously described by Yoel Yaari and colleagues (Yaari et al., 2007)

An increasing amount of evidence shows that proexcitatory alterations to $Na_v1.6$ throughout the hippocampus are a key facilitator of neuronal hyperexcitability in TLE. In light of these studies, future experiments stemming from Chapter V should also aim to target $Na_v1.6$ *in vivo* through pharmacological intervention. Significant strides have recently been made to develop $Na_v1.6$ selective blockers, with experimental compounds now being tested in basic science laboratories. Moving forward, *in vivo* experiments testing the efficacy of these compounds in reducing spontaneous recurrent seizures should be paramount. These experiments would not only provide crucial preliminary data for the development of future clinical AEDs, but it will also expand our knowledge on the importance of $Na_v1.6$ in the initiation and propagation of spontaneous seizures in TLE.

Over 50 million people worldwide suffer from epilepsy and up to 30% of these patients do not respond to clinically available AEDs (WHO, 2018; Kwan and Brodie, 2000). The need for improved therapeutic interventions is crucial to ensure more patients experience a better disease prognosis as well as a superior quality of life. The foundation of new therapies stem from a better understanding of the disease that you are trying to treat. The body of work contained in this dissertation has improved our knowledge of the role of the voltage-gated sodium channel $Na_v1.6$

in multiple epilepsy disorders. By continuing to highlight the significance of this channel in driving pathogenic alterations to the CNS, we hope to further inspire the notion of $Na_v1.6$ as a promising potential target for future therapeutic development.

VII. References

Alonso-Nanclares L, Kastanauskaite A, Rodriguez J-R, Gonzalez-Soriano J, DeFelipe J (2011) A Stereological Study of Synapse Number in the Epileptic Human Hippocampus. Front Neuroanat 5.

Anderson LL, Thompson CH, Hawkins NA, Nath RD, Petersohn AA, Rajamani S, Bush WS, Frankel WN, Vanoye CG, Kearney JA, George AL (2014) Antiepileptic activity of preferential inhibitors of persistent sodium current. Epilepsia 55:1274–1283.

Andrioli A, Alonso-Nanclares L, Arellano JI, DeFelipe J (2007) Quantitative analysis of parvalbumin-immunoreactive cells in the human epileptic hippocampus. Neuroscience 149:131–143.

Androsova G et al. (2017) Comparative effectiveness of antiepileptic drugs in patients with mesial temporal lobe epilepsy with hippocampal sclerosis. Epilepsia 58:1734–1741.

Aronica E, Yankaya B, Troost D, van Vliet EA, Lopes da Silva FH, Gorter JA (2001) Induction of neonatal sodium channel II and III alpha-isoform mRNAs in neurons and microglia after status epilepticus in the rat hippocampus. Eur J Neurosci 13:1261–1266.

Baasch A-L, Hüning I, Gilissen C, Klepper J, Veltman JA, Gillessen-Kaesbach G, Hoischen A, Lohmann K (2014) Exome sequencing identifies a de novo SCN2A mutation in a patient with intractable seizures, severe intellectual disability, optic atrophy, muscular hypotonia, and brain abnormalities. Epilepsia 55:e25-9.

Baek J-H, Rubinstein M, Scheuer T, Trimmer JS (2014) Reciprocal changes in phosphorylation and methylation of mammalian brain sodium channels in response to seizures. J Biol Chem 289:15363–15373.

Barker BS, Nigam A, Ottolini M, Gaykema RP, Hargus NJ, Patel MK (2017) Pro-excitatory alterations in sodium channel activity facilitate subiculum neuron hyperexcitability in temporal lobe epilepsy. Neurobiol Dis 108:183–194.

Barker BS, Ottolini M, Wagnon JL, Hollander RM, Meisler MH, Patel MK (2016) The SCN8A encephalopathy mutation p.Ile1327Val displays elevated sensitivity to the anticonvulsant phenytoin. Epilepsia.

Bertram EH (1997) Functional anatomy of spontaneous seizures in a rat model of limbic epilepsy. Epilepsia 38:95–105.

Bertram EH (2009) Temporal lobe epilepsy: where do the seizures really begin? Epilepsy Behav 14 Suppl 1:32–37.

Bertram EH (2014) Extratemporal lobe circuits in temporal lobe epilepsy. Epilepsy Behav 38:13–18.

Bertram EH, Cornett JF (1994) The evolution of a rat model of chronic spontaneous limbic seizures. Brain Res 661:157–162.

Blanchard MG, Willemsen MH, Walker JB, Dib-Hajj SD, Waxman SG, Jongmans MCJ, Kleefstra T, van de Warrenburg BP, Praamstra P, Nicolai J, Yntema HG, Bindels RJM, Meisler MH, Kamsteeg E-J (2015) De novo gain-of-function and loss-of-function mutations of SCN8A in patients with intellectual disabilities and epilepsy. J Med Genet 52:330–337.

Blumenfeld H, Lampert A, Klein JP, Mission J, Chen MC, Rivera M, Dib-Hajj S, Brennan AR, Hains BC, Waxman SG (2009) Role of hippocampal sodium channel Nav1.6 in kindling epileptogenesis. Epilepsia 50:44–55.

Boerma RS, Braun KP, van de Broek MPH, van Berkestijn FMC, Swinkels ME, Hagebeuk EO, Lindhout D, van Kempen M, Boon M, Nicolai J, de Kovel CG, Brilstra EH, Koeleman BPC (2015) Remarkable Phenytoin Sensitivity in 4 Children with SCN8A-related Epilepsy: A Molecular Neuropharmacological Approach. Neurotherapeutics.

Boiko T, Rasband MN, Levinson SR, Caldwell JH, Mandel G, Trimmer JS, Matthews G (2001) Compact myelin dictates the differential targeting of two sodium channel isoforms in the same axon. Neuron 30:91–104.

Burgess DL, Kohrman DC, Galt J, Plummer NW, Jones JM, Spear B, Meisler MH (1995) Mutation of a new sodium channel gene, Scn8a, in the mouse mutant "motor endplate disease." Nat Genet 10:461–465.

Butler KM, da Silva C, Shafir Y, Weisfeld-Adams JD, Alexander JJ, Hegde M, Escayg A (2017) De novo and inherited SCN8A epilepsy mutations detected by gene panel analysis. Epilepsy Res 129:17–25.

Caldwell JH, Schaller KL, Lasher RS, Peles E, Levinson SR (2000) Sodium channel Na(v)1.6 is localized at nodes of ranvier, dendrites, and synapses. Proc Natl Acad Sci U S A 97:5616–5620.

Carter BC, Bean BP (2009) Sodium Entry during Action Potentials of Mammalian Neurons: Incomplete Inactivation and Reduced Metabolic Efficiency in Fast-Spiking Neurons.

Neuron 64:898–909.

Carvill GL et al. (2013) Targeted resequencing in epileptic encephalopathies identifies de novo mutations in CHD2 and SYNGAP1. Nat Genet 45:825–830.

Cassidy RM, Gale K (1998) Mediodorsal thalamus plays a critical role in the development of limbic motor seizures. J Neurosci 18:9002–9009.

Catterall WA (2000) From ionic currents to molecular mechanisms: the structure and function of voltage-gated sodium channels. Neuron 26:13–25.

Catterall WA, Goldin AL, Waxman SG (2005) International Union of Pharmacology. XLVII. Nomenclature and structure-function relationships of voltage-gated sodium channels. Pharmacol Rev 57:397–409.

Catterall WA, Kalume F, Oakley JC (2010) NaV1.1 channels and epilepsy. J Physiol 588:1849–1859.

Cavazos JE, Jones SM, Cross DJ (2004) Sprouting and synaptic reorganization in the subiculum and CA1 region of the hippocampus in acute and chronic models of partial-onset epilepsy. Neuroscience 126:677–688.

CDC (2017) Epilepsy Fast Facts. Natl Cent Dis Heal Promot

Chanda B, Asamoah OK, Bezanilla F (2004) Coupling interactions between voltage sensors of the sodium channel as revealed by site-specific measurements. J Gen Physiol 123:217–230.

Chen Y, Yu FH, Sharp EM, Beacham D, Scheuer T, Catterall WA (2008) Functional properties and differential neuromodulation of Nav1.6 channels. Mol Cell Neurosci 38:607–615.

Chen Z, Chen S, Chen L, Zhou J, Dai Q, Yang L, Li X, Zhou L (2009) Long-term increasing co-localization of SCN8A and ankyrin-G in rat hippocampal cornu ammonis 1 after pilocarpine induced status epilepticus. Brain Res 1270:112–120.

Clatot J, Hoshi M, Wan X, Liu H, Jain A, Shinlapawittayatorn K, Marionneau C, Ficker E, Ha T, Deschênes I (2017) Voltage-gated sodium channels assemble and gate as dimers. Nat Commun 8:2077.

Cohen I, Navarro V, Clemenceau S, Baulac M, Miles R (2002) On the origin of interictal activity in human temporal lobe epilepsy in vitro. Science (80-) 298:1418–1421.

Cormier JW, Rivolta I, Tateyama M, Yang A-S, Kass RS (2002) Secondary structure of the human cardiac Na+ channel C terminus: evidence for a role of helical structures in modulation of channel inactivation. J Biol Chem 277:9233–9241.

Crill WE (1996) Persistent sodium current in mammalian central neurons. Annu Rev Physiol 58:349–362.

Dawodu S, Thom M (2005) Quantitative neuropathology of the entorhinal cortex region in patients with hippocampal sclerosis and temporal lobe epilepsy. Epilepsia 46:23–30.

de Kovel CGF, Meisler MH, Brilstra EH, van Berkestijn FMC, Slot R van t., van Lieshout S, Nijman IJ, O'Brien JE, Hammer MF, Estacion M, Waxman SG, Dib-Hajj SD, Koeleman BPC (2014) Characterization of a de novo SCN8A mutation in a patient with epileptic encephalopathy. Epilepsy Res 108:1511–1518.

Dolleman-Van Der Weel MJ, Witter MP (1996) Projections from the nucleus reuniens thalami to the entorhinal cortex, hippocampal field CA1, and the subiculum in the rat arise from different populations of neurons. J Comp Neurol 364:637–650.

Drexel M, Romanov RA, Wood J, Weger S, Heilbronn R, Wulff P, Tasan RO, Harkany T, Sperk G (2017) Selective Silencing of Hippocampal Parvalbumin Interneurons Induces Development of Recurrent Spontaneous Limbic Seizures in Mice. J Neurosci 37:8166–8179.

Dyment DA, Tétreault M, Beaulieu CL, Hartley T, Ferreira P, Chardon JW, Marcadier J, Sawyer SL, Mosca SJ, Innes AM, Parboosingh JS, Bulman DE, Schwartzentruber J, Majewski J, Tarnopolsky M, Boycott KM (2015) Whole-exome sequencing broadens the phenotypic spectrum of rare pediatric epilepsy: A retrospective study. Clin Genet 88:34–40.

Ellerkmann RK, Remy S, Chen J, Sochivko D, Elger CE, Urban BW, Becker A, Beck H (2003) Molecular and functional changes in voltage-dependent Na(+) channels following pilocarpine-induced status epilepticus in rat dentate granule cells. Neuroscience 119:323–333.

Engel J, McDermott MP, Wiebe S, Langfitt JT, Stern JM, Dewar S, Sperling MR, Gardiner I, Erba G, Fried I, Jacobs M, Vinters H V, Mintzer S, Kieburtz K (2012) Early surgical therapy for drug-resistant temporal lobe epilepsy: a randomized trial. JAMA 307:922–930.

Estacion M, O'Brien JE, Conravey A, Hammer MF, Waxman SG, Dib-Hajj SD, Meisler MH (2014) A novel de novo mutation of SCN8A (Nav1.6) with enhanced channel activation in a child with epileptic encephalopathy. Neurobiol Dis 69:117–123.

Fisher RS, Acevedo C, Arzimanoglou A, Bogacz A, Cross JH, Elger CE, Engel J, Forsgren L, French JA, Glynn M, Hesdorffer DC, Lee BI, Mathern GW, Moshé SL, Perucca E, Scheffer

IE, Tomson T, Watanabe M, Wiebe S (2014) ILAE official report: a practical clinical definition of epilepsy. Epilepsia 55:475–482.

Frasier CR, Wagnon JL, Bao YO, McVeigh LG, Lopez-Santiago LF, Meisler MH, Isom LL (2016) Cardiac arrhythmia in a mouse model of sodium channel SCN8A epileptic encephalopathy. Proc Natl Acad Sci 113:12838–12843.

Gabrieli JD, Brewer JB, Desmond JE, Glover GH (1997) Separate neural bases of two fundamental memory processes in the human medial temporal lobe. Science 276:264–266.

Gilissen C et al. (2014) Genome sequencing identifies major causes of severe intellectual disability. Nature 511:344–347.

Grieco TM, Malhotra JD, Chen C, Isom LL, Raman IM (2005) Open-channel block by the cytoplasmic tail of sodium channel beta4 as a mechanism for resurgent sodium current. Neuron 45:233–244.

Hamdan FF, Srour M, Capo-Chichi J-M, Daoud H, Nassif C, Patry L, Massicotte C, Ambalavanan A, Spiegelman D, Diallo O, Henrion E, Dionne-Laporte A, Fougerat A, Pshezhetsky A V., Venkateswaran S, Rouleau GA, Michaud JL (2014) De Novo Mutations in Moderate or Severe Intellectual Disability. PLoS Genet 10:e1004772.

Hammer MF, Encinas ADC (2017) Neurotransmitters and Sodium Channelopathies; Possible Link? Pediatr Neurol Briefs 31:7.

Hammer MF, Wagnon JL, Mefford HC, Meisler MH (2016) SCN8A-Related Epilepsy with Encephalopathy.

Hargus NJ, Merrick EC, Nigam A, Kalmar CL, Baheti AR, Bertram EH, Patel MK (2011) Temporal lobe epilepsy induces intrinsic alterations in Na channel gating in layer II medial entorhinal cortex neurons. Neurobiol Dis 41:361–376.

Hargus NJ, Nigam A, Bertram EH, Patel MK (2013) Evidence for a role of Nav1.6 in facilitating increases in neuronal hyperexcitability during epileptogenesis. J Neurophysiol 110:1144–1157.

Harris E, Stewart M (2001) Propagation of synchronous epileptiform events from subiculum backward into area CA1 of rat brain slices. Brain Res 895:41–49.

Herzog RI, Cummins TR, Ghassemi F, Dib-Hajj SD, Waxman SG (2003) Distinct repriming and closed-state inactivation kinetics of Nav1.6 and Nav1.7 sodium channels in mouse spinal sensory neurons. JPhysiol.

Hille B (1977) Local anesthetics: hydrophilic and hydrophobic pathways for the drug-receptor reaction. J Gen Physiol 69:497–515.

Holland KD, Kearney JA, Glauser TA, Buck G, Keddache M, Blankston JR, Glaaser IW, Kass RS, Meisler MH (2008) Mutation of sodium channel SCN3A in a patient with cryptogenic pediatric partial epilepsy. Neurosci Lett 433:65–70.

Hu W, Tian C, Li T, Yang M, Hou H, Shu Y (2009) Distinct contributions of Na(v)1.6 and Na(v)1.2 in action potential initiation and backpropagation. NatNeurosci 12:996–1002.

Joksimovic SM, Eggan P, Izumi Y, Joksimovic SL, Tesic V, Dietz RM, Orfila JE, DiGruccio MR, Herson PS, Jevtovic-Todorovic V, Zorumski CF, Todorovic SM (2017) The role of T-type calcium channels in the subiculum: to burst or not to burst? J Physiol 595:6327–6348.

Jones JM, Meisler MH (2014) Modeling human epilepsy by TALEN targeting of mouse sodium channel Scn8a. Genesis 52:141–148.

Jung HY, Staff NP, Spruston N (2001) Action potential bursting in subicular pyramidal neurons is driven by a calcium tail current. J Neurosci 21:3312–3321.

Kaplan MR, Cho MH, Ullian EM, Isom LL, Levinson SR, Barres BA (2001) Differential control of clustering of the sodium channels Nav1.2 and Nav1.6 at developing CNS nodes of Ranvier. Neuron 30:105–119.

Ketelaars SO, Gorter JA, van Vliet EA, Lopes da Silva FH, Wadman WJ (2001) Sodium currents in isolated rat CA1 pyramidal and dentate granule neurones in the post-status epilepticus model of epilepsy. Neuroscience 105:109–120.

Khaliq ZM, Gouwens NW, Raman IM (2003) The contribution of resurgent sodium current to high-frequency firing in Purkinje neurons: an experimental and modeling study. J Neurosci 23:4899–4912.

Klassen T, Davis C, Goldman A, Burgess D, Chen T, Wheeler D, McPherson J, Bourquin T, Lewis L, Villasana D, Morgan M, Muzny D, Gibbs R, Noebels J (2011) Exome sequencing of ion channel genes reveals complex profiles confounding personal risk assessment in epilepsy. Cell 145:1036–1048.

Knopp A, Kivi A, Wozny C, Heinemann U, Behr J (2005) Cellular and network properties of the subiculum in the pilocarpine model of temporal lobe epilepsy. J Comp Neurol 483:476–488.

Kobayashi M, Wen X, Buckmaster PS (2003) Reduced inhibition and increased output of layer II neurons in the medial entorhinal cortex in a model of temporal lobe epilepsy. J Neurosci

23:8471–8479.

Kohrman DC, Plummer NW, Schuster T, Jones JM, Jang W, Burgess DL, Galt J, Spear BT, Meisler MH (1995) Insertional mutation of the motor endplate disease (med) locus on mouse chromosome 15. Genomics 26:171–177.

Kong W, Zhang Y, Gao Y, Liu X, Gao K, Xie H, Wang J, Wu Y, Zhang Y, Wu X, Jiang Y (2015) SCN8A mutations in Chinese children with early onset epilepsy and intellectual disability. Epilepsia 56:431–438.

Krzemien DM, Schaller KL, Levinson SR, Caldwell JH (2000) Immunolocalization of sodium channel isoform NaCh6 in the nervous system. J Comp Neurol 420:70–83.

Kuo CC, Bean BP (1994) Slow binding of phenytoin to inactivated sodium channels in rat hippocampal neurons. Mol Pharmacol 46:716–725.

Kwan P, Brodie MJ (2000) Early identification of refractory epilepsy. N Engl J Med 342:314–319.

Laezza F, Lampert A, Kozel MA, Gerber BR, Rush AM, Nerbonne JM, Waxman SG, Dib-Hajj SD, Ornitz DM (2009) FGF14 N-terminal splice variants differentially modulate Nav1.2 and Nav1.6-encoded sodium channels. Mol Cell Neurosci 42:90–101.

Larsen J et al. (2015) The phenotypic spectrum of SCN8A encephalopathy. Neurology 84:480–489.

Lee A, Goldin AL (2008) Role of the amino and carboxy termini in isoform-specific sodium channel variation. J Physiol 586:3917–3926.

Lek M et al. (2016) Analysis of protein-coding genetic variation in 60,706 humans. Nature 536:285–291.

Lenkowski PW, Batts TW, Smith MD, Ko SH, Jones PJ, Taylor CH, McCusker AK, Davis GC, Hartmann HA, White HS, Brown ML, Patel MK (2007) A pharmacophore derived phenytoin analogue with increased affinity for slow inactivated sodium channels exhibits a desired anticonvulsant profile. Neuropharmacology 52:1044–1054.

Levin SI, Khaliq ZM, Aman TK, Grieco TM, Kearney J a, Raman IM, Meisler MH (2006) Impaired motor function in mice with cell-specific knockout of sodium channel Scn8a (NaV1.6) in cerebellar purkinje neurons and granule cells. J Neurophysiol 96:785–793.

Lewis AH, Raman IM (2014) Resurgent current of voltage-gated Na(+) channels. J Physiol 592:4825–4838.

Lin X, O'Malley H, Chen C, Auerbach D, Foster M, Shekhar A, Zhang M, Coetzee W, Jalife J, Fishman GI, Isom L, Delmar M (2015) Scn1b deletion leads to increased tetrodotoxin-sensitive sodium current, altered intracellular calcium homeostasis and arrhythmias in murine hearts. J Physiol 593:1389–1407.

Lopez-Santiago LF, Meadows LS, Ernst SJ, Chen C, Malhotra JD, McEwen DP, Speelman A, Noebels JL, Maier SKG, Lopatin AN, Isom LL (2007) Sodium channel Scn1b null mice exhibit prolonged QT and RR intervals. J Mol Cell Cardiol 43:636–647.

Lopez-Santiago LF, Yuan Y, Wagnon JL, Hull JM, Frasier CR, O'Malley HA, Meisler MH, Isom LL (2017) Neuronal hyperexcitability in a mouse model of SCN8A epileptic encephalopathy. Proc Natl Acad Sci U S A 114:2383–2388.

Lothman EW, Bertram EH, Bekenstein JW, Perlin JB (1989) Self-sustaining limbic status epilepticus induced by "continuous" hippocampal stimulation: electrographic and behavioral characteristics. Epilepsy Res 3:107–119.

Macdonald RL, Kelly KM (1994) Mechanisms of action of currently prescribed and newly developed antiepileptic drugs. Epilepsia 35 Suppl 4:S41–S50.

Makinson CD, Tanaka BS, Lamar T, Goldin AL, Escayg A (2014) Role of the hippocampus in Nav1.6 (Scn8a) mediated seizure resistance. Neurobiol Dis 68:16–25.

Makinson CD, Tanaka BS, Sorokin JM, Wong JC, Christian CA, Goldin AL, Escayg A, Huguenard JR (2017) Regulation of Thalamic and Cortical Network Synchrony by Scn8a. Neuron 93:1165–1179.e6.

Mantegazza M, Franceschetti S, Avanzini G (1998) Anemone toxin (ATX II)-induced increase in persistent sodium current: effects on the firing properties of rat neocortical pyramidal neurones. J Physiol 507:105–116.

Mantegazza M, Yu FH, Catterall WA, Scheuer T (2001) Role of the C-terminal domain in inactivation of brain and cardiac sodium channels. Proc Natl Acad Sci U S A 98:15348–15353.

Mantegazza M, Yu FH, Powell AJ, Clare JJ, Catterall W a, Scheuer T (2005) Molecular determinants for modulation of persistent sodium current by G-protein betagamma subunits. J Neurosci 25:3341–3349.

Marionneau C, Carrasquillo Y, Norris AJ, Townsend RR, Isom LL, Link AJ, Nerbonne JM (2012) The sodium channel accessory subunit Navβ1 regulates neuronal excitability through

modulation of repolarizing voltage-gated K^+ channels. J Neurosci 32:5716–5727.

Martin MS, Tang B, Papale LA, Yu FH, Catterall WA, Escayg A (2007) The voltage-gated sodium channel Scn8a is a genetic modifier of severe myoclonic epilepsy of infancy. Hum Mol Genet 16:2892–2899.

Mattia D, Hwa GG, Avoli M (1993) Membrane properties of rat subicular neurons in vitro. J Neurophysiol 70:1244–1248.

Mattia D, Kawasaki H, Avoli M (1997) In vitro electrophysiology of rat subicular bursting neurons. Hippocampus 7:48–57.

McKinney BC, Chow CY, Meisler MH, Murphy GG (2008) Exaggerated emotional behavior in mice heterozygous null for the sodium channel Scn8a (Nav1.6). Genes Brain Behav 7:629–638.

McNally MA, Johnson J, Huisman TA, Poretti A, Baranano KW, Baschat AA, Stafstrom CE (2016) SCN8A Epileptic Encephalopathy: Detection of Fetal Seizures Guides Multidisciplinary Approach to Diagnosis and Treatment. Pediatr Neurol 64:87–91.

Meisler MH et al. (2016) SCN8A encephalopathy: Research progress and prospects. Epilepsia 57:1027–1035 8.

Meisler MH, O'Brien JE, Sharkey LM (2010) Sodium channel gene family: epilepsy mutations, gene interactions and modifier effects. J Physiol 588:1841–1848.

Motoike HK, Liu H, Glaaser IW, Yang A-S, Tateyama M, Kass RS (2004) The Na+ channel inactivation gate is a molecular complex: a novel role of the COOH-terminal domain. J Gen Physiol 123:155–165.

Nadler J V, Perry BW, Cotman CW (1980) Selective reinnervation of hippocampal area CA1 and the fascia dentata after destruction of CA3-CA4 afferents with kainic acid. Brain Res 182:1–9.

Nguyen HM, Goldin AL (2010) Sodium channel carboxyl-terminal residue regulates fast inactivation. J Biol Chem 285:9077–9089.

Noujaim SF, Kaur K, Milstein M, Jones JM, Furspan P, Jiang D, Auerbach DS, Herron T, Meisler MH, Jalife J (2012) A null mutation of the neuronal sodium channel NaV1.6 disrupts action potential propagation and excitation-contraction coupling in the mouse heart. FASEB J 26:63–72.

O'Brien JE, Meisler MH (2013) Sodium channel SCN8A (Nav1.6): properties and de novo

mutations in epileptic encephalopathy and intellectual disability. Front Genet 4:213.

O'Brien JE, Sharkey LM, Vallianatos CN, Han C, Blossom JC, Yu T, Waxman SG, Dib-Hajj SD, Meisler MH (2012) Interaction of voltage-gated sodium channel Nav1.6 (SCN8A) with microtubule-associated protein Map1b. J Biol Chem 287:18459–18466.

O'Mara SM, Commins S, Anderson M, Gigg J (2001) The subiculum: A review of form, physiology and function. Prog Neurobiol 64:129–155.

Ohba C et al. (2014) Early onset epileptic encephalopathy caused by de novo SCN8A mutations. Epilepsia 55:994–1000.

Ottolini M, Barker BS, Gaykema RP, Meisler MH, Patel MK (2017) Aberrant Sodium Channel Currents and Hyperexcitability of Medial Entorhinal Cortex Neurons in a Mouse Model of SCN8A Encephalopathy. J Neurosci 37:7643–7655.

Panayiotopoulos C (2005) The Epilepsies Seizures, Syndromes and Managemen. Oxfordshire: Bladon Medical Publishing.

Papale LA, Beyer B, Jones JM, Sharkey LM, Tufik S, Epstein M, Letts VA, Meisler MH, Frankel WN, Escayg A (2009) Heterozygous mutations of the voltage-gated sodium channel SCN8A are associated with spike-wave discharges and absence epilepsy in mice. Hum Mol Genet 18:1633–1641.

Patel RR, Barbosa C, Brustovetsky T, Brustovetsky N, Cummins TR (2016) Aberrant epilepsy-associated mutant Nav1.6 sodium channel activity can be targeted with cannabidiol. Brain 139:2164–2181.

Patino GA, Isom LL (2010) Electrophysiology and beyond: multiple roles of Na+ channel β subunits in development and disease. Neurosci Lett 486:53–59.

Payandeh J, Scheuer T, Zheng N, Catterall WA (2011) The crystal structure of a voltage-gated sodium channel. Nature 475:353–358.

Petersen A V., Jensen CS, Crépel V, Falkerslev M, Perrier J-F (2017) Serotonin Regulates the Firing of Principal Cells of the Subiculum by Inhibiting a T-type Ca2+ Current. Front Cell Neurosci 11.

Petrovski S, Wang Q, Heinzen EL, Allen AS, Goldstein DB (2013) Genic Intolerance to Functional Variation and the Interpretation of Personal Genomes. PLoS Genet 9.

Plummer NW, Meisler MH (1999) Evolution and diversity of mammalian sodium channel genes. Genomics 57:323–331.

Raman IM, Bean BP (1997) Resurgent sodium current and action potential formation in dissociated cerebellar Purkinje neurons. J Neurosci 17:4517–4526.

Raman IM, Sprunger LK, Meisler MH, Bean BP (1997) Altered subthreshold sodium currents and disrupted firing patterns in Purkinje neurons of Scn8a mutant mice. Neuron 19:881–891.

Rasband MN (2010) The axon initial segment and the maintenance of neuronal polarity. Nat Rev Neurosci 11:552–562.

Rauch A et al. (2012) Range of genetic mutations associated with severe non-syndromic sporadic intellectual disability: An exome sequencing study. Lancet 380:1674–1682.

Remy S, Gabriel S, Urban BW, Dietrich D, Lehmann TN, Elger CE, Heinemann U, Beck H (2003a) A novel mechanism underlying drug resistance in chronic epilepsy. Ann Neurol 53:469–479.

Remy S, Urban BW, Elger CE, Beck H (2003b) Anticonvulsant pharmacology of voltage-gated Na+ channels in hippocampal neurons of control and chronically epileptic rats. EurJNeurosci 17:2648–2658.

Rogawski MA, Loscher W (2004) The neurobiology of antiepileptic drugs. NatRevNeurosci 5:553–564.

Rosker C, Lohberger B, Hofer D, Steinecker B, Quasthoff S, Schreibmayer W (2007) The TTX metabolite 4,9-anhydro-TTX is a highly specific blocker of the Na(v1.6) voltage-dependent sodium channel. Am J Physiol Cell Physiol 293:C783–C789.

Royeck M, Horstmann M-T, Remy S, Reitze M, Yaari Y, Beck H (2008) Role of axonal NaV1.6 sodium channels in action potential initiation of CA1 pyramidal neurons. J Neurophysiol 100:2361–2380.

Rush AM, Dib-Hajj SD, Waxman SG (2005) Electrophysiological properties of two axonal sodium channels, Nav1.2 and Nav1.6, expressed in mouse spinal sensory neurones. J Physiol 564:803–815.

Scalmani P, Rusconi R, Armatura E, Zara F, Avanzini G, Franceschetti S, Mantegazza M (2006) Effects in neocortical neurons of mutations of the Na(v)1.2 Na+ channel causing benign familial neonatal-infantile seizures. J Neurosci 26:10100–10109.

Schaller KL, Caldwell JH (2000) Developmental and regional expression of sodium channel isoform NaCh6 in the rat central nervous system. J Comp Neurol 420:84–97.

Schaub C, Uebachs M, Beck H (2007) Diminished response of CA1 neurons to antiepileptic drugs in chronic epilepsy. Epilepsia 48:1339–1350.

Scheffer IE, Berkovic S, Capovilla G, Connolly MB, French J, Guilhoto L, Hirsch E, Jain S, Mathern GW, Moshé SL, Nordli DR, Perucca E, Tomson T, Wiebe S, Zhang Y-H, Zuberi SM (2017) ILAE classification of the epilepsies: Position paper of the ILAE Commission for Classification and Terminology. Epilepsia 58:512–521.

Seidenberg M, Pulsipher DT, Hermann B (2009) Association of epilepsy and comorbid conditions. Future Neurol 4:663–668.

Shao L-R, Dudek FE (2005) Electrophysiological evidence using focal flash photolysis of caged glutamate that CA1 pyramidal cells receive excitatory synaptic input from the subiculum. J Neurophysiol 93:3007–3011.

Sharp PE, Green C (1994) Spatial correlates of firing patterns of single cells in the subiculum of the freely moving rat. J Neurosci 14:2339–2356.

Singh R, Jayapal S, Goyal S, Jungbluth H, Lascelles K (2015) Early-onset movement disorder and epileptic encephalopathy due to de novo dominant SCN8A mutation. Seizure 26:69–71.

Sloviter RS, Damiano BP (1981) Sustained electrical stimulation of the perforant path duplicates kainate-induced electrophysiological effects and hippocampal damage in rats. Neurosci Lett 24:279–284.

Smith MR, Goldin AL (1997) Interaction between the sodium channel inactivation linker and domain III S4-S5. Biophys J 73:1885–1895.

Spampanato J, Kearney JA, de Haan G, McEwen DP, Escayg A, Aradi I, MacDonald BT, Levin SI, Soltesz I, Benna P, Montalenti E, Isom LL, Goldin AL, Meisler MH (2004) A novel epilepsy mutation in the sodium channel SCN1A identifies a cytoplasmic domain for beta subunit interaction. J Neurosci 24:10022–10034.

Sprissler RS, Wagnon JL, Bunton-Stasyshyn RK, Meisler MH, Hammer MF (2016) Altered gene expression profile in a mouse model of SCN8A encephalopathy. Exp Neurol.

Staff NP, Jung HY, Thiagarajan T, Yao M, Spruston N (2000) Resting and active properties of pyramidal neurons in subiculum and CA1 of rat hippocampus. J Neurophysiol 84:2398–2408.

Stafstrom CE (2005a) The Role of the Subiculum in Epilepsy and Epileptogenesis. Epilepsy Curr 5:121–129.

Stafstrom CE (2005b) Epilepsy and Epileptogenesis. Epilepsy Curr 5:121–129 f.

Stafstrom CE (2007) Persistent Sodium Current and Its Role in Epilepsy. Epilepsy Curr 7:15–22.

Stewart M, Wong RK (1993) Intrinsic properties and evoked responses of guinea pig subicular neurons in vitro. J Neurophysiol 70:232–245.

Swanson LW, Cowan WM (1977) An autoradiographic study of the organization of the efferent connections of the hippocampal formation in the rat. J Comp Neurol 172:49–84.

Takahashi S, Yamamoto S, Okayama A, Araki A, Saitsu H, Matsumoto N, Azuma H (2015) Electroclinical features of epileptic encephalopathy caused by SCN8A mutation. Pediatr Int 57:758–762.

Tang H, Wu G-S, Xie J, He X, Deng K, Wang H, Xu F, Luo H-R (2016) Brain-wide map of projections from mice ventral subiculum. Neurosci Lett 629:171–179.

Taube J (1993) Electrophysiological properties of neurons in the rat subiculum in vivo. Exp Brain Res 96:304–318.

Thurman DJ, Hesdorffer DC, French JA (2014) Sudden unexpected death in epilepsy: assessing the public health burden. Epilepsia 55:1479–1485.

Toyoda I, Bower MR, Leyva F, Buckmaster PS (2013) Early activation of ventral hippocampus and subiculum during spontaneous seizures in a rat model of temporal lobe epilepsy. J Neurosci 33:11100–11115.

Toyoda I, Fujita S, Thamattoor AK, Buckmaster PS (2015) Unit Activity of Hippocampal Interneurons before Spontaneous Seizures in an Animal Model of Temporal Lobe Epilepsy. J Neurosci 35:6600–6618.

Trudeau MM, Dalton JC, Day JW, Ranum LPW, Meisler MH (2006) Heterozygosity for a protein truncation mutation of sodium channel SCN8A in a patient with cerebellar atrophy, ataxia, and mental retardation. J Med Genet 43:527–530.

Twombly DA, Yoshii M, Narahashi T (1988) Mechanisms of calcium channel block by phenytoin. J Pharmacol Exp Ther 246:189–195.

Vacher H, Mohapatra DP, Trimmer JS (2008) Localization and targeting of voltage-dependent ion channels in mammalian central neurons. Physiol Rev 88:1407–1447.

Vaher U, Nõukas M, Nikopensius T, Kals M, Annilo T, Nelis M, Ounap K, Reimand T, Talvik I, Ilves P, Piirsoo A, Seppet E, Metspalu A, Talvik T (2014) De novo SCN8A mutation identified by whole-exome sequencing in a boy with neonatal epileptic encephalopathy,

multiple congenital anomalies, and movement disorders. J Child Neurol 29:NP202-6.

van Drongelen W, Koch H, Elsen FP, Lee HC, Mrejeru A, Doren E, Marcuccilli CJ, Hereld M, Stevens RL, Ramirez J-M (2006) Role of persistent sodium current in bursting activity of mouse neocortical networks in vitro. J Neurophysiol 96:2564–2577.

van Strien NM, Cappaert NLM, Witter MP (2009) The anatomy of memory: an interactive overview of the parahippocampal-hippocampal network. Nat Rev Neurosci 10:272–282.

Vanoye CG, Gurnett CA, Holland KD, George AL, Kearney JA (2014) Novel SCN3A variants associated with focal epilepsy in children. Neurobiol Dis 62:313–322.

Vassilev P, Scheuer T, Catterall WA (1989) Inhibition of inactivation of single sodium channels by a site-directed antibody. Proc Natl Acad Sci U S A 86:8147–8151.

Vassilev PM, Scheuer T, Catterall WA (1988) Identification of an intracellular peptide segment involved in sodium channel inactivation. Science 241:1658–1661.

Veeramah KR, O'Brien JE, Meisler MH, Cheng X, Dib-Hajj SD, Waxman SG, Talwar D, Girirajan S, Eichler EE, Restifo LL, Erickson RP, Hammer MF (2012) De novo pathogenic SCN8A mutation identified by whole-genome sequencing of a family quartet affected by infantile epileptic encephalopathy and SUDEP. AmJHumGenet 90:502–510.

Vissers LELM, Gilissen C, Veltman JA (2015) Genetic studies in intellectual disability and related disorders. Nat Rev Genet 17:9–18.

Vreugdenhil M, Hoogland G, van Veelen CW, Wadman WJ (2004) Persistent sodium current in subicular neurons isolated from patients with temporal lobe epilepsy. EurJNeurosci 19:2769–2778.

Vreugdenhil M, van Veelen CW, van Rijen PC, Lopes da Silva FH, Wadman WJ (1998) Effect of valproic acid on sodium currents in cortical neurons from patients with pharmaco-resistant temporal lobe epilepsy. Epilepsy Res 32:309–320.

Vreugdenhil M, Wadman WJ (1999) Modulation of sodium currents in rat CA1 neurons by carbamazepine and valproate after kindling epileptogenesis. Epilepsia 40:1512–1522.

Wagnon JL, Barker BS, Hounshell JA, Haaxma CA, Shealy A, Moss T, Parikh S, Messer RD, Patel MK, Meisler MH (2015a) Pathogenic mechanism of recurrent mutations of SCN8A in epileptic encephalopathy. Ann Clin Transl Neurol:n/a-n/a.

Wagnon JL, Barker BS, Ottolini M, Park Y, Volkheimer A, Valdez P, Swinkels MEM, Patel MK, Meisler MH (2017) Loss-of-function variants of SCN8A in intellectual disability

without seizures. Neurol Genet 3:e170.

Wagnon JL, Korn MJ, Parent R, Tarpey TA, Jones JM, Hammer MF, Murphy GG, Parent JM, Meisler MH (2015b) Convulsive seizures and SUDEP in a mouse model of SCN8A epileptic encephalopathy. Hum Mol Genet 24:506–515.

Wagnon JL, Meisler MH (2015) Recurrent and non-recurrent mutations of SCN8A in epileptic encephalopathy. Front Neurol 6.

Walter RD (1969) Clinical Aspects of Temporal Lobe Epilepsy. Calif Med 110:325–329.

Watanabe E, Fujikawa A, Matsunaga H, Yasoshima Y, Sako N, Yamamoto T, Saegusa C, Noda M (2000) Nav2/NaG channel is involved in control of salt-intake behavior in the CNS. J Neurosci 20:7743–7751.

Wellmer J, Su H, Beck H, Yaari Y (2002) Long-lasting modification of intrinsic discharge properties in subicular neurons following status epilepticus. Eur J Neurosci 16:259–266.

Whitaker WR, Faull RL, Dragunow M, Mee EW, Emson PC, Clare JJ (2001a) Changes in the mRNAs encoding voltage-gated sodium channel types II and III in human epileptic hippocampus. Neuroscience 106:275–285.

Whitaker WR, Faull RL, Waldvogel HJ, Plumpton CJ, Emson PC, Clare JJ (2001b) Comparative distribution of voltage-gated sodium channel proteins in human brain. Brain Res Mol Brain Res 88:37–53.

WHO (2018) Epilepsy Factsheet. World Heal Organization

Wiebe S, Blume WT, Girvin JP, Eliasziw M (2001) A randomized, controlled trial of surgery for temporal-lobe epilepsy.

Wieser H-G, ILAE Commission on Neurosurgery of Epilepsy (2004) ILAE Commission Report. Mesial temporal lobe epilepsy with hippocampal sclerosis. Epilepsia 45:695–714.

Witter MP (2007) The perforant path: projections from the entorhinal cortex to the dentate gyrus. Prog Brain Res 163:43–61.

Witter MP, Griffioen AW, Jorritsma-Byham B, Krijnen JL (1988) Entorhinal projections to the hippocampal CA1 region in the rat: an underestimated pathway. Neurosci Lett 85:193–198.

Witter MP, Groenewegen HJ (1990) The subiculum: cytoarchitectonically a simple structure, but hodologically complex. Prog Brain Res 83:47–58.

Witter MP, Groenewegen HJ, Lopes da Silva FH, Lohman AH (1989) Functional organization of the extrinsic and intrinsic circuitry of the parahippocampal region. Prog Neurobiol 33:161–

253.

Witter MP, Naber PA, van Haeften T, Machielsen WC, Rombouts SA, Barkhof F, Scheltens P, Lopes da Silva FH (2000a) Cortico-hippocampal communication by way of parallel parahippocampal-subicular pathways. Hippocampus 10:398–410.

Witter MP, Wouterlood FG, Naber PA, Van Haeften T (2000b) Anatomical organization of the parahippocampal-hippocampal network. Ann N Y Acad Sci 911:1–24.

Wolff M et al. (2017) Genetic and phenotypic heterogeneity suggest therapeutic implications in SCN2A-related disorders. Brain 140:1316–1336.

Wong JC, Makinson CD, Lamar T, Cheng Q, Wingard JC, Terwilliger EF, Escayg A (2018) Selective targeting of Scn8a prevents seizure development in a mouse model of mesial temporal lobe epilepsy. Sci Rep 8:126.

Woodruff-Pak DS, Green JT, Levin SI, Meisler MH (2006) Inactivation of sodium channel Scn8A (NA v1.6) in Purkinje neurons impairs learning in morris water maze and delay but not trace eyeblink classical conditioning. Behav Neurosci 120:229–240.

Wouterlood FG, Saldana E, Witter MP (1990) Projection from the nucleus reuniens thalami to the hippocampal region: light and electron microscopic tracing study in the rat with the anterograde tracer Phaseolus vulgaris-leucoagglutinin. J Comp Neurol 296:179–203.

Wozny C, Knopp A, Lehmann T-N, Heinemann U, Behr J (2005) The subiculum: a potential site of ictogenesis in human temporal lobe epilepsy. Epilepsia 46 Suppl 5:17–21.

Yaari Y, Yue C, Su H (2007) Recruitment of apical dendritic T-type Ca2+ channels by backpropagating spikes underlies de novo intrinsic bursting in hippocampal epileptogenesis. J Physiol 580:435–450.

Yamada-Hanff J, Bean BP (2013) Persistent sodium current drives conditional pacemaking in CA1 pyramidal neurons under muscarinic stimulation. J Neurosci 33:15011–15021.

Yarov-Yarovoy V, DeCaen PG, Westenbroek RE, Pan C-Y, Scheuer T, Baker D, Catterall WA (2012) Structural basis for gating charge movement in the voltage sensor of a sodium channel. Proc Natl Acad Sci 109:E93–E102.

Yu FH, Mantegazza M, Westenbroek RE, Robbins CA, Kalume F, Burton KA, Spain WJ, McKnight GS, Scheuer T, Catterall WA (2006) Reduced sodium current in GABAergic interneurons in a mouse model of severe myoclonic epilepsy in infancy. Nat Neurosci 9:1142–1149.

Yue C, Remy S, Su H, Beck H, Yaari Y (2005) Proximal persistent Na+ channels drive spike afterdepolarizations and associated bursting in adult CA1 pyramidal cells. J Neurosci 25:9704–9720.